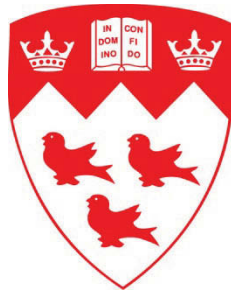


**Impact of seismic retrofit and presence of *terra cotta*
masonry walls on the dynamic properties of a hospital
building in Montréal, Canada**

by

Amin Asgarian

December 2011



Department of Civil Engineering and Applied Mechanics

McGill University, Montreal

A Thesis submitted to the Faculty of Graduate Studies and Research in partial fulfillment of the requirements of the degree of Master of Engineering

© Amin Asgarian 2011

Abstract

Unreinforced masonry (URM) infill walls are widely used in structures in North America. In several “pre-code” hospital buildings constructed before the 1970s, *terra cotta* masonry blocks have been used extensively. Although unreinforced *terra cotta* infill walls play a structural role, interior partitions are generally considered as non-structural components (NSCs) and their stiffness effects on the structure are often ignored in seismic analysis and design, while their weight/mass is included as uniformly distributed load/inertia. *Terra cotta* infill walls interact with their bounding frame during earthquakes and increase the lateral stiffness and strength of the structure, which in turn influences the dynamic response of the building. Of course, as they get damaged in strong earthquakes, their stiffness is degrading and they either become locally detached from the frame or they simply collapse. *In situ* vibration measurements and observations of past earthquake-induced damage clearly demonstrate the necessity of considering the effect of infill walls on structural response, particularly for post-critical buildings such as hospitals which have to remain functional after severe design-level seismic shaking.

To illustrate the structural contribution of infill *terra cotta* walls, two eleven-storey buildings have been selected which are two wings (Blocks #7 and #8) of CHU Sainte-Justine, a paediatric research hospital located in Montréal, Canada. The two buildings are almost identical in terms of floor plans, elevations and dimensions. This hospital campus was initially built in the late 1950s and Block #7 was seismically retrofitted in 2008 by adding a full-height reinforced concrete shear wall at its free end and connecting the other end of the building to the adjacent Block #9, using structural anchor bars at each floor slab and along the height of interfacing columns. Block #8 was not retrofitted and has remained unattached to adjacent Block 9. A detailed

linear elastic finite element analysis model of each building was created where the infill unreinforced *terra cotta* walls have been modeled. Only linear models were created at this stage as the hospital buildings have to remain practically linear elastic to fulfill their functionality performance objectives. Two different techniques were adopted for modeling these infill walls, namely using panel elements and compression strut models. For the compression strut models, three different formulas suggested in the literature were used to calculate the effective width and properties of the strut. In parallel, in situ Ambient Vibration Measurements (AVMs) were done in both buildings and their dominant dynamic properties including the lowest natural frequencies, corresponding mode shapes, and effective damping ratios have been extracted using two different operational modal analysis techniques- namely, Frequency Domain Decomposition-Peak Picking (FDD) and Enhanced Frequency Domain Decomposition-Peak Picking (EFDD). The AVM results were used for validation and also calibration of the numerical models. The calibrated models were subjected to a set of 12 synthetic ground accelerograms compatible with the NBC Uniform Hazard Spectra (UHS) for Montréal in both principal horizontal directions independently. Selecting two floors in each block (top floor #7 and middle floor # 3), Floor Response Spectra (FRS) and Interstorey-Drift curves were developed for each record. The effects of seismic rehabilitation and presence of infill walls on the dynamic properties of the building and also on the performance of their NSCs were addressed by comparing the results of different models (i.e. models including and excluding infill walls). Finally, a detailed study of the NSC's seismic behaviour (both Interstorey-Drift-sensitive components and Acceleration-sensitive components) was done using FRS and Interstorey-Drift curves provided for the two selected floors.

Finally, the lateral stiffness of the rehabilitated block # 7 is significantly improved compared to block # 8 which means it is subjected to larger accelerations; for example the maximum acceleration at the 7 floor is on

average three times the acceleration of the same floor in block # 8 for the twelve earthquake scenarios. The non-structural components that are sensitive to accelerations are subjected to higher forces in block 7. Since the inter-storey drifts are much reduced in block 7 to very low values justifying the linear analysis, the performance of architectural components and functional components connected at several levels (e.g. pipes and conduits) is improved.

Résumé

Les murs en maçonnerie non armée (MNA) sont très présents dans les bâtiments nord-américains, en particulier dans les bâtiments publics comme les écoles, les centres communautaires et sportifs, et les hôpitaux. Dans plusieurs hôpitaux « pré-code » construits avant l'adoption des normes parasismiques dans les années 1970, la maçonnerie de blocs en *terra cotta* a été abondamment utilisée. Bien que les murs de remplissage jouent effectivement un rôle structural dans la réponse sismique des bâtiments, les murs qui servent simplement de cloisons internes sont considérés comme des composants non-structuraux (architecturaux) et leur influence structurale est négligée dans les analyses sismiques alors que leur masse/poids est pris(e) en compte comme une inertie/force uniformément distribuée appliquée au plancher. Les murs de remplissage en *terra cotta* interagissent avec leur cadre périphérique durant les séismes et augmentent la rigidité latérale et la résistance des ossatures, ce qui influence directement leur réponse dynamique. Évidemment, à mesure que ces murs sont endommagés par fissuration lors de violents séismes, leur rigidité se dégrade et la maçonnerie se détache progressivement du cadre périphérique ou s'effondre. Des mesures de vibrations ambiantes dans les bâtiments de même que les observations de dommages lors de séismes antérieurs ont prouvé la nécessité de tenir compte de l'influence structurale des murs de remplissage, particulièrement pour les bâtiments de protection civile comme les hôpitaux qui se doivent de rester fonctionnels suite au séisme de conception.

Cette thèse illustre la contribution structurale de murs de remplissage en *terra cotta* à l'aide d'une étude de cas détaillée de deux bâtiments de onze étages du Centre hospitalier universitaire (CHU) Sainte-Justine – les blocs #7 et #8, un hôpital pédiatrique situé sur l'île de Montréal. Les deux bâtiments sont quasi identiques en termes de géométrie des planchers, coupes en

élévation et dimensions. Cet hôpital a été construit à la fin des années 1950 et le bloc #7 a fait l'objet d'une réhabilitation parasismique en 2008; un mur de refend sismique en béton armé a été construit sur la pleine hauteur de la façade libre dans l'axe faible et le bâtiment a été connecté à son bâtiment adjacent (le bloc #9) par des tiges d'ancrage en acier dans les dalles de chaque plancher et le long des colonnes d'interface. Le bloc #8, par contre, n'a subi aucune réhabilitation parasismique et demeure non-relié à son bâtiment adjacent. Un modèle détaillé pour l'analyse par éléments finis de chacun des deux blocs a été mis au point, avec modélisation des murs de remplissage en *terra cotta*. Seuls des modèles linéaires élastiques ont été créés pour cette étude considérant que les bâtiments doivent rester pratiquement en mode de réponse linéaire pour satisfaire leur objectif de performance sismique. Deux techniques ont été appliquées pour la modélisation des murs de remplissage : la définition de panneaux continus et la méthode des bielles comprimées équivalentes. Pour cette dernière technique, trois formules différentes bien documentées ont été utilisées pour calculer la largeur effective des bielles de compression. En parallèle avec ces études numériques, une campagne de mesures de vibrations ambiantes a été réalisée pour les deux blocs et les propriétés dynamiques dominantes des bâtiments ont été identifiées, incluant les périodes naturelles fondamentales, les déformées modales correspondantes, ainsi que les rapports d'amortissement modal visqueux. L'analyse des mesures s'est faite à l'aide de deux techniques d'analyse modale opérationnelle en sélectionnant les pics des fonctions obtenues par décomposition des mesures dans le domaine des fréquences, soit la méthode de base(FDD) et une version dite améliorée (EFDD). Les résultats des mesures de bruit ambiant ont été utilisés pour valider et calibrer les modèles numériques. Une fois calibrés, les modèles ont été analysés sous l'effet de 12 séismes représentés par des accélérographes synthétiques compatibles avec le spectre de l'aléa sismique uniforme défini au Code National du Bâtiment pour Montréal. Les accélérographes ont été appliqués indépendamment dans les deux directions géométriques

principales des bâtiments. Deux étages spécifiques ont été sélectionnés pour une analyse approfondie des résultats : le plancher du 7^e étage et le plancher du 3^e étage. Les spectres de réponse de ces planchers ainsi que les historiques des déplacements inter-étages (7-8) et (3-4) ont été générés pour chacun des scénarios d'analyse sismique.

L'étude comparative des résultats obtenus avec les différents modèles d'analyse par éléments finis (i.e. excluant et incluant les murs de remplissage, et selon les diverses approches de modélisation) a permis d'étudier les effets de la réhabilitation parasismique du bloc #7 et l'influence de la présence des murs de remplissage dans les blocs #7 et #8 sur leurs propriétés dynamiques. Finalement, les analyses sismiques ont permis de quantifier l'influence de ces effets sur le comportement des composants non-structuraux en comparant les spectres de planchers et les déplacements inter-étages. Au final, le bloc réhabilité a considérablement amélioré sa rigidité et par le fait même subi des accélérations de beaucoup supérieures à celles du bloc 8 non réhabilité – les composants non structuraux sensibles aux accélérations sont ainsi plus sollicités au bloc #7. Par contre, les déplacements inter-étages sont réduits à des valeurs très faibles (qui justifient pratiquement les analyses linéaires), ce qui améliore la performance des composants architecturaux et des composants fonctionnels connectés à plusieurs niveaux (ex. tuyauteries et conduites).

Acknowledgments

I am grateful for the financial support provided by Natural Sciences and Engineering Research Council of Canada (NSERC) in the form of a research assistantship as part of the NSERC strategic research network on reducing urban seismic risk (CSRN).

I wish to express my profound and sincere gratitude to my research advisor, Professor Ghyslaine McClure, for her continuous help and support, constant encouragement, and skilful guidance throughout this research. Her kindness always made me feel like a colleague rather than a subordinate and I am so glad to have had the opportunity to work with her.

This research could not have been possible without the help of technical personnel from Sainte-Justine Hospital who provided building data and allowed our team to perform ambient vibration measurements; thanks are due to Mr. Jonathan St-Jean, Mr. Stéphane Daraïche, and Ms. Marie-Claude Lefebvre.

I sincerely thank all my friends who encouraged and helped me during this research project; Farshad Mirshafiei, Iman Shamim, Alireza Mirzaei, and Helene Tischer.

At last but not the least, my greatest thank-you goes to my lovely family (my father, Mohammad Hossein, my mother, Zahra, my brother, Ali, and my sister, Azin) for their invaluable and irreplaceable love, constant support, and all the difficulties through which they have put themselves during these years to reach me to this stage. They have been always on my side and they are the reason for who I am today and will be tomorrow.

Table of contents

Abstract	I
Résumé	IV
Acknowledgments	VII
Table of contents	VIII
List of Figures	XIII
List of Tables	XVIII
List of symbols	XXI
Acronyms	XXII
1. Introduction	1
1.1 Research motivation.....	1
1.2 Research objectives	5
1.3 Research Methodology	6
1.4 Organization of thesis	7
2. Background and literature review	9
2.1 CHU Sainte-Justine Hospital[2]	9
2.1.1 General information about the Hospital.....	9

2.1.2	Seismic retrofitting plan of Hospital	12
2.2	Risk of a strong earthquake in Montreal	13
2.3	Experimental modal analysis and ambient vibration testing.....	15
2.3.1	Forced Vibration Testing (FVT)	15
2.3.2	Free response testing.....	16
2.3.3	Earthquake response testing	16
2.3.4	Ambient Vibration Testing (AVT)	17
2.4	Behaviour and analysis of unreinforced masonry infill walls.....	18
2.4.1	Equivalent diagonal compression struts	19
2.4.2	Finite element models	23
3	Experimental study: In situ Ambient Vibration Test (AVT).....	25
3.1	Data collection	25
3.1.1	Instrument.....	25
3.1.2	Distribution of measurement points.....	27
3.1.3	Test procedure.....	30
3.2	Data analysis and modal identification	31
3.2.1	Synchronization	31

3.2.2	Theoretical concepts of modal analysis	32
3.2.2.1	Spectral density function	32
3.2.3	Operational modal analysis techniques.....	33
3.2.3.1	Peak-picking method (PP).....	34
3.2.3.2	Frequency Domain Decomposition-Peak Picking (FDD).....	34
3.2.3.3	Enhanced Frequency Domain Decomposition (EFDD)	39
3.3	AVT results	44
3.4	Comparison between AVT results and NBCC-2010 period equation...	45
4	Numerical study: Finite element modeling and analysis.....	47
4.1	General properties of the buildings	47
4.1.1	Geometric properties	47
4.1.2	Structural Properties.....	49
4.2	Description of different FE models	51
4.2.1	Bare-frame models (the models excluding masonry infill walls)	52
4.2.1.1	Block #8.....	54
4.2.1.2	Block #7	55
4.2.2	Full-frame models (with masonry infill walls)	68

4.2.2.1	Continuum model (Panel element model)	69
4.2.2.2	Equivalent diagonal compression struts	74
4.3	Calibration of numerical models using AVT results.....	80
4.4	Time-history seismic analysis and development of Floor Respons Spectra and Interstorey-Drift curves.....	81
5	Results and discussion.....	86
5.1	Bare-frame model results.....	86
5.2	Full-frame model results.....	91
5.2.1	Results of Block#8.....	92
5.2.2	Results of Block #7.....	96
5.3	FE Model Calibration with AVT results	101
5.3.1	Discussion of block#8 results	102
5.3.2	Discussion of block#7 results	103
5.4	Effect of seismic retrofit and masonry infill walls on the performance of NSCs	105
5.4.1	Results and discussion for Block#8.....	106
5.4.2	Results and discussion for Block#7	114
6	Conclusions and Futur Work	121

Appendix A - Acceleration floor response spectra 123

References.....128

List of Figures

Figure 1 -- <i>Terra Cotta</i> infill masonry wall in CHU Sainte-Justine in	3
Figure 2 – Brittle shear failure of reinforced concrete column, 1972, Managua earthquake. [41].....	4
Figure 3 – Failure due to creating the soft first storey, Beichuan, China,	4
Figure 4 - RDP plan[2]	10
Figure 5 - General layout of the hospital.....	11
Figure 6 - Exterior wall cross-section.....	11
Figure 7 - Side elevation of block#4: a) during construction; b) after adding concrete shear wall and new masonry wall	13
Figure 8 – Diagonal compression strut	20
Figure 9 - Infilled frame [16]	21
Figure 10-Failure mechanisms of infilled frames [17].....	22
Figure 11 - Continuum model [27]	24
Figure 12 – TROMINO sensor connected to the radio antenna	26

Figure 13- Architectural Drawing, Block#8, Floor#1.....	28
Figure 14- Distribution of measurement points in horizontal plane	28
Figure 15- Vertical distribution of measurement points: a) 2D view; b)3D view.....	29
Figure 16 - FDD-Peak picking, Aug 2010, Block#8, Singular value plot.....	37
Figure 17 - FDD-Peak picking, Aug 2010, Block#8, Estimated mode shape corresponding to first peak (Translational mode in Y-direction)	38
Figure 18 - EFDD-Peak picking, Identification of SDOF spectral bell (Aug 2010, Block#8)	41
Figure 19 - SDOF autocorrelation function in Time-Domain.....	42
Figure 20 - Improved estimate of frequency using zero crossings	43
Figure 21 - Estimate of viscous damping using logarithmic decrement.....	43
Figure 22 - Geometric properties: a) Elevation view; b)Plan view	48
Figure 23 - 3D view of bare-frame model, Block#8	54
Figure 24 - 3D extruded view of bare-frame model-Block#8	55
Figure 25 - Close-up view of anchor locations before casting the shear wall	56

Figure 26 - Connection between new shear wall and existing building[2].....	57
Figure 27- Anchor details: a) Plan view of connection; b) Cross-section	57
Figure 28- Inter-Storey drift (average displacement).....	61
Figure 29- MDOF system: a)schematic view of N degree-of-freedom system;	64
Figure 30- a) Shear model of block#8 and b) corresponding stiffness matrix	66
Figure 31- 3D view of bare-frame model-Block#7	67
Figure 32-3D extruded view of bare-frame model-Block#7	68
Figure 33-Full-frame model using panel elements - Block#8: a & b) 3D views;	72
Figure 34- Full-frame model using panel elements - Block#7: a & b)3D views;	73
Figure 35 – Diagonal Compression strut- Effective width.....	74
Figure 36- Full-frame model using diagonal compression struts - Block#8: a & b) 3D views;	78
Figure 37- Full-frame model using diagonal compression struts - Block#7: a & b)3D views;	79

Figure 38- NBC 2005 UHS for Montreal.....	83
Figure 39- Example of ground motion record (E70701): a) Time-history, b) Response spectrum.....	84
Figure 40- Comparison between response spectrum of E70701 and UHS: a)Unscaled RS; b)Scaled RS based on 1 st mode; c) Scaled RS based on 2 nd mode; d) Scaled RS based on 3 rd mode (best match)	85
Figure 41- First mode of vibration of bare-frame models: a)Block#8; b)Block#7-.....	90
Figure 42- Layout of AVT measurement points distribution in second test series in block#7 and dimensions of balcony.....	100
Figure 43 - Averaged FRS of block#8-7 th floor-X-direction: a) Pseudo acceleration;.....	106
Figure 44 - Averaged FRS of block#8-3 rd floor-X-direction: a) Pseudo acceleration;.....	107
Figure 45 -Averaged FRS of block#8-7 th floor-Y-direction: a) Pseudo acceleration;.....	108
Figure 46 - Averaged FRS of block#8-3 rd floor-Y-direction: a) Pseudo acceleration;.....	109
Figure 47 - Inter-storey drift curve - Block#8 - 3 rd floor - X direction - E701001 record:	110

Figure 48 - Averaged FRS of block#7-7th floor-X-direction: a) Pseudo acceleration;.....114

Figure 49 - Averaged FRS of block#7-3rd floor-X-direction: a) Pseudo acceleration;.....115

Figure 50 - Averaged FRS of block#7-7th floor-Y-direction: a) Pseudo acceleration;.....116

Figure 51 - Averaged FRS of block#7-7th floor-Y-direction: a) Pseudo acceleration;.....117

Figure 52 - Inter-storey drift curve - Block#8 - 3rd floor - X direction - E701001 record:118

Figure 53 - Floor Response acceleration, Block#8, Continuum model, 7th floor, X-direction124

Figure 54 - Floor Response acceleration, Block#8, Continuum model, 7th floor, Y-direction125

Figure 55 - Floor Response acceleration, Block#7, Continuum model, 7th floor, X-direction126

Figure 56 - Floor Response acceleration, Block#7, Continuum model, 7th floor, Y-direction127

List of Tables

Table 1 - Seismic history of Quebec [6]	14
Table 2 - Block # 8	44
Table 3 - Block # 7	44
Table 4 – Fundamental period calculation based on NBCC-2010.....	45
Table 5 – Comparison between AVT result and NBCC-2010	45
Table 4 - Concrete properties	50
Table 5 - Concrete properties	50
Table 6 - Calculation of spring stiffness in X direction (Inter-storey drift method)	62
Table 7 - Calculation of spring stiffness in Y direction (Inter-storey drift method)	63
Table 8 - Clay masonry properties based on the masonry unit strength and the mortar type (Amrhein 1998; Committee 2005a; Committee 2005b)	71
Table 9 - Initial properties of terra cotta infill wall	71
Table 10 - Characteristics of M-R scenarios considered for Montreal	81

Table 11 – Scaling factor and PGA of scaled records	82
Table 12 - Scale factor calculation based on first three modes-E70701	84
Table 13 - Bare-frame model results - Block#8	87
Table 14 - Bare-frame model results - Block#7	87
Table 15 - Comparison between calculated natural frequencies of Block 8 and Block 7	88
Table 16 - Comparison between calculated natural frequencies of two models of block#7	89
Table 17 - Comparison of bare-frame model and AVT results- Block#8	92
Table 18 - Comparison of full-frame model (continuum model) and AVT results- Block#8	93
Table 19 - Comparison of full-frame model (Stafford Smith model for diagonal compression strut) and AVT results- Block#8.....	93
Table 20 - Comparison of full-frame model (Durrani & Luo model model for diagonal compression strut) and AVT results- Block#8.....	94
Table 21 - Comparison of full-frame model (FEMA-356 model for diagonal compression strut) and AVT results- Block#8.....	94
Table 22 - Comparison of the full-frame models with the bare-frame model	95

Table 23 - Comparison of bare-frame model and AVT results- Block#7	96
Table 24 - Comparison of full-frame model (continuum model) and AVT results- Block#7	97
Table 25 - Comparison of full-frame model (Stafford Smith model for diagonal compression strut) and AVT results- Block#7.....	97
Table 26 - Comparison of full-frame model (Durrani & Luo model model for diagonal compression strut) and AVT results- Block#7.....	98
Table 27 - Comparison of full-frame model (FEMA-356 model for diagonal compression strut) and AVT results- Block#7	98
Table 28 - Comparison of the full-frame models with the bare-frame model	99
Table 29 - Calibrated properties of terra cotta infill wall	101
Table 30 - Maximum Inter-storey drift - Block#8.....	111
Table 31 - Modal periods and frequencies of bare-frame and continuum....	112
Table 32 - Maximum Inter-storey drift - Block#7.....	119
Table 33 – Natural periods and frequencies of bare-frame and continuum models	120

List of symbols

X, Y, Z	Global coordinate axes
ω	Variable corresponding to frequency [in rad/s]
k	Stiffness of an SDOF oscillator
$[K]$	Stiffness matrix for a linear MDOF oscillator
$[F]$	Flexibility matrix for a linear MDOF oscillator
N	Number of DOF
$\{\varphi_r\}$	Mode shape r
$f(t)$	Applied force to an SDOF oscillator
$F(\omega)$	Fourier spectrum obtained from Fourier transform of applied force $f(t)$
$x(t)$	Arbitrary time history record (or signal)
$X(\omega)$	Fourier spectrum of signal $x(t)$
$G_{jk}(\omega)$	Spectral density between records and $x_j(t)$ and $x_k(t)$
$[G(\omega)]$	Output spectral density matrix (also denoted $[G_{xx}(\omega)]$ for emphasis)
$[U]$	Left-singular vector matrix
$\{u_i(\omega)\}$	i^{th} singular vector at frequency ω
$[V]$	Right-singular vector matrix
f_m^l	Specified compressive strength of clay masonry assemblages
E_m	Modulus of elasticity of masonry infill
E_v	Modulus of rigidity (Shear modulus) of masonry infill

W_{eff} Effective width of diagonal strut

Acronyms

AVT Ambient vibration test

CG Center of gravity

CR Center of rigidity

DOF Degree-of-freedom

EFDD Enhanced frequency domain decomposition

FDD Frequency domain decomposition

FE Finite element

FFT Fast Fourier transform

FRF Frequency response function

FRS Floor response spectra

FVT Forced Vibration test

GPS Global positioning system

IFFT Inverse fast Fourier transform

LLRS Lateral load resisting system

MAC Modal assurance criteria

MDOF Multi degree-of-freedom

NSCs Non-structural components

OFCS Operational and functional building components

<i>RC</i>	Reinforced concrete
<i>RDP</i>	Retrofitting and development plan
<i>SDF</i>	Spectral density function
<i>SISO</i>	Single-input-single-output
<i>SVD</i>	Singular value decomposition
<i>UHS</i>	Uniform hazard spectra
<i>URM</i>	Unreinforced masonry

1 Introduction

1.1 Research motivation

A building is composed of two types of components: structural components and non-structural components (NSCs) or operational and functional components (OFCs). NSCs can be categorized into three sub-components according to their functionality: Architectural (external or internal), Building services (mechanical, electrical, and telecommunication), and Building contents (common and specialized)[1]. Unreinforced masonry (URM) infill walls are an example of architectural component which is frequently used as interior and exterior walls in both reinforced concrete and steel structures. In several pre-code hospital buildings constructed before the 1970s, *terra cotta* masonry blocks have been used extensively both as infill walls and partitions (Figure 1). As *terra cotta* infill walls are normally considered non-structural, their effect in stiffening and strengthening the structure is simply neglected by engineers in seismic analysis and design, while their weight is taken into the account as a uniformly distributed dead load. However, infill walls tend to interact with their surrounding frame under seismic actions which leads to an increase in lateral stiffness and strength, resulting in a significant change in the dynamic characteristics of buildings. On the one hand, such interaction may be beneficial to the performance of the structure as the infill walls effectively strengthen the moment-resisting frame of the building until they reach their collapse state.

On the other hand, this increase in strength which accompanies an increase in the initial stiffness of the structure may consequently attract additional seismically induced lateral inertia forces for which the structure is not designed. The presence of URM infill walls can also cause some undesired behaviour such as brittle shear failure of reinforced concrete columns and

short column phenomena, over-strengthening of the upper stories of the structure, induce a soft first storey and torsional effects due to in-plane irregularity (Figures 2 and 3).

These issues, observed in several post-earthquake damage surveys, clearly demonstrate the importance and necessity of considering the effect of URM infill walls on the dynamic properties of structures, particularly for post-critical buildings such as hospitals which have to remain functional after severe design-level seismic motions. This fact was the main motivation behind this research.

The performance of NSCs themselves and their functionality during and after an earthquake is of great importance especially in post-disaster structures as “Risk to safety, damage to property, and loss of function and operation in a building can be significantly affected by the failure or malfunction of operational functional components even if the building structural system has performed well during an earthquake” [1]. Hence, the other motivating factor for this research was to focus on the NSCs behaviour when the structure is subjected to design seismic ground motions. In this regard, the influence of seismic retrofitting of the selected hospital case study and the influence of *terra cotta* infill walls on the performance of NSCs have both been selected as the main targets of the research.



Figure 1 - Terra Cotta infill masonry wall in CHU Sainte-Justine in Montréal (Asgarian, 2010)



J84. Two-story reinforced concrete building, Managua, Nicaragua, damaged in the 1972 Managua Earthquake. The slide shows a reinforced concrete column which was part of the structural system and which failed due to its shortening because of the effect of the masonry wall. The masonry walls were considered as non-structural elements.

Figure 2 - Brittle shear failure of reinforced concrete column, 1972, Managua earthquake. [41]



Figure 3 - Failure due to creating the soft first storey, Beichuan, China, 12 May 2008 earthquake [42]

1.2 Research objectives

The scope of this study is to achieve better understanding of the effect of the non structural components, in this case unreinforced *terra cotta* infill walls, on the structural response of buildings during earthquakes and to find a reliable way to account for their effect in numerical modeling and design. The other goal of the project was to assess the influence of seismic retrofitting and the presence of infill walls on NSCs performance. These objectives will be achieved through a detailed case study analysis of two eleven-storey wings (Blocks #7 and #8) of CHU Sainte-Justine, a paediatric research hospital located in Montréal, Canada. The two buildings are almost identical in terms of floor plans, elevations and dimensions. This hospital campus was initially built in the late 1950s and Block #7 was seismically retrofitted in 2008 by adding a full-height reinforced concrete shear wall at its free end and connecting the other end of the building to the adjacent Block #9, using structural anchor bars at each floor slab and along the height of interfacing columns. Block #8 was not retrofitted and has remained unattached to adjacent Block 9. More details will be presented in Chapter 2. The specific research objectives are:

Study the effects of unreinforced *terra cotta* infill walls on the dynamic characteristics of the structures - namely, their natural frequencies, mode shapes, and modal damping ratios.

Simulate and evaluate the effects of seismic rehabilitation on the dynamic behaviour of the hospital structure.

Find the best available technique for modeling masonry infill walls (i.e. the technique which leads to the closest results to the experimental ones).

Assess the impact of the seismic rehabilitation of Block #7 and the presence of masonry infill walls on the performance of their NSCs.

1.3 Research Methodology

The methodology adopted for this study is to develop a detailed numerical model for Blocks #7 and #8 and then conduct the Ambient Vibration Tests (AVT) in both blocks of the hospital to be able to calibrate and verify the numerical models using experimental results. Having the calibrated models, the study can be further advanced towards the other objectives. Therefore, this research project can be divided into two main phases:

1) - Numerical Study: in which the detailed linear elastic finite element analysis models of each building have been generated where the infill unreinforced *terra cotta* walls are explicitly modeled using two different techniques, namely panel elements and simplified compression strut models.

2) - Experimental Study: in which Ambient Vibration Measurements (AVM) have been conducted on Blocks #7 and #8 separately. Then, the dominant dynamic properties of both buildings including the lowest natural frequencies, corresponding mode shapes, and effective modal damping ratios were extracted using operational modal analysis techniques.

The generated finite element models have been then calibrated and verified taking advantage of AVM results. Finally, the effect of seismic rehabilitation and infill walls on the dynamic properties of the building and also on the performance of their NSCs is evaluated by comparing the different models and by developing Floor Response Spectra (FRS) and Inter-storey Drift curves after subjecting the calibrated models to different generated ground accelerograms.

1.4 Organization of thesis

Chapter 2 begins with the general information about the case study - CHU Sainte – Justine Hospital. This is followed by the description of different experimental modal analysis testing techniques- namely, Forced Vibration Testing (FVT), free response testing, Earthquake response testing, and Ambient Vibration Testing (AVT). Then the behaviour of unreinforced masonry infill walls under cycling loading is explained. The previous research studies on numerical modeling of masonry infill walls are described. Afterwards, two different methods for modeling the infill walls proposed in literatures are introduced as the last part of this chapter.

Chapter 3 discusses in detail the methods used in this study to collect and analyze ambient vibration data to identify the dynamic properties of the buildings. First, the relevant technical specifications of the testing equipment are discussed and the testing procedure is described. The theory behind the enhanced frequency domain decomposition (EFDD) method, which was used in this study to extract the dynamic properties from the recorded ambient motions, is then summarized. Lastly, the AVT results are presented for both blocks separately.

Chapter 4 describes the finite element models generated for both blocks. Two series of models are introduced: Bare-frame models and Full-frame models. The particular attention is given to details of the modeling of infill walls. This is followed by the description of calibration and verification of numerical finite element models using experimental results. Then the procedure of subjecting the calibrated models to the series of generated ground accelerograms and developing the Floor Response Spectra (FRS) and Inter-storey drift curves are discussed.

Chapter 5 presents the dynamic properties of both Block #7 and #8 extracted from different finite element models. The results are compared to each other and discussed in details. The effect of infill walls and seismic retrofitting of Block#7 on dynamic response of the buildings and also on dynamic behaviour of their NSCs during earthquake are explained by presenting the FRS and Interstorey-drift curves developed for each building.

Finally, Chapter 6 summarizes the main conclusions of this research. These are followed by a reiteration of the limitations of this study and recommendations on future work.

2 Background and literature review

2.1 CHU Sainte-Justine Hospital [2]

2.1.1 General information about the Hospital

The CHU Sainte-Justine is a paediatric research hospital affiliated to the *Université de Montréal*. It is the largest mother-child centre in Canada and one of the four most important paediatric centres in North America [3]. The hospital inauguration dates back to 1907. For supplying the high health service demand of the last century, a new complex of 64,739 m² was added to the main part of hospital between 1950 and 1957. All the blocks being considered in this project (i.e. blocks# 7, 8, and 9) have been constructed in the 1950s.

Due to the accelerated increase in health needs during the last decades and in order to move at the same pace and respond to the people health needs appropriately, the hospital management has developed a document on Retrofitting and Development Planning (RDP). The RDP is composed of three parts: 1) need for a modern hospital, 2) upgrading requirements of the existing building for an area of 15,000 m² represented in white color in Figure 4, and 3) new construction of about 30,000 m² expected by the end of 2011 represented in blue in Figure 4.

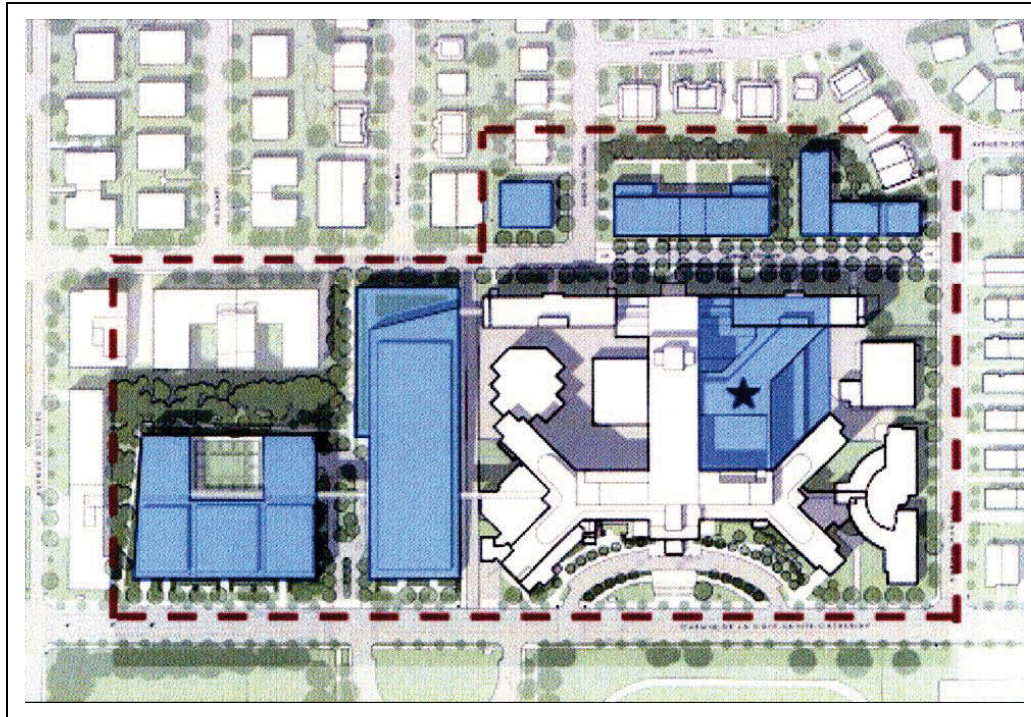


Figure 4 - RDP plan[2]

The hospital is composed of 12 blocks that are individual buildings (Figure 5). Most of the buildings have four basements and up to 9 floors above ground level. The structural system is reinforced concrete frames with URM infill walls. It is comprised of closely-spaced square and rectangular beams of relatively small dimensions (sectional dimensions of 28cm×50cm on average), a 130-mm concrete slab, and exterior walls composed of a 100-mm brick layer, a 200-mm *terra cotta* infill, a 25-mm air gap, another 100mm *terra cotta* infill, and 25-mm of plaster panel. The interior walls are made of 200-mm *terra cotta* masonry (Figure 6).

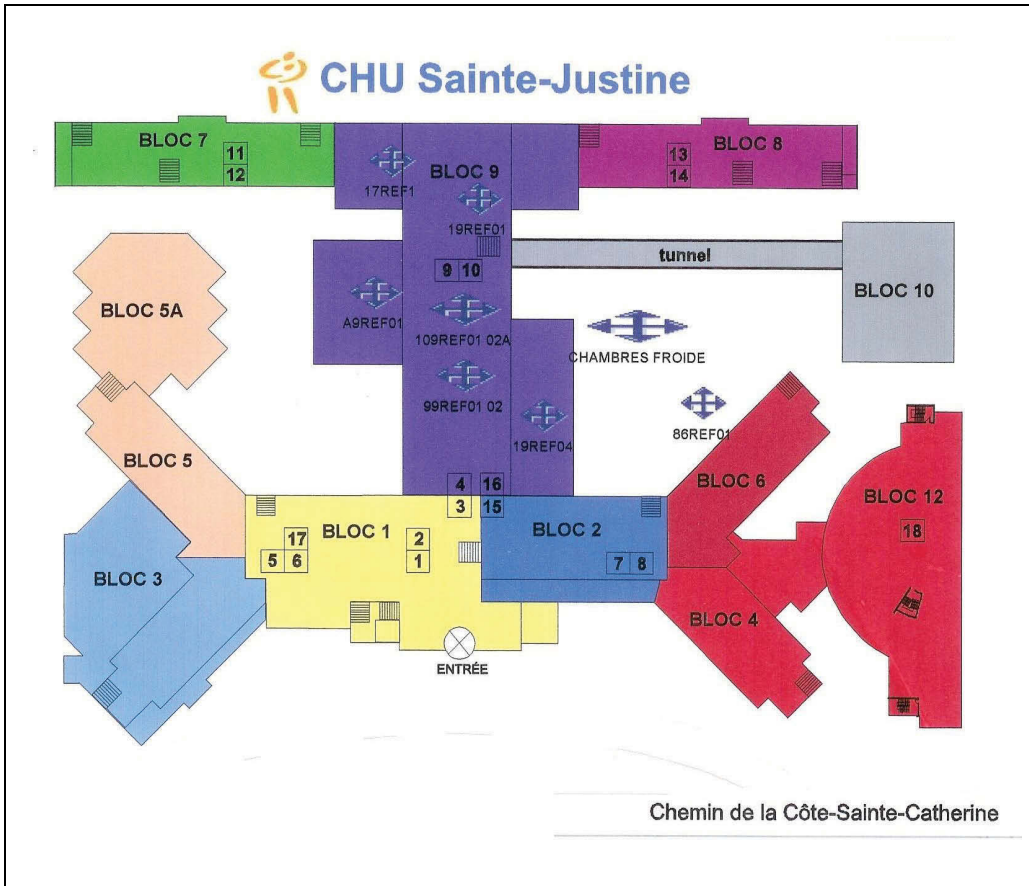


Figure 5 - General layout of the hospital

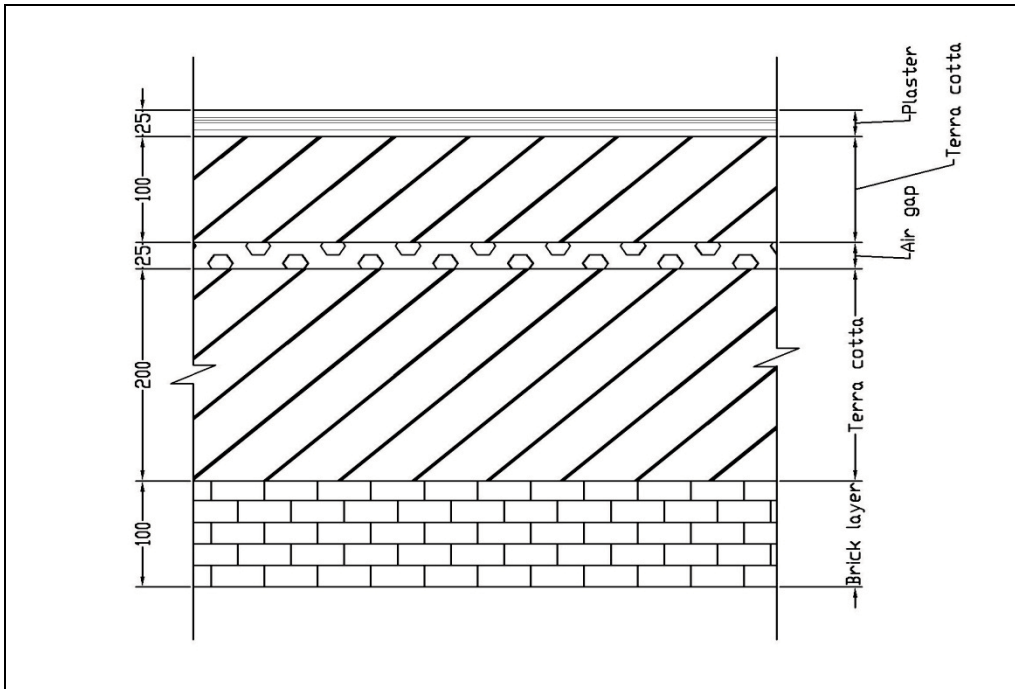


Figure 6 - Exterior wall cross-section

Since all the design was based on the building code of the 1950s, the engineers apparently have been counting on the bare frame behaviour (i.e. beams and columns resistance) and the additional stiffness coming from the exterior and interior infill walls to resist the lateral wind forces. Besides, there is no indication that the lateral inertia forces induced by an earthquake have been taken into account. Hence, none of the blocks had any specific seismic force resisting system (neither shear wall nor bracing system) before the recent implementation of the RDP.

In the 1950s, it was also a common practice for design engineers to separate the buildings using narrow construction joints to avoid cracking problems arising from concrete shrinkage. Therefore, every building was separated from each other using xx-mm joints. It is worthy of mention that the hospital is founded on good quality rock, soil site class C-Very dense soil and soft rock[4]. Thus, there is no concern regarding the amplification of ground motion due to poor soil condition.

2.1.2 Seismic retrofitting plan of Hospital

The objective of the retrofitting plan was to provide sufficient lateral stiffness for the hospital to preserve its integrity and stability during the maximum design earthquake and to ensure its continuous functionality even after strong ground motions. The latter, in its turn, requires functionality of NSCs as well.

Since the hospital had to remain operational during construction and major disturbance was intolerable, all construction activities had to be done from outside, and it was decided to build reinforced concrete shear walls outside the existing buildings. The construction started in summer 2008. There were a total of twelve walls to build directly on the exterior existing brick walls

(i.e. the exterior masonry wall is conserved). Every meter, steel reinforcing bars of 55mm diameter have linked the existing structure (edge beams or columns) with the new wall sections. Additionally, the construction joints separating existing buildings were blocked using structural anchor bars. Figure 7 shows Block#4 before and after adding the concrete shear wall to its free end. A similar process was undertaken for Block #7.

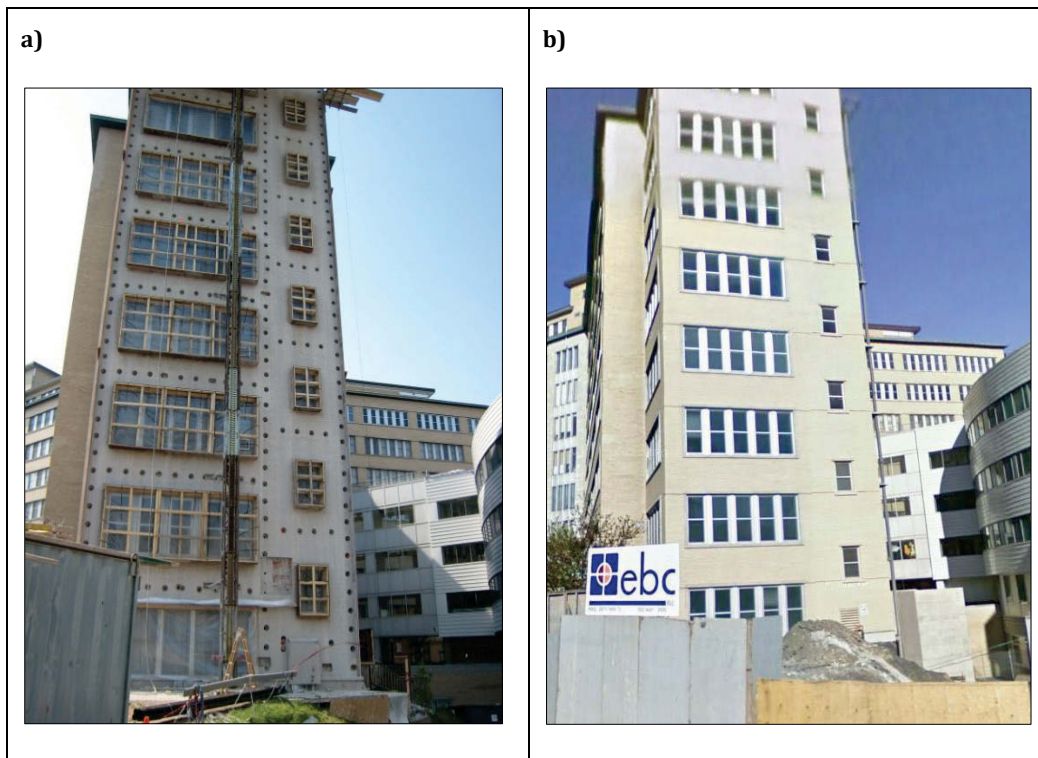


Figure 7 - Side elevation of block#4: a) during construction; b) after adding concrete shear wall and new masonry wall

2.2 Risk of a strong earthquake in Montreal

According to the Tectonic Plate Theory, the earth's crust is divided into a small number of large and rigid pieces known as tectonic plates. These plates are continuously moving apart (diverge) in some areas and moving toward each other (converge) at other locations, or sliding past each other. More than 97% of the world's earthquakes are caused near these plates

boundaries as a result of the stresses that build up as the plates tend to move and interact with another [5].

Eastern Canada is located in a stable continental region within the North American Plate and, as a consequence, has a relatively low rate of earthquake activity. However, there is a possibility of having large and damaging earthquakes in this area as they have occurred here in the past. Annually, about 450 earthquakes take place in eastern Canada. Of this number, approximately four exceed magnitude 4, thirty surpass magnitude 3, and about twenty-five events are reported felt. A decade, on average, comprises three events greater than magnitude 5 which is generally the threshold of observed damage to buildings [6]. As eastern Canada is part of the stable interior of the North American plate, the rate and size of seismic activity cannot be directly related to the plate interaction. Consequently, the causes of earthquakes in eastern Canada are not well understood.

The Island of Montreal is located in the Western Quebec seismic zone. Historical the seismic activity record of this region shows that the province of Quebec has been shaken by several significant earthquakes since the beginning of last century, as listed in Table 1.

Table 1 - Seismic history of Quebec [6]

Year	Province of Quebec region	Richter Magnitude
1732	Montreal	5.8
1925	Charlevoix-Kamouraska	6.2
1935	Temiscamingue	6.2
1988	Saguenay	5.9
1989	Ungava	6.3

These earthquakes above magnitude 6 likely exceed the limit that the existing structures in Montreal are able to resist without significant damage. They would also damage the NSCs and cause their failure or malfunction. These issues become increasingly important when considering post-critical buildings such as hospitals. As a result, although Montreal is considered as a moderate seismic region, seismic evaluation and eventual rehabilitation of existing buildings is important.

2.3 Experimental modal analysis and ambient vibration testing

As mathematical models cannot capture all the details of three-dimensional interactions of structural and NSCs and the quality of construction, full-scale dynamic testing of existing buildings is an appropriate method commonly used by researchers to validate and refine the computational models of buildings. The main purpose of these tests is to identify the dominant dynamic properties of real structures from vibration measurements, which is referred to as experimental modal analysis (EMA). There are different approaches for dynamic testing which are as follows [7]:

2.3.1 Forced Vibration Testing (FVT)

Forced vibration testing is the traditional technique for EMA. Briefly explaining, FVT is subjecting a structure to a known input (i.e. known load function) at a particular degree-of-freedom (DOF) and measuring the response of structure at a specific DOF. This is referred as single-input-single-output (SISO) modal testing. Knowing both input and output, the frequency response function (FRF) which relates these two functions can be estimated. The FRF itself depends on natural frequencies, mode shapes, and damping ratios of the structure. Therefore by knowing FRF, the dynamic properties can be extracted. This type of analysis is also called input-output

modal identification. A few shortcomings for this method are that it involves relatively expensive equipment and it is labour intensive. Moreover, in some cases it might require to shut down the daily operation of a building for doing the test. However, because of the larger amplitude of vibration and knowing both the input and output, the results are believed to be very reliable.

2.3.2 Free response testing

Free response testing consists of imposing a set of initial conditions on a structure such as initial displacement or initial velocity and then releasing it to oscillate freely and measuring the free vibration response over time. If the initial conditions are selected carefully, the response which would be an exponentially decaying oscillatory function will be dominated by a single mode of vibration. The corresponding natural frequency can be calculated using the number of zero crossings and the viscous damping ratio can also be extracted using the logarithmic decrement technique.

2.3.3 Earthquake response testing

In this category of tests, the sensors are permanently installed in the building under consideration, waiting for a relatively strong ground motion to happen and then measure the ground motion and corresponding building response during the time of occurrence. Dynamic properties are determined using transfer functions between the acceleration responses of upper floors and the measured ground acceleration. Some drawbacks of this method are considerable amount of time needed for accomplishing the test and also permanent use of instruments. However, when the test is successful, the results are invaluable.

2.3.4 Ambient Vibration Testing (AVT)

For testing the large civil structures which are difficult to excite artificially (i.e. using FVT) or in special cases (like hospitals) in which exciting the structure is not permitted, ambient vibration testing is the preferred method. In AVT instead of artificially exciting the structure, the ambient vibrations in the building are monitored. These low-amplitude vibrations are generated by ambient sources such as wind load, mechanical equipment in operation, micro-tremors, traffic, loads due to use and occupancy, and other environmental loads. It means that in AVT the signature of the input forces driving the building motion is not exactly known. Therefore, for the dynamic properties extraction the excitation is assumed to be a broadband white noise (i.e. the excitation having approximately equal energy content throughout the frequency range of interest [8]). AVT is also called Operational Modal Analysis or Output-only Modal Identification since dominant modal properties are identified from measured response only.

Assuming a constant input spectrum at each input DOF (white noise), the FRF is directly related to the output spectra. Since the FRF between any two DOF shows peaks at the natural frequencies of the building, these frequencies can be detected directly from output spectra. This is the basic concept behind all the frequency domain modal identification techniques using ambient vibration data [7].

Since the ambient response of the structure is small and often contaminated with noises, and also the input is unknown, the modal identification process becomes more difficult than for the other methods described above. The main difficulties are the need for sensitive equipment\sensors and careful data analysis. But AVT has several advantages in comparison with the other techniques, namely: 1- Testing is relatively cheap and fast, 2- There is no

interference with the normal everyday operation of the structure. It should be noted that the measured response is representative for the real operating conditions of the structure [9]. Due to the advantages and simplicity of the method, AVT has been used for a wide variety of structures including buildings [7, 10, 11], and bridges [12, 13]. Moreover, many studies done in this field have shown that the dynamic properties obtained from AVT are in good agreement with those ones extracted from FVT [10]. Besides, in some cases like Ste-Justine Hospital, the case study for this project, any kind of interference in the normal operation of the building is strictly prohibited. As a result, AVT is adopted to evaluate the dynamic properties of the structure in this research.

2.4 Behaviour and analysis of unreinforced masonry infill walls

Unreinforced Masonry (URM) infill walls are commonly used for low- and medium-rise buildings all over the world in regions of low to high seismicity, especially in developing countries where the labour costs are not very high. The walls are added to the structural frame as exterior (cladding) and interior walls (partition). Although they are considered as NSCs, yet during the earthquake, they tend to interact with the surrounding frame and may result in different undesirable failure modes both to the frame and to the infill wall. The brittle behaviour of infill walls, with little or no ductility, causes the structural and non-structural parts to suffer from various types of damages ranging from invisible microcracking to crushing and eventually disintegration. Thus, ignoring the frame-wall interaction is not always on the conservative side and it may lead to erroneous estimation of the lateral stiffness, strength, and ductility of the structure as well as the interaction between seismic demand and supply.

The URM infill walls have long been known to affect the dynamic characteristics of structures and numerous studies have been done on this topic during last five decades. However, the professionals still have not reached a consensus on the way for modelling the infill walls in seismic analysis. This problem is partly attributed to incomplete knowledge of the behaviour of URM infill walls. Furthermore, the presence of a large number of interacting parameters and many possible failure modes for infill walls - described later in this section- makes it difficult for one model to account for the parameters precisely.

In general, available techniques for modelling masonry walls can be divided into two groups including: 1- Equivalent diagonal compression struts and 2- Finite element models.

2.4.1 Equivalent diagonal compression struts

The first published research on infilled RC frames subjected to racking load is by Polyakov (1956) [14]. In this study a number of large-scale tests including square and rectangular frames were performed. The masonry infill and frame elements were observed to behave monolithically until separation cracks between the infill and the frame develop around the perimeter of the infill except for small regions at the two diagonally opposite corners. As the load is increased, the compression diagonal starts to shorten and the tension diagonal to lengthen until the masonry infill cracks along the compression diagonal. The structural assemblage continues to resist an increasing load in spite of the diagonal cracks that continue to propagate and new cracks appear. The system failure is defined at the time of the appearance of large cracks. Observing this type of behaviour, he suggested that the infilled frame system is equivalent to a braced frame with a compression diagonal strut replacing the infill wall (Figure 8). Holmes [15] proposed a method for

predicting the deformations and strength of infilled frames based on the equivalent diagonal strut concept. His assumption was that the infill wall acts as a diagonal compression strut of the same thickness and elastic modulus as the infill with a width equal to one-third the diagonal length (Figure 8).

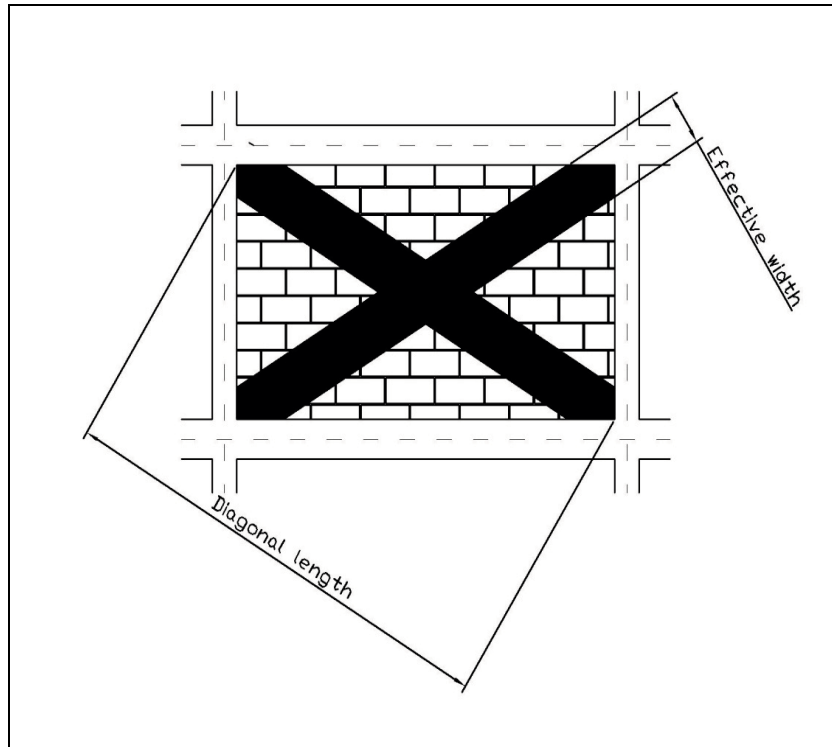


Figure 8 - Diagonal compression strut

Stafford Smith [16] conducted a series of tests in which double-storey model infilled frames were laterally loaded to failure. He investigated the influence on lateral stiffness and strength of varying beam section, column section, and the length/height proportions of the infill. Monitoring the model deformations during the tests showed that the frame separated from the infill over a large part of the length of each side after subjecting to racking load, and region of contacts remain only adjacent to the corners at the end of the compression diagonal (Figure 9). These observations led to the conclusion that the wall could be replaced by an equivalent diagonal strut connecting the loaded corners. The term of “effective width” of the wall was introduced

which is the width of an equally stiff uniform strut whose length is equal to the diagonal of the wall, whose thickness and modulus of elasticity is the same as the wall. It was determined that the effective width is dependent on the wall's aspect ratio, relative stiffness of the column and infill but not on the stiffness of the beams. Two modes of infill failure were observed: 1- Tensile cracking failure along the loaded diagonal and 2- Compressive failure in one of the loaded corners.

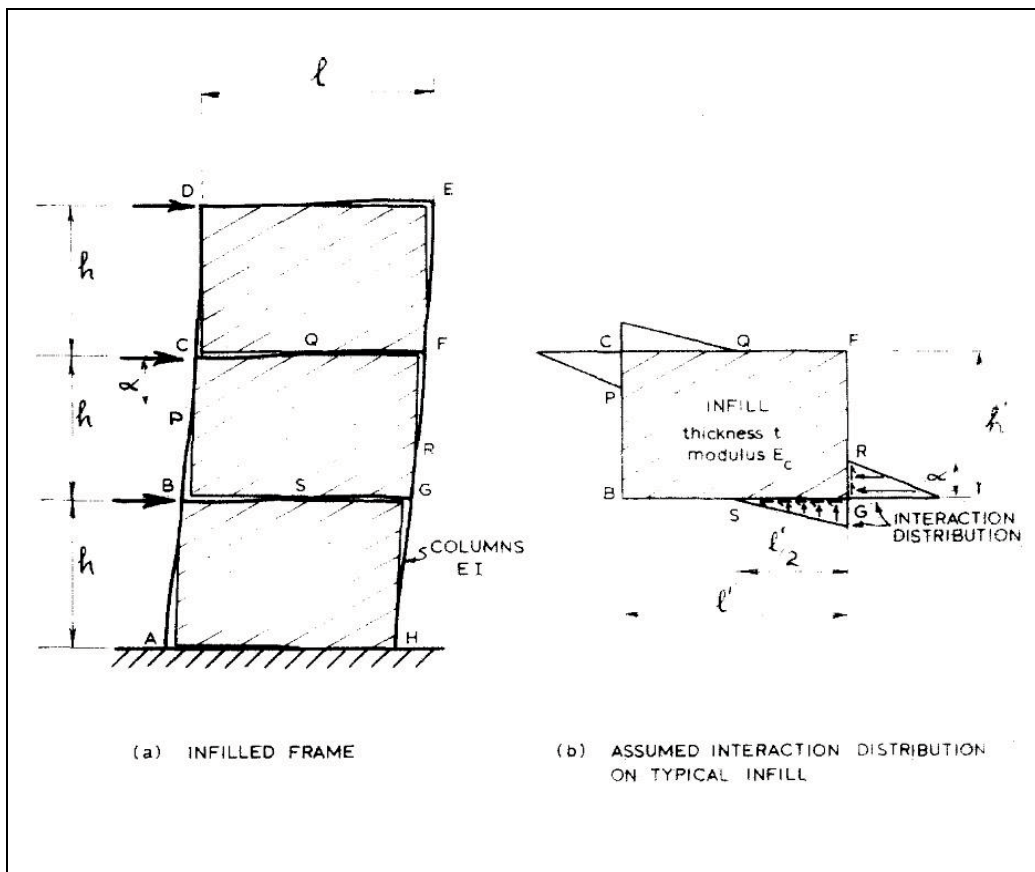


Figure 9 - Infilled frame [16]

Further studies have shown that infilled frames can develop other failure mechanisms in addition to the ones mentioned by Stafford Smith. Shing and Mehrabi [17] characterized five main failure mechanisms for infilled frames (Figure 10). They are as follows:

- A. Purely flexural mode in which the frame and the infill act as an integral flexural element.
- B. Horizontal sliding crack at the mid-height of an infill which introduces short-column behaviour.
- C. Diagonal cracks which propagate from one loaded corner to the other; and these can sometimes be joined by a horizontal crack at mid-height.
- D. Sliding of multiple bed-joints in the masonry infill that occurs often in infills with weak mortar joints.
- E. Distinct diagonal strut mechanism with two distinct parallel cracks that are often accompanied by corner crushing or sometimes by crushing at the centre of the infill.

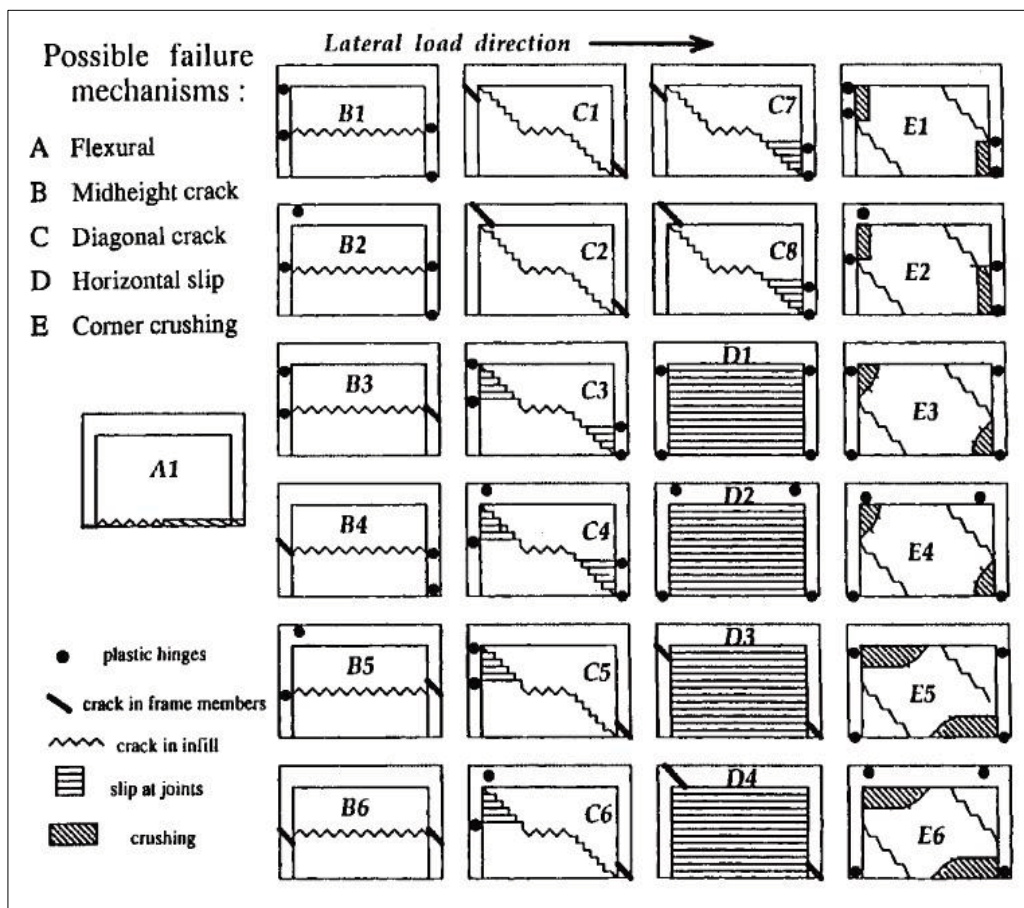


Figure 10-Failure mechanisms of infilled frames [17]

Durrani and Luo [18, 19] have analysed a series of Finite Element (FE) models of masonry infills. Based on empirical fitting to the FE results, they proposed an approach for calculating the effective width of an equivalent compression strut. Unlike the other suggested formulations which neglected the stiffness of beams in determining the effective width factors, their approach takes this parameter into account as well. However, they indicated that the beam section has only a slight effect on effective width.

In the FEMA-356 document[20], published by the Federal Emergency Management Agency (FEMA) in 2000 to provide a set of nationally applicable guidelines for the seismic rehabilitation of existing buildings, the equivalent strut model is suggested in order to include the beneficial effect of the infill walls in the analysis of retrofitted buildings. Accordingly, the elastic in-plane stiffness of a solid URM infill wall prior to cracking shall be represented with an equivalent diagonal compression strut with the same thickness and modulus of elasticity as the infill wall and effective width calculated from the formulation suggested. Further investigation on the concept of diagonal strut has been done by Mainstone [21] , Hendry [22] , and El-Dakhkhni [23-25]. Among all the approaches, Stafford Smith[16], Durrani and Luo[18, 19], and FEMA-356[20] have been adopted in the calculation performed in this work.

2.4.2 Finite element models

Considerable advances in computer technology and availability of increased computational resources brought another more detailed approach for modeling masonry infill walls using finite elements. The biggest complexity in this type of modeling is resulting from the characteristics of the interface between the masonry and the mortar, and that between the infill panel and frame [26]. One of the developed FE techniques for modeling infill walls is to consider the masonry as a homogeneous material including the masonry

units and the mortar together as a continuum. This is what is called as “a homogeneous isotropic continuum” in the literature (Figure 11). The other difficulty in this method is to define the material properties to properly represent the composite behaviour of the wall (i.e. masonry block units and mortar). This is the other method used in this study for modeling the masonry infill walls. The walls are modeled using the panel element with equivalent properties.

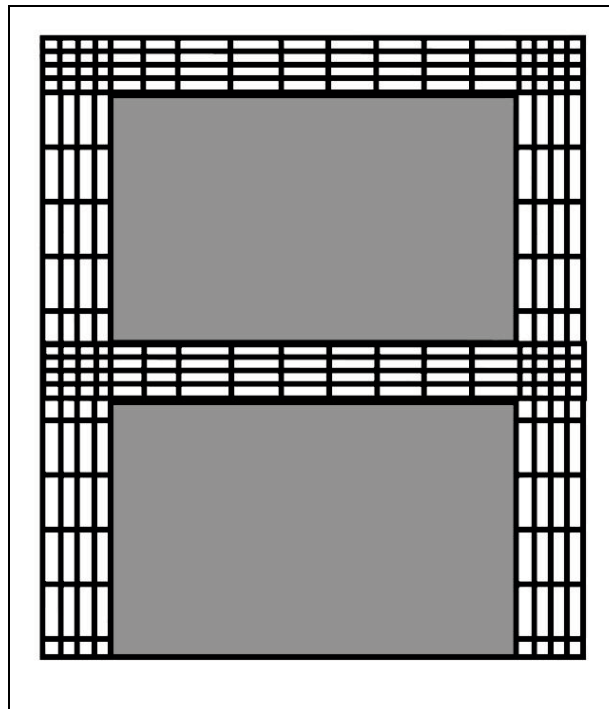


Figure 11 - Continuum model [27]

3 Experimental Study: In situ Ambient Vibration Test (AVT)

As previously explained, for the purpose of verifying and calibrating the numerical models, ambient vibration tests (AVT) were performed in both selected buildings (Blocks #7 and #8) of CHU Sainte-Justine. Using TROMINO sensors, velocities induced by ambient excitations in both horizontal directions and along the vertical were recorded at several locations in each building. Analysis of recorded data has been done using two different operational modal analysis techniques- namely, Frequency Domain Decomposition-Peak Picking (FDD) and Enhanced Frequency Domain Decomposition-Peak Picking (EFDD) and the dominant dynamic properties of both buildings including the lowest natural frequencies, corresponding mode shapes, and effective modal damping ratios have been extracted. The AVT results have been used for calibrating the numerical models. The first series of AVT tests was done in August and September 2010 in both blocks. Due to some discrepancies between AVT results and numerical models of block#7, another test series was conducted only in this block in July 2011 to clarify the source of inconsistency. The comprehensive discussion of the experimental methods used to collect and analyze the data will follow.

3.1 Data collection

3.1.1 Instrument

The instrument used to measure ambient vibrations of the buildings was TROMINO® sensor (portable ultra-light seismic noise acquisition system); classification of CISPR 11 - EN 55011(Figure 12). Each instrument is equipped with three orthogonal high resolution electrodynamic velocimeters and three orthogonal digital accelerometers. This makes the sensor capable of measuring minute velocities and accelerations induced by ambient

excitations in three orthogonal directions: two in the horizontal plane and one along the vertical. The sensors are also equipped with internal/external GPS antennas to allow synchronization among different units outdoor and with a radio transmitter for indoor synchronization as well. The sensors are wireless, and their acquisition frequency range is 0.1 - 256 Hz which suffices to include all natural frequencies of buildings [28]. Setting TROMINO® into operation is very easy thanks to its LCD and set of 4 soft-touch keys which let the user to communicate with the system and set all the measurement parameters such as the acquisition mode, record length, sampling rate and etc [28]. The other instrument utilized in AVT was Radio Antenna (Figure 12) which helps sensors to communicate with each other at longer distances. TROMINO stores data on compact flash memory supports (i.e. internal memory card provided in sensors). The sensors can be connected to a personal computer using a USB cable and the recorded data can be downloaded with the proprietary Grilla software.



Figure 12 - TROMINO sensor connected to the radio antenna

3.1.2 Distribution of measurement points

The first step before doing the actual AVT is determining the test setup configuration. It means deciding how to distribute the measurement points spatially (i.e. both horizontally and vertically), how many floors to monitor, and how many points on each floor are needed to be measured. In order to do this, the architectural drawings (Figure 13) of the building have to be consulted to figure out which floor areas are easily accessible. The main criterion in selecting the measurement points, is distributing them such that they can capture the possible dominant mode shapes to be identified. Accordingly, measurements were taken at three locations on each floor of both blocks (except roof and basement in which no measurements were done). These three points were located along a principal axis of rigidity, to permit the identification of both translational and torsional modes. For practical considerations, the principal axis of rigidity was approximated by the building axis of symmetry.

Having a long continuous corridor at all floors (which is the axis of symmetry as well), the measurement points were located at the two ends and middle point of the corridor. Point distribution both in horizontal plane and vertical direction is illustrated in Figures 14 and 15.

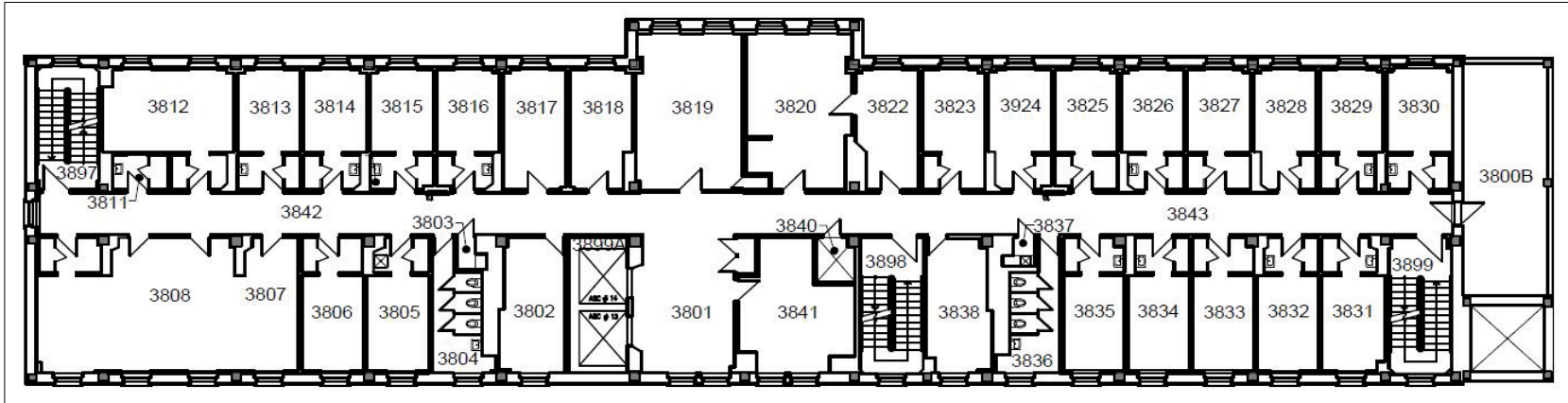


Figure 13- Architectural Drawing, Block#8, Floor#1

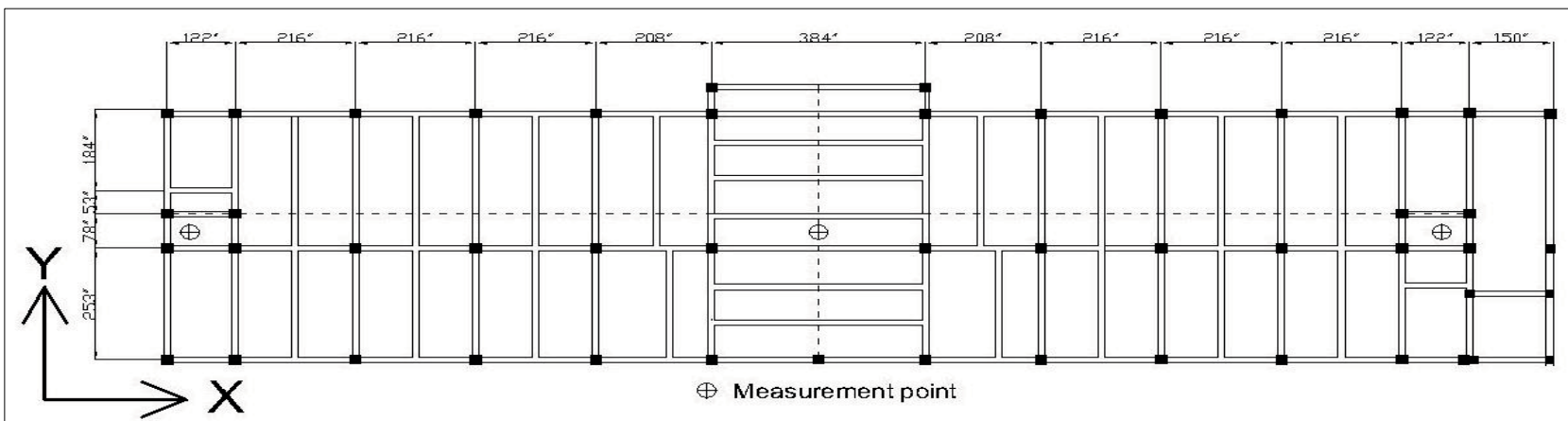
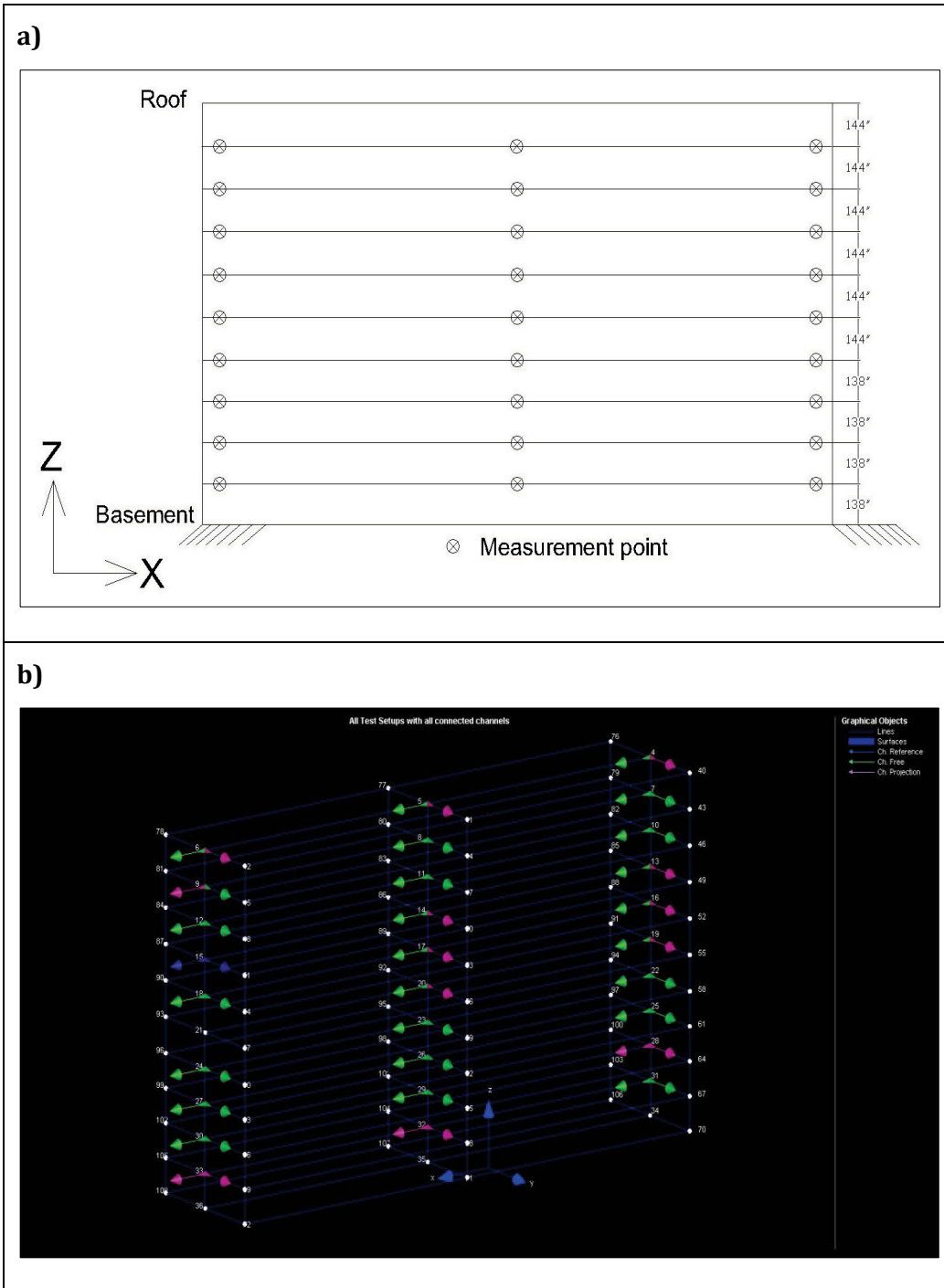


Figure 14- Distribution of measurement points in horizontal plane



3.1.3 Test procedure

The total number of six and seven TROMINO sensors has been used for the AVT done in 2010 and 2011, respectively. Due to the number of sensors available, it was decided to measure three points on every floor except at the roof and basement. Since the number of measurement points is usually more than that of the transducers, selected points are divided into different groups- so-called test setups. The sensor(s) which is common in all test setups and remains at the same location is called the reference sensor. The other sensors that move around until measuring all the points is completed are called roving sensors. The main rule in positioning the reference sensor is to place it in a point where all the modes to be identified have a significant contribution to the response (i.e. far away from any modal node). In the AVT done in both blocks of Ste-Justine hospital, two reference sensors were always used, one located at 2nd floor and the other at the 4th floor. Having more than one reference sensor has several advantages including:

- 1- It is a more conservative approach since if anything happens to one of the reference sensors and makes its data inappropriate to use in analysis, there is another reference sensor as backup and there is no need to repeat all the measurements.
- 2- As the reference sensors are typically located at different points in the building, it is less likely that all of them are on modal nodes in one setup (if their location were selected carefully). In other words, in every setup at least one reference sensor is excited by all the modes of vibration of interest.

In general, 8 minute long data records were taken at sampling frequency of 128 Hz for each measurement setup. The sampling frequency was selected based on the Nyquist sampling theorem[29], which stipulates

that aliasing (error) caused by discretization of a continuous signal can be avoided if the sampling frequency is greater than twice the maximum component frequency. Hence, in this case the sampling frequency should be at least twice the highest fundamental frequency of interest. For buildings we are typically interested in frequencies below 25 Hz, hence the selected sampling frequency of 128 Hz is satisfactory [29].

3.2 Data analysis and modal identification

Modal identification means to determine the modal parameters from experimental data. The modal parameters of both B#7 and #8, including the lowest natural frequencies, corresponding mode shapes, and effective modal damping ratios have been extracted using two different operational modal analysis techniques - namely, Frequency Domain Decomposition-Peak Picking(FDD) and Enhanced Frequency Domain Decomposition-Peak Picking (EFDD), as implemented in the commercial software ARTeMIS Extractor TM. Different steps of operational modal analysis are briefly explained below [9].

3.2.1 Synchronization

The first step before doing any kind of analysis on raw AVT data is to synchronize the measured records. Generally speaking, the synchronization is the process of making the starting time of all records the same so as to be able to analyze them together and extract the mode shapes precisely. This pre-processing step is essential whenever AVT is started manually using GPS (Global Positioning System) which lead to having non-synchronous data. The quickest way to synchronize recordings among several TROMINO[®] units is radio communication. It means that the sensors can form a wireless chain and communicate with each other using radio antennas.

Among all devices on the chain, one sensor plays the role of the master sensor and the others are slave ones. The master can send commands to other slave sensors. Hence, starting measurement on the master sensor will automatically start the recording on the other slave units simultaneously. This method results in having synchronous data from the beginning and eliminates the need for further synchronization. In AVT performed in Sainte-Justine hospital, careful arrangement of test setups made it possible to use radio communication for all measurements. Consequently, all the recorded data were synchronous and ready to analyze.

3.2.2 Theoretical concepts of modal analysis

Prior to describing the different operational modal analysis techniques used in this study, it is necessary to explain the principal concepts behind modal analysis [30].

3.2.2.1 Spectral density function

The spectral density of a time signal describes how the energy (or variance) of that time series is distributed with frequency. Hence, it is a useful mean to identify modal parameters since after determining the spectral density function, the frequencies which carry the most energy content of the signal can be recognized easily as peaks. The spectral density function (SDF), $G_{xy}(\omega)$, between two time history records $x(t)$ and $y(t)$, having corresponding Fourier transforms $X(\omega)$ and $Y(\omega)$, is defined as[30]:

$$G_{xy}(\omega) = E[X(\omega)Y(\omega)^*] \quad (3.1)$$

where * denotes the complex conjugate. An initial estimate can be obtained by performing a Fast Fourier Transform (FFT) for each raw time signal to

obtain $X(\omega)$ and $Y(\omega)$ and simply omitting the expected value operation. According to equation 3.1, the spectral density, $G_{xx}(\omega)$, of the signal, $x(t)$, is the square of the magnitude of the Fourier transform of the signal. Therefore, the unit of SDF is the square of the unit of the original signal, $x(t)$, per unit frequency. For instance, in our case that the signals are velocity time histories, the SDFs have unit of $[(m/s)^2/Hz]$. However, SDF is typically presented in decibel (db). The decibel is a logarithmic unit that indicates the ratio of a physical quantity (usually power or intensity) relative to a specified or implied reference level. As an example, taking the reference quantity equal to $1(m/s)^2/Hz$, the SDF is calculated in db unit as:

$$SDF[db] = 10 \log_{10} \left(\frac{SDF[(m/s)^2/Hz]}{1[(m/s)^2/Hz]} \right) \quad (3.2)$$

Now assuming a multiple-degree-of-freedom system (MDOF) composed of N degrees-of-freedom (DOF) in which ambient vibrations were measured at all nodes simultaneously, the SDF between all the different measured signals can be estimated. To produce the Power Spectral Density (PSD) matrix, $[G]$, all the estimated SDFs must be arranged in a matrix in such order that the entry in row i and column j represents the SDF between DOFs i and j .

So far, the SDF and PSD matrix concepts have been explained briefly. Now, the different techniques for operational modal analysis can be presented.

3.2.3 Operational modal analysis techniques

As mentioned before, two different modal identification methods have been used in this study to determine the dynamic properties of the buildings. They are:

- 1- Frequency Domain Decomposition-Peak Picking (FDD).
- 2- Enhanced Frequency Domain Decomposition-Peak Picking (EFDD).

3.2.3.1 Peak-picking method (PP)

The peak-picking method is the simplest known method for modal identification. This method is initially based on the fact that the SDFs go through extreme values around the natural frequencies. As an explanation, presuming that the structure is being excited by a broadband stationary white noise (i.e. constant input spectral density matrix over the frequency range of interest), the output PSD matrix is directly related to the FRF matrix of the structure which contains information about its dynamic properties. Hence, plotting the SDF related to one element of the PSD matrix shows peaks at resonant frequencies of structure. The mode shapes are determined by examining the relative magnitudes of the SDF of different elements of the PSD matrix at each resonant frequency. Using the half-power bandwidth method, the modal damping ratio can also be approximated [31]. The peak-picking technique gives reasonable estimates of the natural frequencies and mode shapes if the modes are well separated. However, in the case of closely-spaced modes, it is difficult to distinguish them [32]. In spite of this drawback, peak-picking is a widely accepted method for modal identification because its implementation is simple and processing is speedy. The peak-picking technique was further improved by using Frequency Domain Decomposition (FDD) which will be explained below [9, 29].

3.2.3.2 Frequency Domain Decomposition-Peak Picking (FDD)

The main idea of the Frequency Domain Decomposition (FDD) technique is to carry out an approximate decomposition of the system response into a set of independent single-degree-of-freedom (SDOF) systems, one for each mode.

The FDD method is also based on the fact that the response of the structure shows extreme values around the natural frequencies which, therefore, can be determined by selecting the generated peaks. The difference between FDD and peak-picking is that, in FDD, the peaks will be picked on singular value plots instead of SDF plots. Hence, the Singular Value Decomposition (SVD) of the PSD matrix should be carried out first. The SVD is the factorization of a matrix into a set of three matrices in the following form:

$$[G] = [U][S][V]^* \quad (3.3)$$

where $[G]$ is the matrix to be decomposed (in this case, the output PSD matrix), $[S]$ is a diagonal matrix with non-negative real numbers on the diagonal known as singular value matrix of $[G]$, $[U]$ is a real or complex unitary matrix, and V^* (the conjugate transpose of V) is a real or complex unitary matrix. The $[U]$ and the $[V]$ are called the left and right singular vectors of $[G]$, respectively. The singular values are sorted in descending order along the main diagonal of $[S]$. Since the PSD matrix is Hermitian (i.e. the entries on opposite sides of the main diagonal are complex conjugates), the $[U]$ and $[V]$ are transposed matrix of each other. Interestingly, the columns of $[U]$ or the rows of $[V]$ are orthonormal eigenvectors of $[G]$, called singular vectors, and the diagonal non-negative real values of $[S]$ are the corresponding eigenvalues, called singular values [33]. Therefore, at a particular frequency, the singular vector is representative of the building's mode shapes and the corresponding singular values indicate the contribution of each mode in the total energy carried by the response signal at that frequency. It should be noticed that SVD must be carried out separately for each PSD matrix corresponding to each discrete frequency. Now plotting the singular values versus frequency, the natural frequencies of the structure are recognized as peaks. The first singular vector corresponding to each selected peak provides an estimate of the associated mode shape. Usually the first few

singular values are plotted. For well-separated modes, all mode shapes of interest can be picked on the first singular value alone (Figures 16 and 17). However, in case of close or repeated modes, the attention should be also given to the second or third singular value as well.

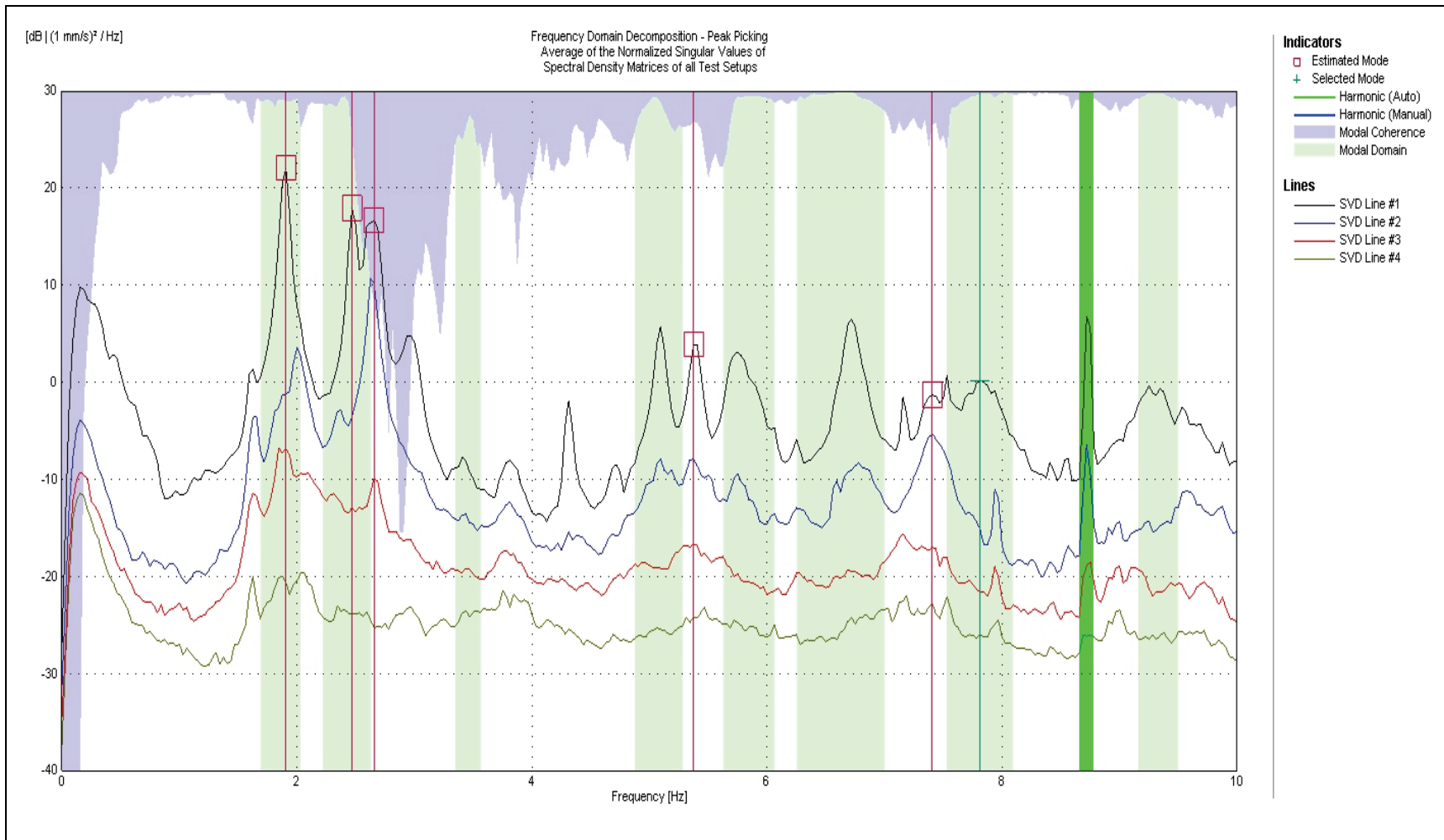


Figure 16 - FDD-Peak picking, Aug 2010, Block#8, Singular value plot

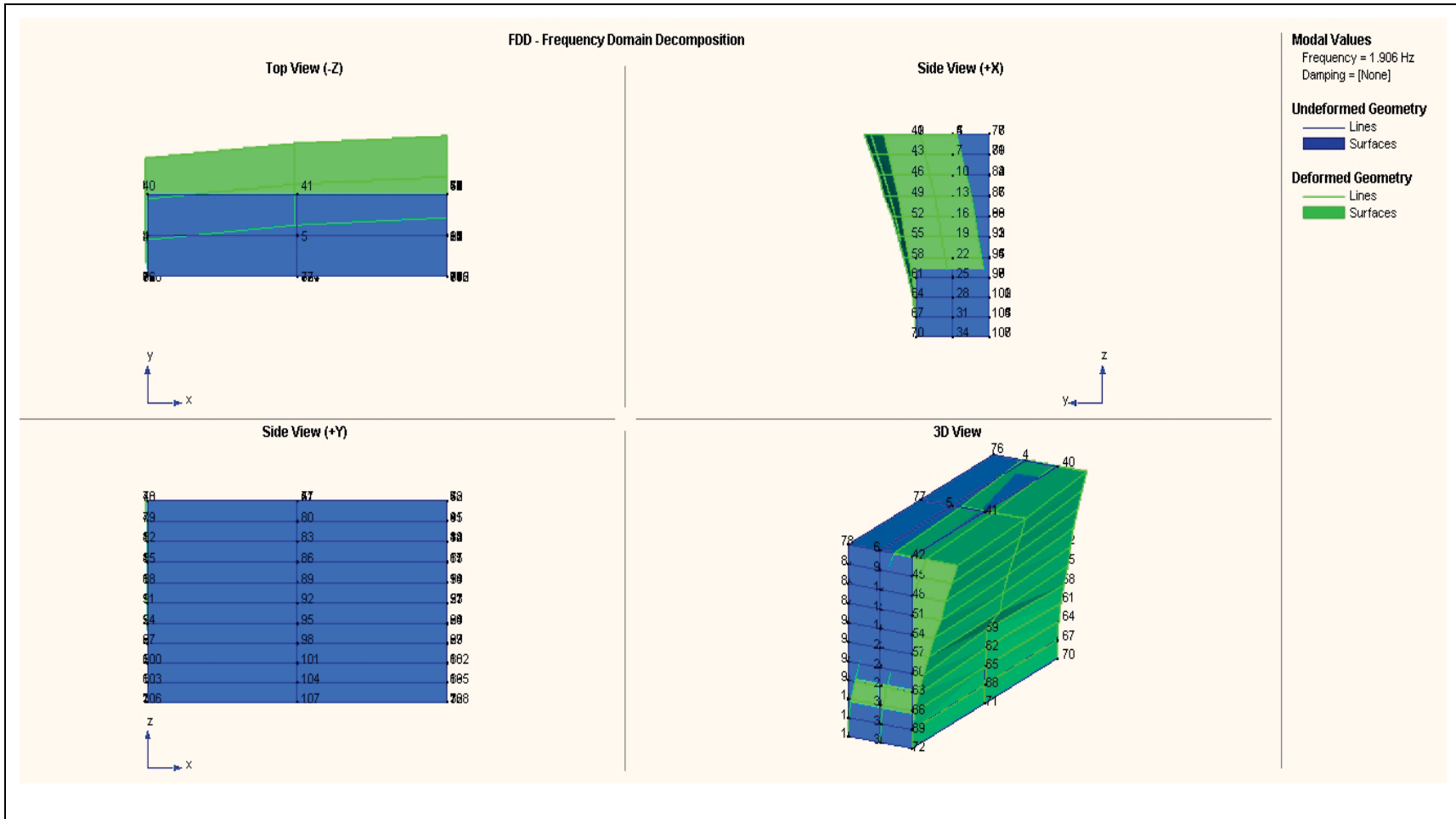


Figure 17 - FDD-Peak picking, Aug 2010, Block#8, Estimated mode shape corresponding to first peak (Translational mode in Y-direction)

3.2.3.3 Enhanced Frequency Domain Decomposition (EFDD)

The Enhanced Frequency Domain Decomposition (EFDD) emerges as an improvement of the FDD technique. In FDD-peak picking, the accuracy of modal estimation depends on how precisely the peaks are picked by the user. Therefore, imprecise peak-picking will lead to inaccurate estimates of natural frequencies and corresponding mode shapes. Contrary to the FDD technique in which all estimations are only based on one point (i.e. selected peak point), in EFDD the modal parameters are estimated using a range of frequencies in the neighbourhood of the peak point, which is called a Single-Degree-Of-Freedom (SDOF) spectral bell. As a result, the imprecision related to the FDD method will be eliminated using EFDD technique. Besides, EFDD can also yield an estimate of modal viscous damping ratios and the uncertainty associated to modal estimation (for both the frequency and damping ratio), which is not possible with the standard FDD method[7, 9].

Prior to describing the EFDD method, the Modal Assurance Criterion (MAC) should be explained. The MAC is one of the main concepts in identification of the SDOF bell. It provides a measure of consistency (correlation) between estimates of two modal vectors. Given two mode shapes $\{\varphi_1\}$ and $\{\varphi_2\}$, the MAC function is calculated as follows:

$$\text{MAC}(\{\varphi_1\}, \{\varphi_2\}) = \frac{|\{\varphi_1\}^H \{\varphi_2\}|^2}{|\{\varphi_1\}^H \{\varphi_1\}| \cdot |\{\varphi_2\}^H \{\varphi_2\}|} \quad (3.4)$$

The MAC value can vary in the range of [0-1]. The zero value indicates that the mode shapes are not consistent and a value near unity shows the consistency (complete orthogonality) of two mode shapes.

The modal estimation in EFDD technique proceeds in two steps. The first step is to perform peak-picking, exactly in the same way as described for FDD. The second step is to use the FDD determined mode shapes to identify the SDOF spectral bell functions and then to estimate both the frequency and viscous damping ratio using these bells.

- Identification of SDOF spectral bell

The identification of the SDOF spectral bell is performed using the FDD identified mode shape. At each resonant frequency, the corresponding singular vector is considered as reference vector. Moving on both sides of the peak, the MAC vector between the reference vector and singular vector corresponding to each neighbouring frequency is calculated. If the MAC value of this vector is above a user-specified rejection level the corresponding singular value is included in the description of the SDOF bell. The search on either side of the modal peak is continued until no MAC values are found above the rejection level. For the remaining frequencies, the values of the SDOF spectral bell are set to zero. It should be noted that the identification of the SDOF bell has to be accomplished for each mode and for each setup individually (Figure 18).

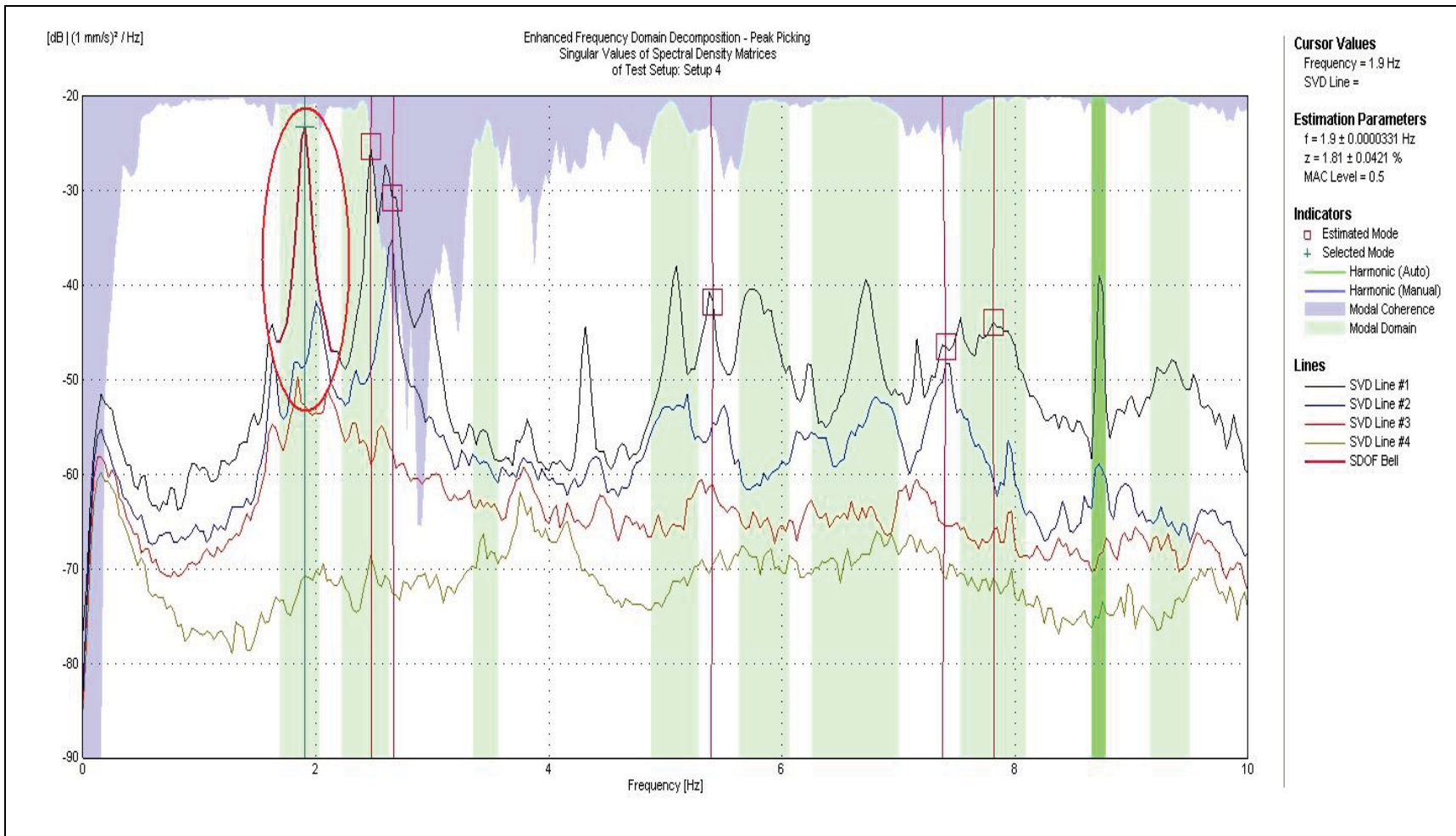


Figure 18 - EFDD-Peak picking, Identification of SDOF spectral bell (Aug 2010, Block#8)

- Improved estimate of mode shape

Following the identification of the SDOF spectral bell, an improved estimate of the mode shape is obtained by weighted averaging. All singular vectors, u_i , included in the identified SDOF bell at frequency, ω , are weighted by multiplying them with their corresponding singular value, s_i . This means that the closer the singular vector is to the peak of the SDOF bell, the more influence it has on the mode shape estimate. The weighted mean operation is performed as follows [9]:

$$\{\varphi(\omega)\} = \frac{\sum s_i(\omega)\{u_i(\omega)\}}{\sum s_i(\omega)} \quad (3.5)$$

$\{\varphi(\omega)\}$ is the averaged mode shape at resonant frequency of ω that has the effect of all the singular vectors included in the corresponding SDOF bell.

- Improved estimate of frequency and modal viscous damping ratio

For estimating the natural frequency and damping ratio of each mode, the corresponding identified SDOF bell is brought back to the time domain using Inverse Fast Fourier Transform (IFFT). This transformation yields a SDOF autocorrelation function which is an exponentially decaying function that oscillates at the damped natural frequency of the corresponding mode shape (Figure 19).

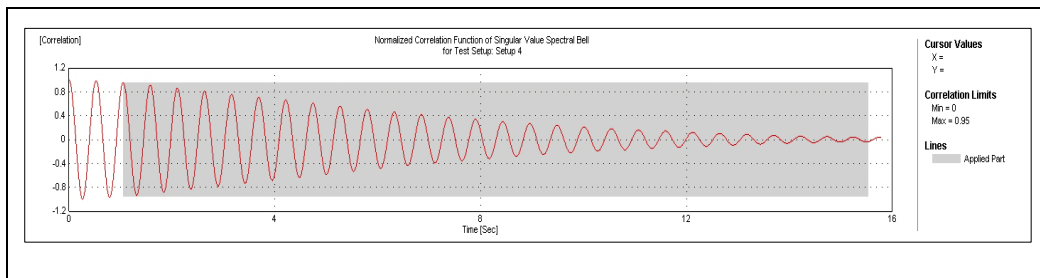


Figure 19 - SDOF autocorrelation function in Time-Domain.

For estimation of the natural frequency, the zero crossings (on the time axis) of the SDOF autocorrelation function are plotted against time and a linear regression is then performed. The slope of the fitted line is equal to the number of zero crossings per second, which is twice the number of cycles per second. Consequently, the natural frequency can be obtained easily (Figure 20).

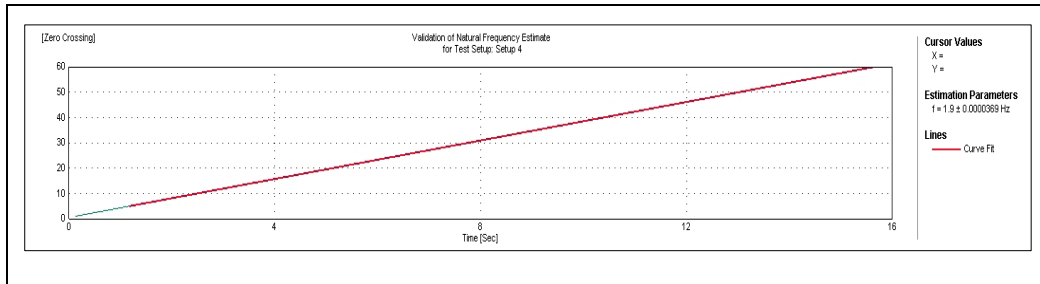


Figure 20 - Improved estimate of frequency using zero crossings

As mentioned before, the SDOF autocorrelation function decays exponentially in a similar way to the linear viscously damped SDOF system in free vibration. Hence, the logarithmic decrement technique [31] can be used to find the modal damping ratio. In summary, after the identification of the peaks of the autocorrelation function is performed, the decaying curve that connects the peaks along with their corresponding times is determined. For viscous damped linear SDOF system, taking the logarithm of this decaying curve will result in a straight line on which the damping ratio can be estimated by linear regression (Figure 21). The detailed explanation can be found in thesis by Damien Gilles [7].

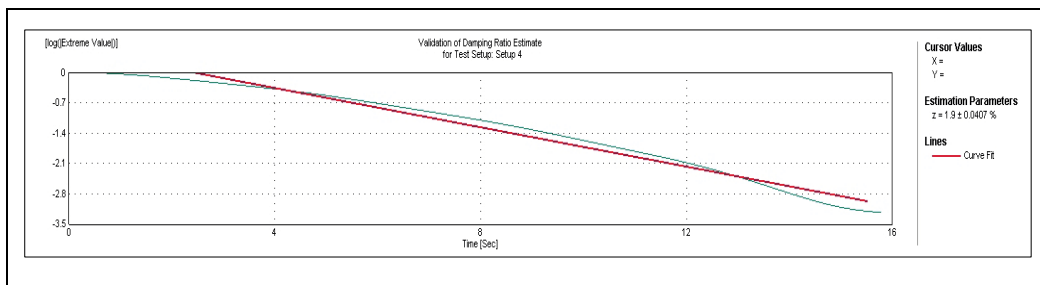


Figure 21 - Estimate of viscous damping using logarithmic decrement

3.3 AVT results

Table 2 - Block # 8

Block#8												
Mode shape	1 st transverse mode		1 st longitudinal mode		1 st torsional mode		2 nd transverse mode		2 nd longitudinal mode		2 nd torsional mode	
Models	Period (s)	Frequency (Hz)	Period (s)	Frequency (Hz)	Period (s)	Frequency (Hz)	Period (s)	Frequency (Hz)	Period (s)	Frequency (Hz)	Period (s)	Frequency (Hz)
ARTEMIS-EFDD-Aug 2010	0.53	1.90	0.38	2.67	0.40	2.48	0.19	5.39	0.14	7.40	0.13	7.82

Table 3 - Block # 7

Block#7						
Mode shape	1 st transverse mode		1 st longitudinal mode		1 st torsional mode	
Models	Period(s)	Frequency(Hz)	Period(s)	Frequency(Hz)	Period(s)	Frequency(Hz)
ARTEMIS-EFDD-Sep 2010	0.54	1.86	0.49	2.05	0.33	3.06
ARTEMIS-EFDD-July 2011	0.55	1.83	0.50	2.00	0.35	2.88

3.4 Comparison between AVT results and NBCC-2010 period equation

In this part the fundamental sway mode period of both blocks are calculated based on the empirical formula recommended in NBCC-2010-Sentence 4.1.8.11. 3)-a)-ii [4] for concrete moment-resisting frames (see Table 4) and then, it is compared with the fundamental period extracted from AVT records, in Table 5.

Table 4 – Fundamental period calculation based on NBCC-2010

Empirical period-NBCC 2010		
$T_a=0.075(h_n)^{3/4}$		
Building height	h_n (m)	36.11
Fundamental period	T_a (s)	1.10
Fundamental frequency	f (Hz)	0.91

Table 5 – Comparison between AVT result and NBCC-2010

Blocks	Models	Fundamental Period (s)
Block # 8	NBCC 2010	1.10
	ARTEMIS-EFDD-Aug 2010	0.53
	Difference (%)	110%
Block # 7	NBCC 2010	1.10
	ARTEMIS-EFDD-Sep 2010	0.54
	Difference (%)	106%
	NBCC 2010	1.10
	ARTEMIS-EFDD-July 2011	0.55
Difference (%)	102%	

The results show that the fundamental period of the buildings extracted from ambient vibration records measured in the operational condition of the structure is roughly half the period calculated based on NBCC. Of course, AVT are conducted at very low strain levels, very far from the slightly damaged state that is expected during a design level earthquake. On the other hand, operational conditions include the real reactive mass of the structure as well as the presence of non-structural components (in particular the effect of stiff partitions and infilled walls), and the effect of the foundations and soil at the site. This considerable difference in fundamental period implies that the period selected for design procedure according to NBCC results in underestimated earthquake load (i.e. selecting a lower acceleration on the Design Spectrum).

4 Numerical study: Finite element modeling and analysis

As previously discussed, in order to illustrate the structural contribution of unreinforced *terra cotta* infill walls, two eleven-storey buildings of CHU Sainte-Justine hospital have been selected and a detailed linear elastic finite element analysis model of each building is generated in commercial software SAP 2000 v.14.0.0 (Integrated software for structural analysis and design)[34].

In this chapter, the different parts of the numerical study of these two buildings (Block#7 and #8) are described in detail. It includes: a description of the various Finite Element (FE) models created for each block (models excluding and including masonry infill walls), a presentation of the different techniques used for modelling the masonry infill walls, the calibration and verification of the FE models using AVT results. The calibrated models are then analysed for a set of generated ground accelerograms, and Floor Response Spectra (FRS) and Inter-storey drift curves are generated for selected floors using the results of dynamic analysis. The numerical results of the different models will be presented, compared and discussed at the end of the chapter.

4.1 General properties of the buildings

4.1.1 Geometric properties

The selected buildings are two wings (Blocks #7 and #8) of CHU Sainte-Justine, a paediatric hospital located in Montréal, Canada (Figure 5). They mainly serve as the research area of the hospital with laboratories and office space. The two blocks are mostly identical in terms of floor plans, elevations and dimensions. The buildings are nearly rectangular in shape having the

plan dimensions of 63 m × 14.5 m (206'-7" × 47'-6") and total height of 39.7 m (130'-6") from the base. Both blocks consist of 11 stories from which the lowest four stories (starting from the basement) have the height of 3.5 m (11'-6") and the other seven upper ones (ending to the roof) have the height of 3.65 m (12") (Figure 22). The identification of the different stories of the two blocks is also illustrated in Figure 22, which is used in later explanations and discussions.

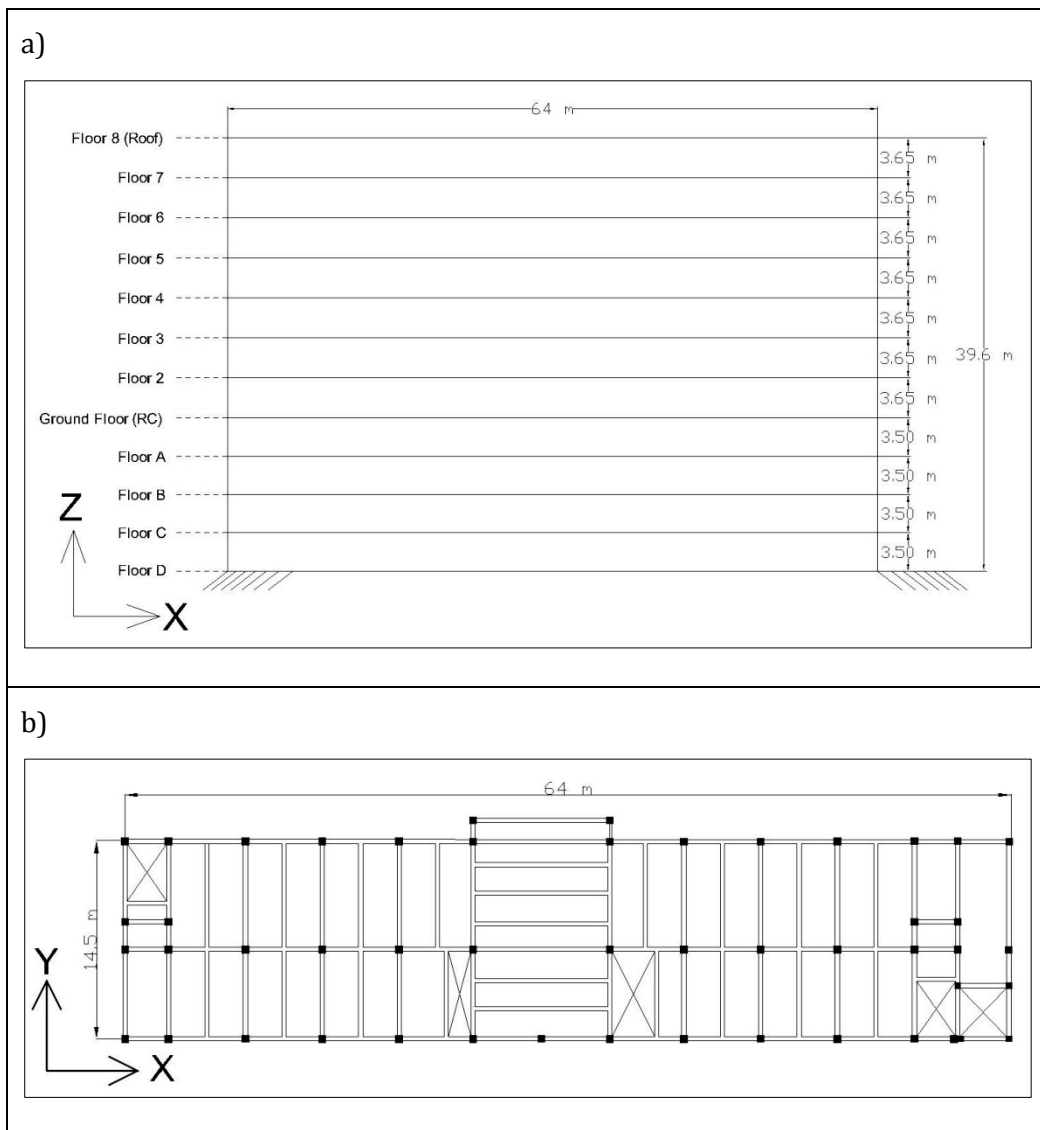


Figure 22 - Geometric properties: a) Elevation view; b) Plan view

4.1.2 Structural Properties

- Structural elements

The hospital campus was initially built in the late 1950s when no specific seismic engineering considerations existed for Montreal. The structural system of both buildings (Blocks#7 and #8) is a reinforced concrete (RC) moment frame comprised of closely-spaced square and rectangular columns, small dimension beams, thin concrete slab (typically 100 mm or 4"), exterior walls composed of 100 mm brick layer, 200mm *terra cotta*, 25mm air gap, 100mm *terra cotta*, and 25mm of plaster, and interior wall including 200mm *terra cotta*.

- Lateral Load-Resisting System (LLRS)

As explained in chapter 2, both blocks were built according to the available building code and the engineers apparently have been counting on the RC moment frame (bare frame) behaviour and the additional stiffness coming from the infill walls to resist the lateral wind forces. Moreover, there is no indication of taking the seismic lateral forces into account. Therefore, the lateral load-resisting system (LLRS) of both blocks was non-ductile RC moment-resisting frame initially. However, as a part of the RDP, block #7 was seismically retrofitted in 2008 by adding a full-height reinforced concrete shear wall at its free end and connecting the other end of the building to the adjacent block #9 using structural anchor bars (55 mm diameter) at each floor slab and along the height of interfacing columns at every meter. Block #8 was not retrofitted and has remained unattached to its adjacent building. To summarize, the LLRS of block#8 is still RC moment-resisting frame, as it was before, while for block#7, the LLRS has been enhanced by adding the concrete shear wall and connecting this block to the adjacent block#9.

- Material properties

Linear elastic material properties are used for 3D modal analysis. These properties are nominal values indicated on the structural drawings and were not verified by physical tests. The specified compressive strength of concrete, f'_c , is 3000 psi (21 MPa) for all the structural members (i.e. beams, slabs, and concrete shear wall) except for the columns. For the columns, f'_c is taken as 5000 psi (35 MPa) for the lower seven floors starting from the basement and 3000 psi (21 MPa) for the rest of the floors up to the roof. It should be mentioned that the same nominal concrete material as the existing lower-strength concrete (3000 psi) was used in the seismic shear wall added to block#7. The other properties used in the numerical models are listed in Tables 4 and 5.

Table 4 - Concrete properties

3000 psi Concrete	
Compressive strength (f'_c)	2.07E+04 kN/m ²
mass per unit volume	2.40 tons/m ³
weight per unit volume	23.6 kN/m ³
modulus of elasticity	2.15E+07 kN/m ²
Poisson's ratio	0.2
shear modulus	8.97E+06 kN/m ²

Table 5 - Concrete properties

5000 psi concrete	
Compressive strength (f'_c)	3.45E+04 kN/m ²
mass per unit volume	2.40 tons/m ³
weight per unit volume	23.6 kN/m ³
modulus of elasticity	2.78E+07 kN/m ²
Poisson's ratio	0.2
shear modulus	1.16E+07 kN/m ²

In contrary to the concrete material properties specified on the design drawings, determining the properties of the masonry infill wall is not an easy-task to do, especially that this project did not involve any experimental tests on material samples. The difficulty of finding realistic nominal properties is also related to the complexity of infill wall's structural behaviour. Therefore, the properties of terra cotta infill masonry had to be defined such how that it could represent the composite behaviour of the wall (i.e. terra cotta units and mortar)properly. This matter will be further discussed later.

4.2 Description of different FE models

To study the effect of seismic retrofitting and masonry infill walls on the dynamic characteristics of the two buildings, different 3D finite element models were generated in SAP2000. It should be noted that the main use of these models is to compare different structural assumptions: it is very difficult to represent the accurate response of the actual buildings, but it is deemed useful nonetheless to use elastic models in a comparative analysis. In order to build these FE models, a number of assumptions were made as follows:

- 1- Linear elastic material properties were used for 3D modal analyses.
- 2- Beam-to-column connections are assumed to be fixed (RC moment-resisting frame).
- 3- The frames are fixed at the base of the columns.
- 4- Since the hospital is sitting on good quality rock, the author has assumed soil site class C: very dense soil and soft rock [4], so that there is no amplification factor because of soil behaviour. Hence, the soil-structure interaction is neglected.

- 5- The floor diaphragms are rigid in their own planes and flexible normal to their planes.
- 6- The mass source is defined to be generated by the dead loads. It means that the software generates masses from the loads and lumps them at the joints. The self weight of the frame is also included in the dead load. These reactive masses will determine the amount of inertia force created by the ground acceleration.
- 7- Only permanent gravity loads are considered in the seismic analyses – no floor live load of any environmental loads on the walls and roof are combined (i.e. D+E only).

In general, the generated models can be divided into two categories: 1- Bare-frame models or models excluding infill walls, 2- Full-frame models or models including infill walls. The detailed description of each model and their numerical results will follow.

4.2.1 Bare-frame models (the models excluding masonry infill walls)

The numerical simulation of both blocks was started by creating the bare frame models for each block separately. It means that in the first step of modeling, the infill masonry walls are excluded from the models and the structural elements are only columns, beams, thin concrete slabs, peripheral concrete wall (17" thick) going all around the buildings between floor D and C, and the concrete shear wall (only for block#7). At each floor, the joints are constrained together using the diaphragm constraint which causes them to move together as a planar diaphragm that is rigid against membrane deformation.

- Mass\Self-weight

Using the material and geometrical properties (i.e. density and cross section, respectively) assigned to each element, the software automatically calculates the mass\self-weight of the element. The mass is then lumped at the element joints and used to compute the inertial forces in dynamic analysis. However, the self-weight is also a force being distributed along the length of the element (frame element) or uniformly distributed over the plane of the element (shell or plane element) and always acts downward [34].

Although the partitions are not modeled in this 'bare-frame' step, the self-weight (dead load) associated with them must be included in the models. Thus, according to the NBCC 2005- Division B-4.1.4.1.(3) [4], the dead load of 1 kPa has been distributed uniformly on all floor areas (except roof) to account for partition weight.

The only part which remains to account for its weight is the stair slabs. As it can be seen in the typical plan view shown in Figure 13, there are three staircases (from the ground floor to the last), two at the ends and one in the middle. Using the structural drawings, the volume of the stairs slabs was calculated between every two consecutive floors. Then having the concrete density, their weight was determined. For each story, the staircase is supported by two beams, one at the upper floor and the other one at the lower floor. Therefore, the stairs load was divided between the supporting beams and applied to them as a uniformly distributed span load (i.e. a load distributed along the length of frame element). The other relevant modeling details of each block will be explained separately below.

4.2.1.1 Block #8

As mentioned before, block#8 has not been retrofitted seismically and, hence, it does not have any concrete shear wall or connection to the adjacent block#9. Therefore, the complexity of this block is less than block#7 in terms of numerical modeling. The self-weight of elements, stair weight, and partition weight were included in the model as explained above. All the frames are fixed at the base of the columns. Figures 23 and 24 illustrate the bare-frame model of block#8.

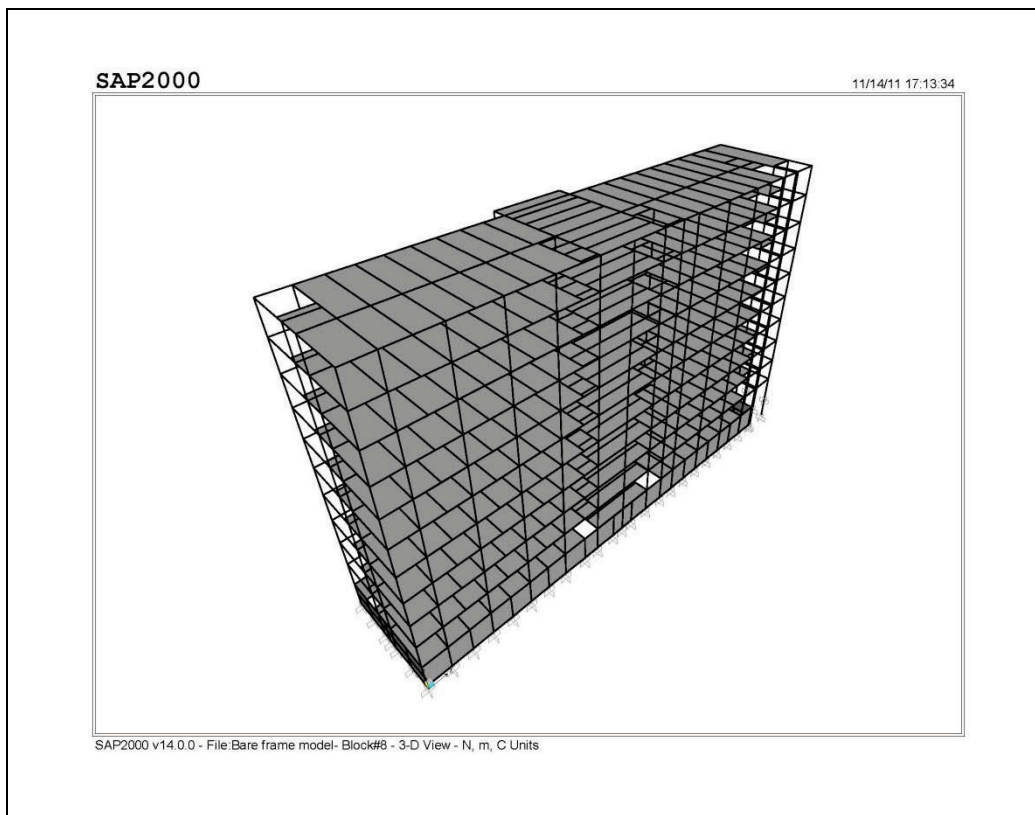


Figure 23 - 3D view of bare-frame model, Block#8

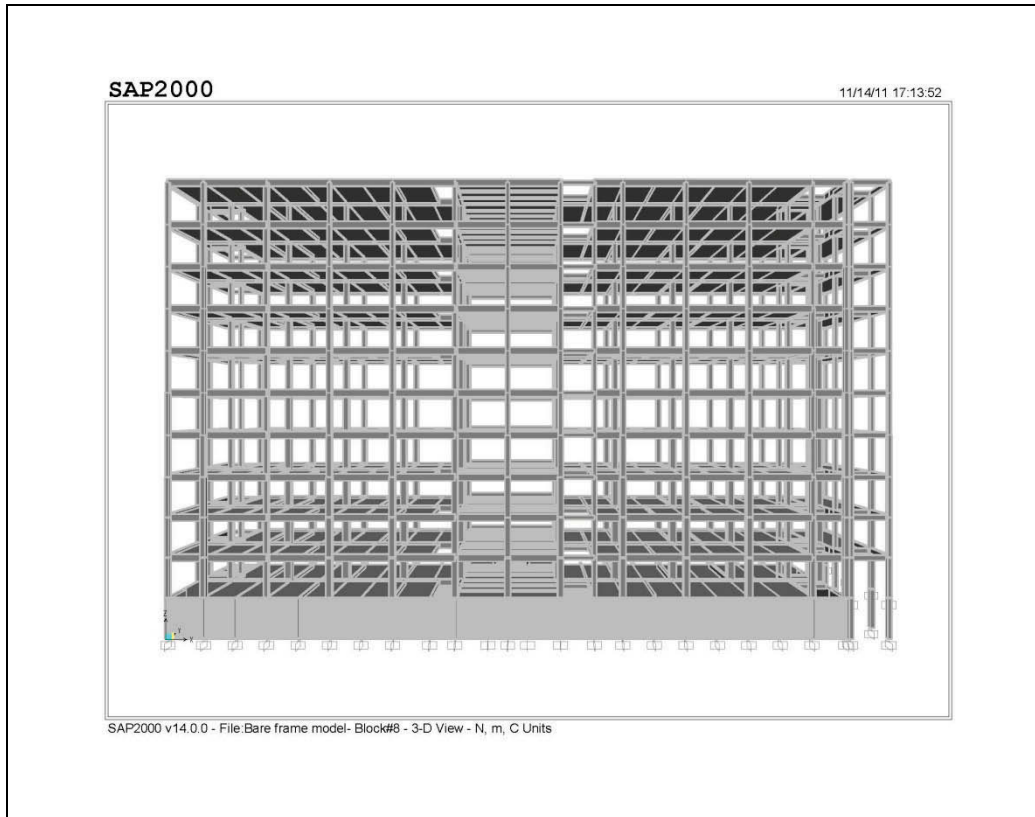


Figure 24 - 3D extruded view of bare-frame model-Block#8

4.2.1.2 Block #7

Block#7 has been seismically retrofitted in 2008 by adding a full-height reinforced concrete shear wall at its free end and connecting the other end of the building to the adjacent Block #9. These changes make the model of block#7 more complex than block #8. Regardless of these differences, the other parts of this block were modeled using exactly the same approach as block #8. The modeling details of the added concrete shear wall and connections to block #9 are explained below.

- Concrete shear wall

At the first step of modeling, the existing part of block#7 (the main structural frame) has been created in SAP2000. Then the concrete shear wall has been

added to this first model. The concrete used to model the shear wall has the same nominal compressive strength as defined for the concrete of the slab and upper levels of the existing part (Concrete 3000 psi). The geometry and dimensions of the shear wall, its openings, and the coupling beams were taken from the structural drawings and have been modeled in details. The concrete shear wall has been connected to the building (existing part of block #7) using structural anchor bars of 55 mm diameter at each floor slab and along the height of interfacing columns, at 1 meter spacing (see Figure 25).



Figure 25 - Close-up view of anchor locations before casting the shear wall

To provide a complete composite action of the shear wall with the rest of the building, the rebars are welded to a 13 mm plate located in the shear wall and anchored with epoxy in the existing structural elements at the other side (Figure 26). All the rebars have been covered by concrete at the distance between the interfaces of the shear wall and the existing building. Hence, the connecting links have a square cross-section of 250mm×250mm (Figure 27).

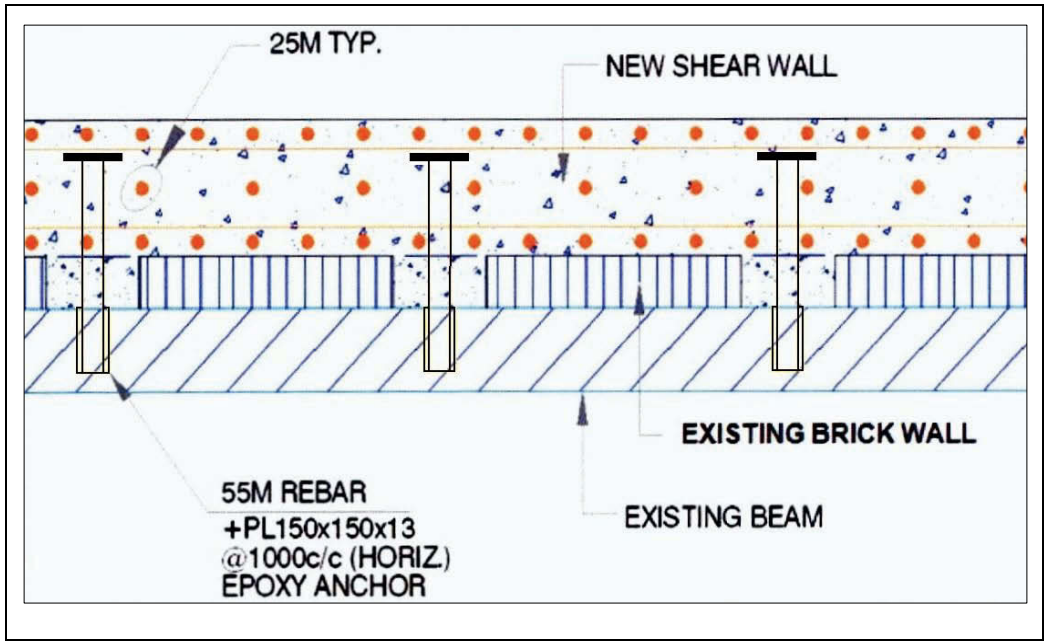


Figure 26 - Connection between new shear wall and existing building[2].

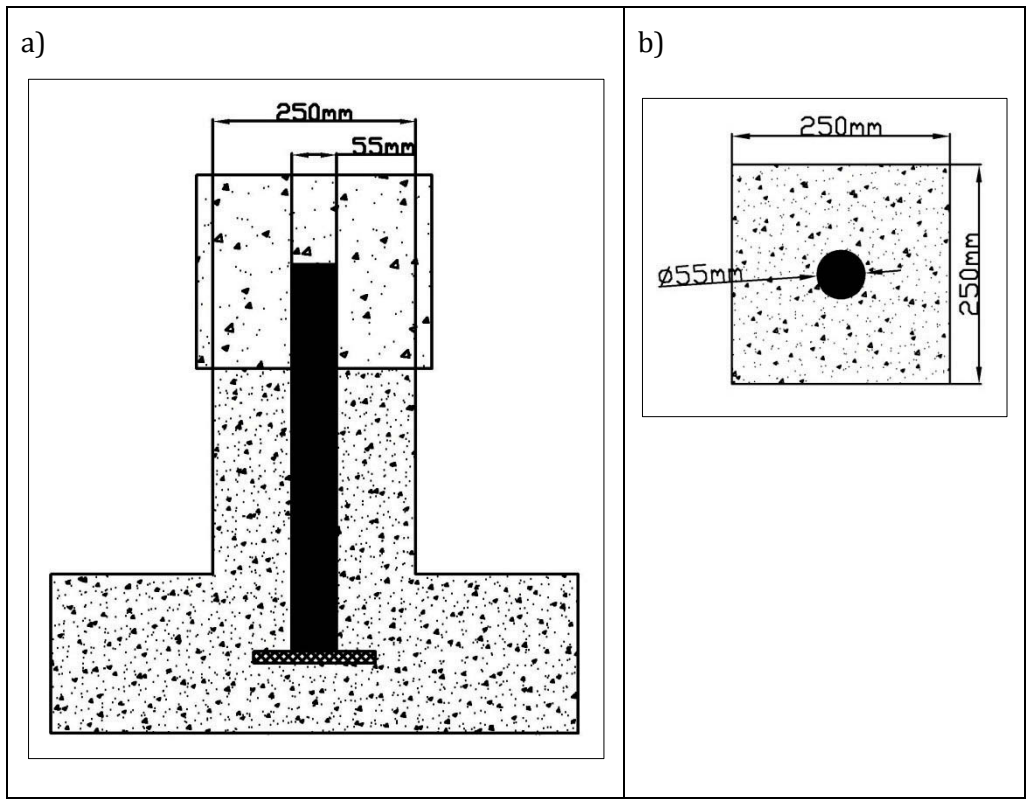


Figure 27- Anchor details: a) Plan view of connection; b) Cross-section

The first approach used to connect the shear wall to the building in the numerical model is to constrain the shear wall joints and floor joints all together by means of a rigid diaphragm constraint at each floor. This causes the wall joints to move as a planar diaphragm at each level with the corresponding floor joints.

In the second approach, the connections have been modeled using an equivalent frame element (with equivalent steel cross-section). Each link (connection) is defined by a start and an end point. The start point represents the interface between the link and the shear wall, whereas the end point defines the connectivity between the link and the existing building. Three different link systems have been assigned to both ends of links: Fixed-Fixed, Fixed-Pinned, and Pinned-Pinned connections, to compare their effects on the dynamic properties of the whole model when running an eigenvalue analysis.

Comparing the results of these models shows that the differences between the diaphragm, Fixed-Fixed, and Fixed-Pinned models are negligible. The only model that has different results (resonant frequencies) is the Pinned-Pinned model. However, the Pinned-Pinned system is not a good representation because the connections are nearly fixed at the shear wall interface due to the provided anchoring details. The main reason for testing these different types of connection models was in an attempt to explain the discrepancies observed between AVT and numerical results for this block (block #7). This matter will be comprehensively explained in chapter 5.

- Connections to the block #9

The other seismic retrofitting action done in block#7 was connecting this building to the adjacent block#9 using structural anchor bars. The

connections start at floor 1 and continue up to the roof level. Clearly, these connections add significant lateral stiffness to block#7, in addition to eliminating the risk of pounding of the two separate buildings (#7 and #9) under very strong shaking. The connected points of block#7 cannot move freely anymore since their displacement is contingent upon inducing the same displacement in corresponding points of block#9(if the connection links are assumed to be rigid). This behaviour should be considered in the numerical model of block#7. To do so, the connecting links are simulated by means of support elastic springs two sets of spring supports are defined in the model, in each orthogonal horizontal direction (X and Y directions in the model). Since the structural details of block#9 were not available for this study (and indeed, the evaluation of this building is not an objective of this project), a simplifying assumption has been made to estimate the equivalent stiffness of the support springs, taking the approximate stiffness of the springs considering that the adjacent building was block#8 instead of block#9. It means that the stiffness of spring supports at each floor has been estimated by the lateral stiffness of the corresponding floor of block#8. To calculate the floor lateral stiffness of block#8 two different techniques have been utilized: Drift method and Flexibility Matrix method.

- Drift method

By definition, for a SDOF system, stiffness is the force required to produce a unit displacement along the same direction of the DOF. Therefore, having the applied force (F) and induced relative inter-story displacement (X), the stiffness (K) can be calculated as follows:

$$K = \frac{F}{X} \quad (4.1)$$

Therefore, in this method the lateral stiffness of the building is calculated using the lateral displacements (lateral drift) of the building induced by a prescribed lateral force. The step by step explanation of the procedure used is presented next.

1- Applying the lateral force:

In the first step, a lateral force is applied to the roof of the block#8 model in each horizontal direction (X and Y) separately. The force must be exerted at the center of rigidity (CR) of the roof (or floor) to prevent any torsional effect; otherwise a portion of the lateral displacement is caused by the generated torque which is undesired. Due to the symmetry of LLRS of block#8, the principal axes of the rigidity are approximated by the axes of symmetry. In other words, the CR can be replaced by the geometric center (centroid) of the building plan. Hence, the force is simply applied at the centroid.

2- Determining the Inter-Storey drift:

After applying the lateral force and running the model, the total lateral displacement (lateral drift) of each storey and, subsequently, inter-storey drifts are determined. Replacement of CR with the centroid causes a small torsional effect (the centre of twist does not coincide with the centroids) but it was found negligible, and the averaged lateral displacement is used to eliminate the torsional displacement (see Figure 28).

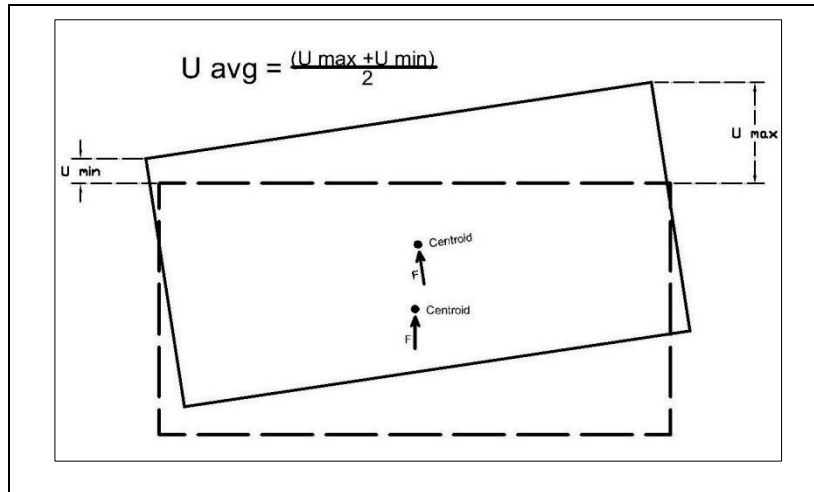


Figure 28- Inter-Storey drift (average displacement)

3- Calculating the lateral stiffness of each storey:

Now, the applied force and the lateral displacements of each storey are both known. Using equation 4.1, the lateral stiffness of each storey is simply calculated. In the model the stiffness of each storey is simulated by two spring supports in each orthogonal horizontal direction (X and Y). These springs are located at two corners of the common side of block#7 with block#9. Therefore, the equivalent stiffness of the springs in each direction is half of the lateral stiffness of corresponding floor in that particular direction.

It should be noted that the aforementioned procedure is applied for each horizontal direction (X and Y) separately. Therefore, four spring supports are defined at each floor level of block#7 (from floor#1 up to the roof), two in X direction and two in Y. These springs are assigned to the two common corners of block#7 and block#9. Tables 6 and 7 illustrate the calculation of spring stiffness in X and Y directions, respectively.

Table 6 - Calculation of spring stiffness in X direction (Inter-storey drift method)

X - direction						
Lateral force applied to the roof (F) = 920 N						
Floor#	Lateral displacement (mm)×10 ⁻³			Inter-storey drift (mm) ×10 ⁻³	Lateral stiffness of each storey (N/m)	Equivalent stiffness of spring support (N/m)
	First corner (U _{min})	Second Corner (U _{max})	Average (U _{avg})			
8	31.566	31.925	31.746	5.709	1.61E+08	8.06E+07
7	25.905	26.169	26.037	4.883	1.88E+08	9.42E+07
6	21.065	21.243	21.154	3.905	2.36E+08	1.18E+08
5	17.193	17.306	17.250	3.468	2.65E+08	1.33E+08
4	13.747	13.816	13.782	3.084	2.98E+08	1.49E+08
3	10.678	10.718	10.698	2.772	3.32E+08	1.66E+08
2	7.918	7.935	7.927	2.553	3.60E+08	1.80E+08
1	5.372	5.376	5.374	2.152	4.28E+08	2.14E+08
A	3.218	3.227	3.223	1.917	4.80E+08	2.40E+08
B	1.301	1.310	1.306	1.287	7.15E+08	3.57E+08
C	0.019	0.018	0.019	0.019	4.97E+10	2.49E+10
D	0	0	0	0	-----	-----

Table 7 - Calculation of spring stiffness in Y direction (Inter-storey drift method)

Y - direction						
Lateral force applied to the roof (F) = 920 N						
Floor#	Lateral displacement (mm)×10 ⁻³			Inter-storey drift (mm) ×10 ⁻³	Lateral stiffness of each storey (N/m)	Equivalent stiffness of spring support (N/m)
	First corner (U _{min})	Second Corner (U _{max})	Average (U _{avg})			
8	38.17	40.12	39.15	6.56	1.40E+08	7.01E+07
7	31.78	33.39	32.58	5.84	1.58E+08	7.88E+07
6	26.02	27.46	26.74	4.89	1.88E+08	9.41E+07
5	21.28	22.43	21.85	4.39	2.09E+08	1.05E+08
4	17.03	17.90	17.46	3.92	2.35E+08	1.17E+08
3	13.21	13.88	13.54	3.53	2.61E+08	1.30E+08
2	9.72	10.31	10.02	3.24	2.84E+08	1.42E+08
1	6.56	6.99	6.77	2.74	3.36E+08	1.68E+08
A	3.92	4.15	4.04	2.39	3.86E+08	1.93E+08
B	1.62	1.68	1.65	1.56	5.90E+08	2.95E+08
C	0.10	0.08	0.09	0.09	1.03E+10	5.17E+09
D	0	0	0	0	-----	-----

- Flexibility matrix method

By definition, for a SDOF system, flexibility is the displacement induced in the system by a unit force applied in the same direction as the DOF. Dealing with a multi-degree-of-freedom (MDOF) system, flexibility coefficients populate the flexibility matrix, $[F]$. Defining a system composed of N DOFs defined at each floor level, one can obtain a N -by- N flexibility matrix, $[F]_{n \times n}$ (Figure 29-a). By definition, the flexibility coefficient f_{ij} , the entry in row i and column j , is the displacement along the i^{th} DOF induced by a unit force applied to the j^{th} DOF.

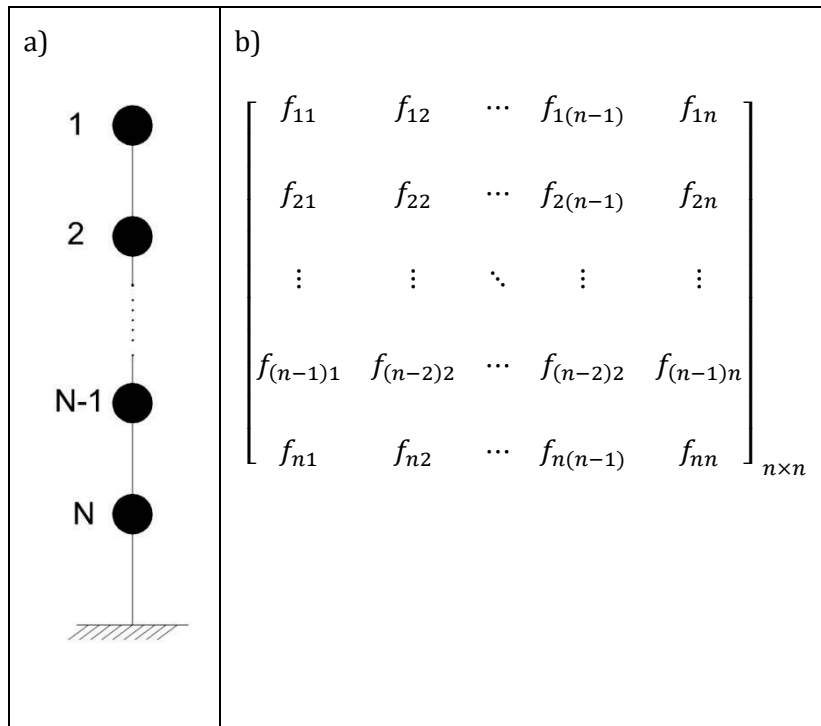


Figure 29- MDOF system: a) schematic view of N degree-of-freedom system;
b) Flexibility matrix of MDOF system

To generate the $[F]_{n \times n}$, a unit force must be applied to one DOF at a time. This procedure is repeated for all DOFs individually. In this way, each time one column of the matrix is completed and, consequently, the entire matrix, $[F]_{n \times n}$, is generated. The stiffness matrix, $[K]_{n \times n}$, of the system is obtained by inverting the flexibility matrix, $[F]_{n \times n}$ (Equation 4.2).

$$[K]_{n \times n} = [F]_{n \times n}^{-1} \quad (4.2)$$

Using this approach, the flexibility matrix of block#8 has been generated in both horizontal directions (X and Y) individually.

To extract the lateral stiffness of each storey of block#8 (in X and Y directions) from the stiffness matrix, a simplified model of the building is obtained by assuming that:

- 1- The mass is concentrated at the center of gravity (CG) of each floor level (lumped-mass system).
- 2- The floors are rigid in bending and in the axial direction (diaphragm action).
- 3- The columns are axially rigid.

Together these assumptions allow for the generation of a model commonly known as a “shear building model”, where displacements at each floor level may be described by one DOF alone (Figure 30-a). Accepting the shear building assumption, the stiffness matrix of block#8 becomes a tridiagonal matrix as shown below:

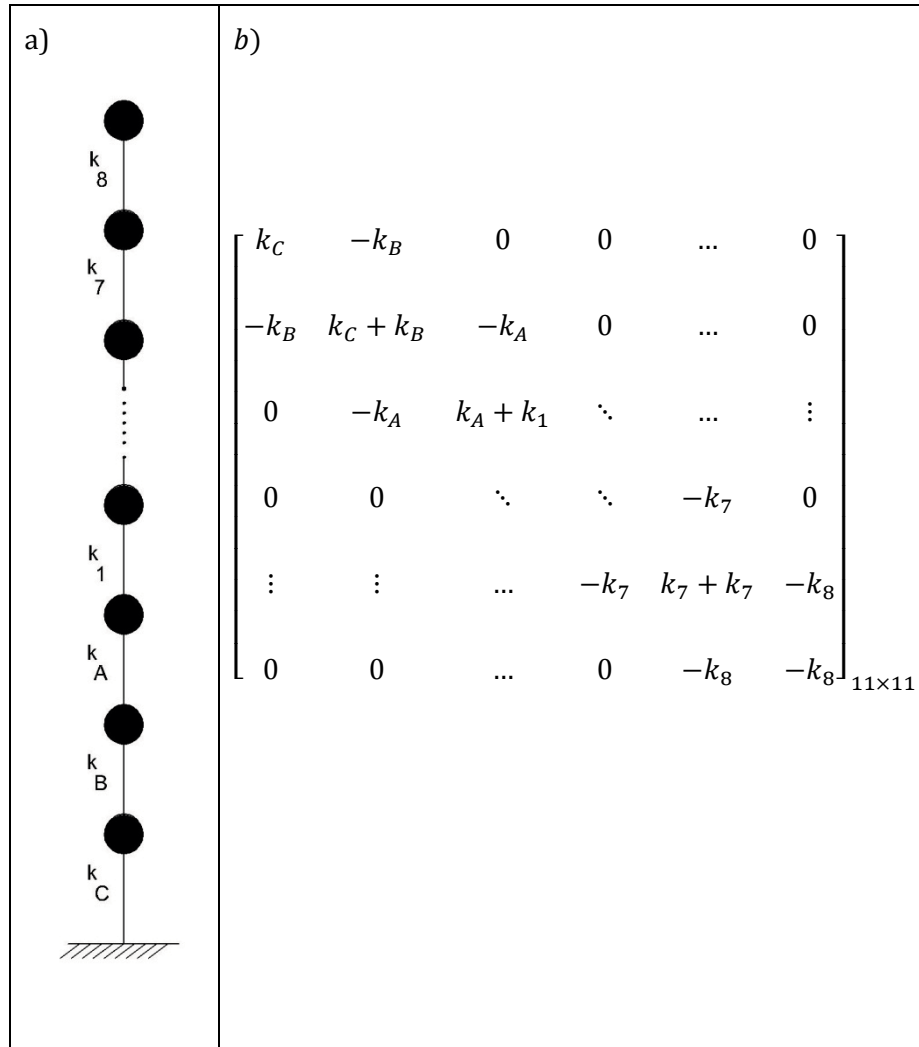


Figure 30- a) Shear model of block#8 and b) corresponding stiffness matrix

Comparing this tridiagonal matrix with the stiffness matrix already provided, the lateral stiffness of each storey and equivalent stiffness of spring supports are directly determined. However, as expected, the comparison between these two matrices showed that the calculated stiffness matrix using the flexibility method is not exactly consistent with the parametric stiffness matrix presented in Figure 30. It means that the acceptance of the shear building model assumption for block#8 is not accurate. The observed difference between the lateral stiffness calculated using this method and drift method is another indication for this matter. Another reason for this inconsistency is that in the generated numerical model of block#8, the mass

is not lumped at CG of each floor level, rather it is distributed among the joints of each element.

In the end, it was decided to use the spring stiffness calculated by the drift method (Tables 6 and 7) to simulate the connections between blocks#7 and #9. Figures 31 and 32 illustrate the bare-frame model of block#7.

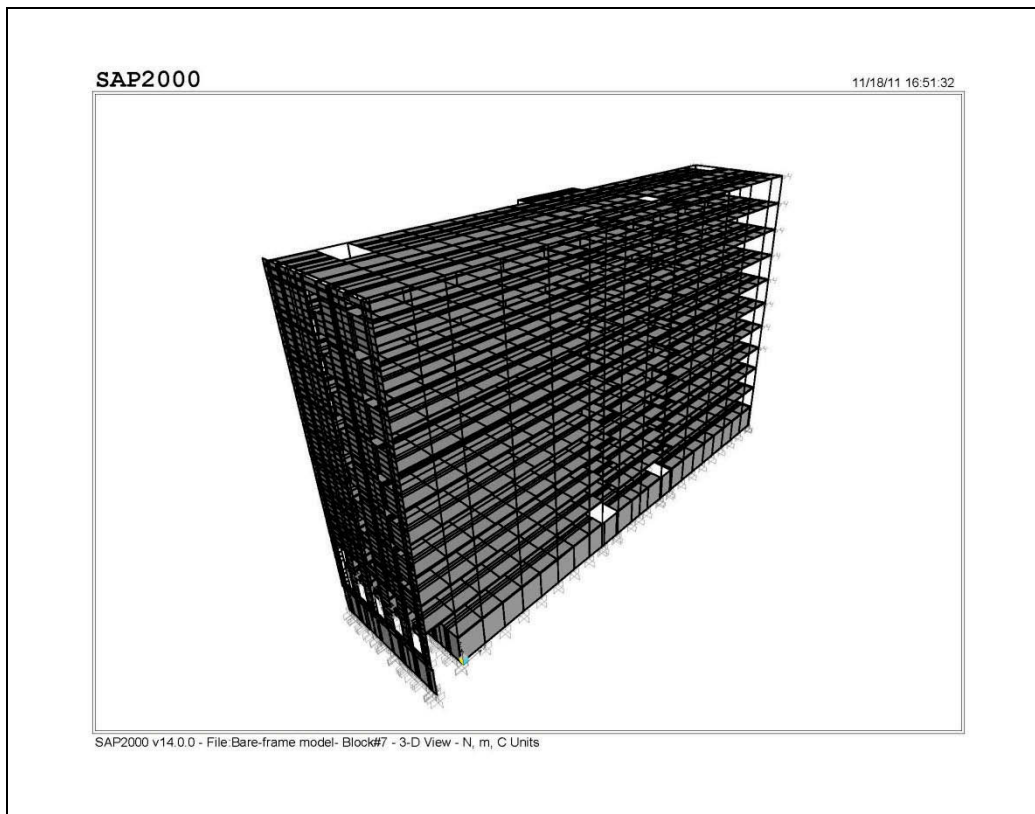


Figure 31- 3D view of bare-frame model-Block#7

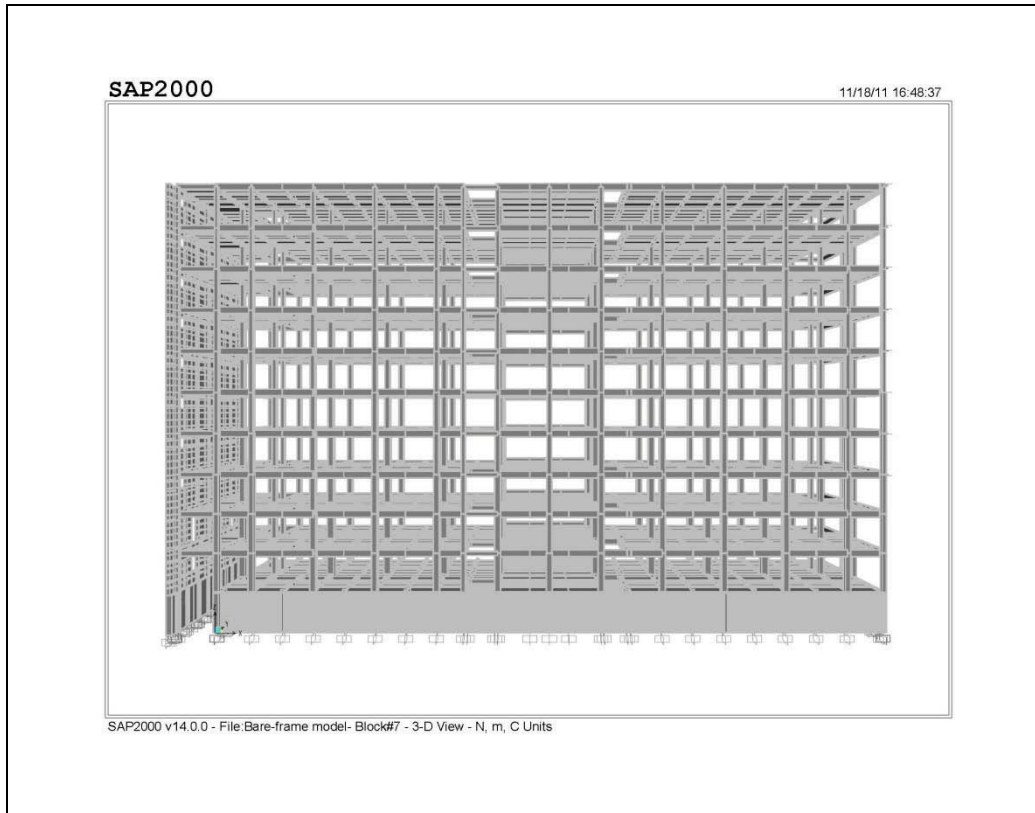


Figure 32-3D extruded view of bare-frame model-Block#7

4.2.2 Full-frame models (with masonry infill walls)

After generating the bare-frame models of both blocks, the masonry infill walls were added to the initial models, to evaluate their effect on the dynamic behaviour of the buildings. The masonry infill walls of the hospital have been constructed using *terra cotta* masonry units. To model the infill walls, their structural details and the properties of *terra cotta* blocks are required. To obtain this information and verify the construction of these walls, beside the literature review and consulting the structural drawings of the hospital, both blocks have been visited in February 2011. In the visit, all floors were inspected and the alterations done in interior partitions after RDP were checked.

As described in chapter 2, two different techniques were adopted in this study for modeling the *terra cotta* infill walls: 1- Continuum model or panel element model, 2- Equivalent diagonal compression struts. The details of each model are explained below.

It should be noted that in modeling, only those infill walls which are surrounded by frame elements (i.e. beam and column) have been added to the models. For the rest of the URM partition walls, their weight is calculated and counted in the model as a uniformly distributed dead load. Thus, the 1-kPa dead load which was already considered for partitions is eliminated.

4.2.2.1 Continuum model (Panel element model)

As previously explained, one way to model the masonry infill walls is to consider them as a homogeneous material including the masonry units and the mortar together as a continuum. This is what is called as “a homogeneous isotropic continuum” in the literature (Figure 11). Adopting this technique, the infill wall (*terra cotta* blocks and mortar) has been simulated using the panel element. The key part of this method is to define the equivalent properties of the material in such a way that the panel element can represent the composite behaviour of the wall properly. In order to determine the equivalent material properties of material, a number of references were used [35-37]. The first step is to determine the properties of each component including: 1- mortar type and 2-compressive strength of clay masonry units.

Mortars are categorized into different types based on their specifications and their construction suitability- namely, M, S, N, and O types. The type N is suitable mortar for general use in above grade masonry, interior walls and partitions, and masonry veneer and non-structural masonry partitions [36]. Therefore Type N has been selected as the mortar type for the case study.

The other material parameter to be determined is the compressive strength of the clay masonry units. Initially, the smallest nominal published value of compressive strength (4000 psi = 27.58 MPa) was selected as a starting point. Later, this value has been adjusted to match the AVT results. Having these two factors, the specified compressive strength of clay masonry assemblages, f_m , can be determined directly using Table 8. Subsequently, the modulus of elasticity, $E_m = 700 \times f_m$, and the modulus of rigidity (shear modulus), $E_v = 0.4 E_m$, are calculated. Assuming the masonry wall material as homogenous isotropic linear elastic, the Poisson's ratio, ν , is determined as follows:

$$\nu = \frac{E_m}{2 \times E_v} - 1 = \frac{E_m}{2 \times 0.4 \times E_m} - 1 = 0.25 \quad (4.3)$$

There are two more parameters remained to be determined: the equivalent panel thickness and density of the infill wall. The panel element is a solid element while the infill wall is composed of hollow *terra cotta* units. Therefore, the equivalent solid thickness (EST), which is the volume of solid material divided by the face of the wall), should be calculated. This is done by subtracting the thickness of the perforations from the total thickness of the wall (4"). Since the perforated masonry units are replaced by solid units, the same thing should be done regarding density. In other words, the density of solid brick should be used instead of hollow brick density. The properties used for panel elements in this step are listed in Table 9.

Figures 33 and 34 illustrate the generated full-frame models of both blocks #7 and #8 using panel elements.

Table 8 - Clay masonry properties based on the masonry unit strength and the mortar type (Amrhein 1998; Committee 2005a; Committee 2005b)

Type N Mortar							
Compressive Strength of Clay Masonry		Specified Compressive Strength of Clay Masonry Assemblage f_m		Modulus of Elasticity		Modulus of Rigidity (Shear Modulus)	
				$E_m = 700 \times f_m$ (psi) E_m (max) = 3,000,000 (psi)		$E_v = 0.4 \times E_m = 280 \times f_m$ (psi) E_v (max) = 1,200,000 (psi)	
psi	MPa	psi	MPa	psi	MPa	psi	MPa
14,000 or more	96.53 or more	4,400	30.34	3.08E+06	2.12E+04	1.23E+06	8.49E+03
12,000	82.74	3,800	26.20	2.66E+06	1.83E+04	1.06E+06	7.34E+03
10,000	68.95	3,330	22.96	2.33E+06	1.61E+04	9.32E+05	6.43E+03
8,000	55.16	2,700	18.62	1.89E+06	1.30E+04	7.56E+05	5.21E+03
6,000	41.37	2,200	15.17	1.54E+06	1.06E+04	6.16E+05	4.25E+03
4,000	27.58	1,600	11.03	1.12E+06	7.72E+03	4.48E+05	3.09E+03

Table 9 - Initial properties of terra cotta infill wall

Terra cotta infill wall	
Compressive strength (f_m')	11.03E+03 kN/m ²
mass per unit volume	2.0E+00 tons/m ³
weight per unit volume	1.96E+01 kN/m ³
modulus of elasticity	7.72E+06 kN/m ²
shear modulus (modulus of rigidity)	3.09E+06 kN/m ²
Poisson's ratio	0.25
Equivalent thickness	40 mm

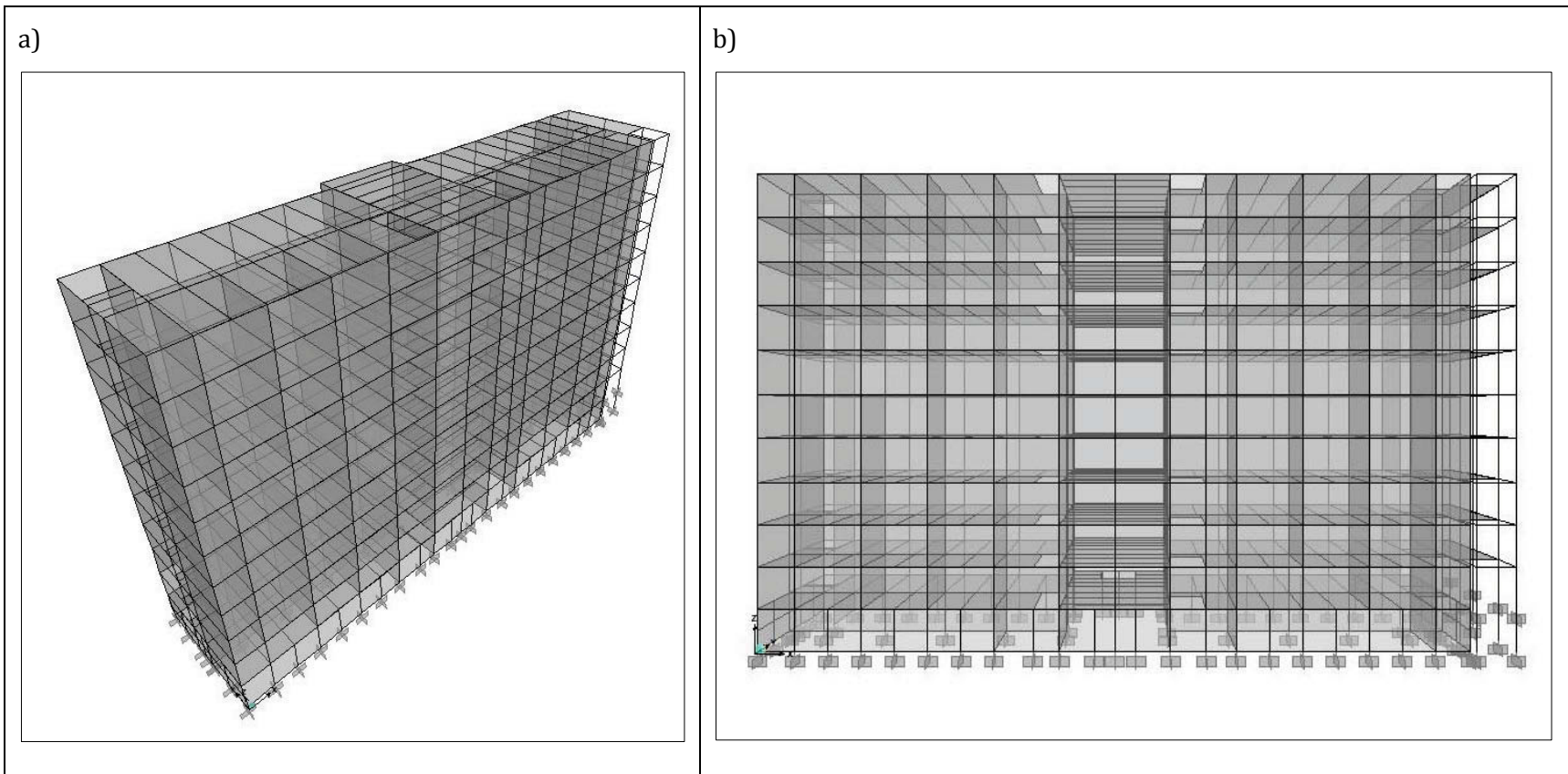


Figure 33-Full-frame model using panel elements - Block#8: a & b) 3D views;

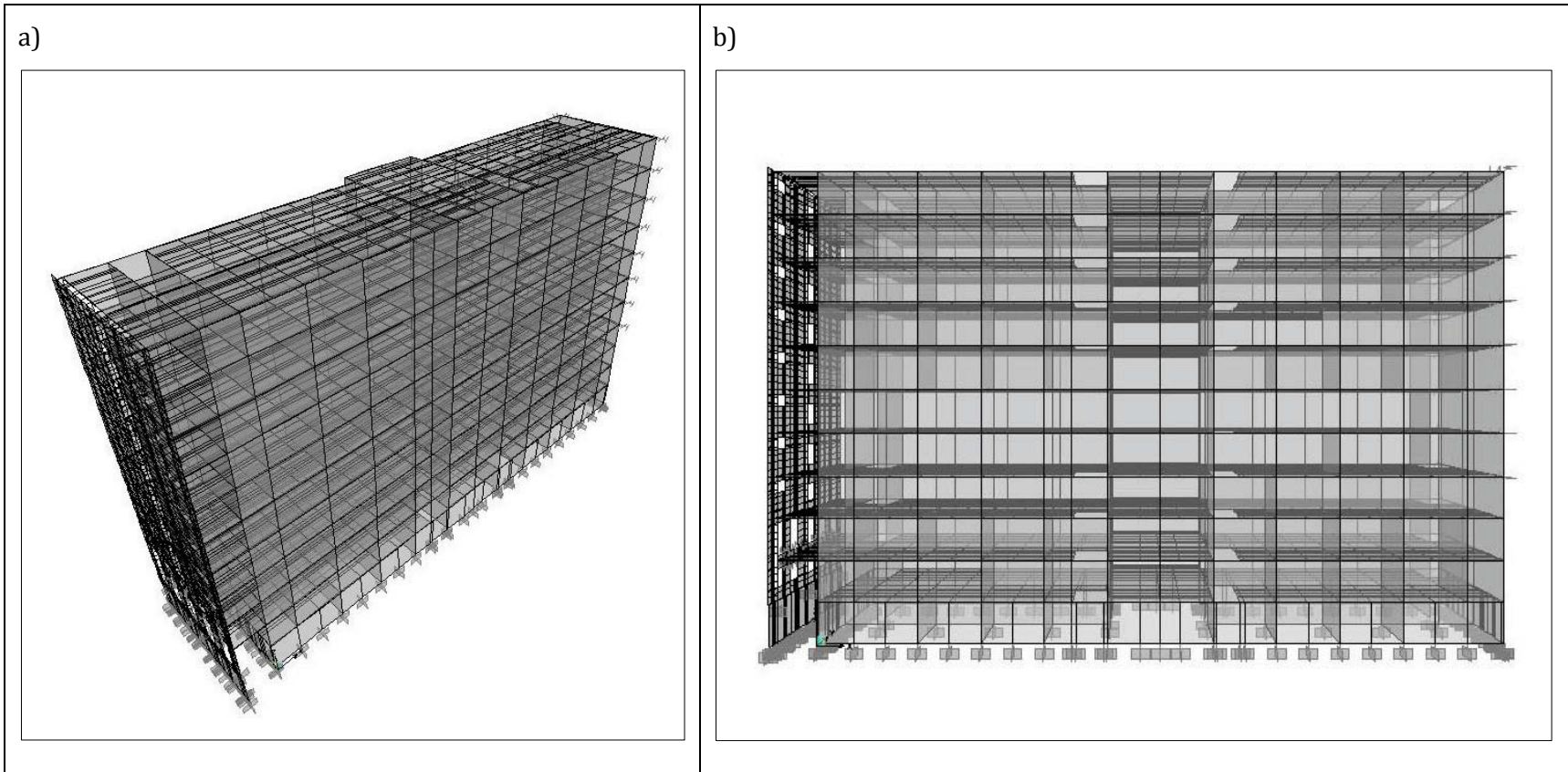


Figure 34- Full-frame model using panel elements - Block#7: a & b)3D views;

4.2.2.2 Equivalent diagonal compression struts

The other method for modeling the in-plane response of masonry infill walls is the equivalent diagonal compression strut model. It means that the wall bounded by beams and columns could be replaced by an equivalent diagonal strut connecting the four corners of the bounding frame. The strut has a length equal to the diagonal of the wall and its thickness (in out-of-plane direction) and modulus of elasticity are the same as the wall's. The width of the strut, which is called "effective width", is a function of different parameters such as the wall's aspect ratio, relative stiffness of the column and infill, and stiffness of the beams. Among all the studies carried out in this field, three different formulas suggested in the literature were used to calculate the effective width of the strut (see Figure 35); they are as follows:

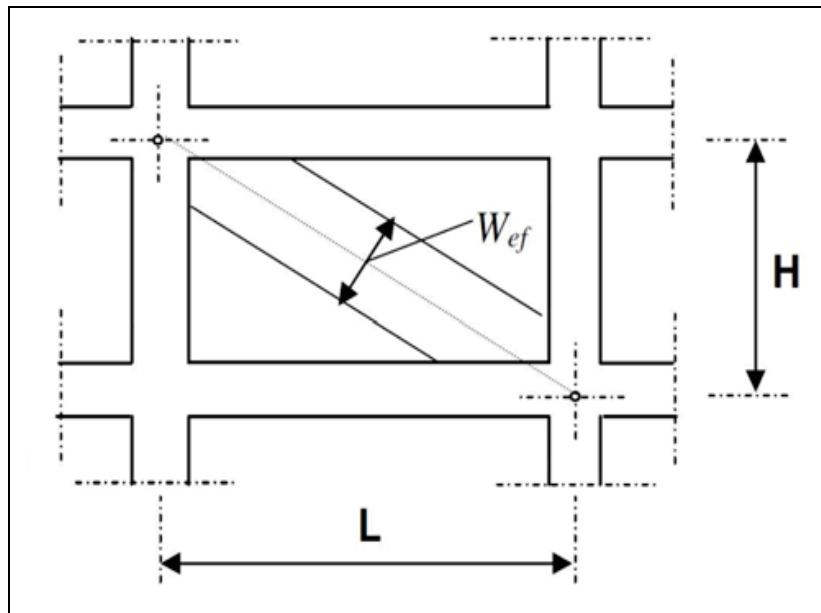


Figure 35 – Diagonal Compression strut- Effective width

1- Stafford Smith, B[16]

$$\lambda h = \sqrt[4]{\left(\frac{E_c \times t \times \sin 2\theta}{4EIh'}\right)} \times h \quad (4.4)$$

In which E_c , t , and h' are the elastic modulus, thickness, and height of the brick masonry infill respectively; E and I are the Young's modulus and second moment of area of the surrounding frame member (Column), h is the column height; and θ is the angle between the infill diagonal and the horizontal. λ is a non-dimensional parameter that is a characteristic of the infill frame for a rectangular frame. Then, λh , represents the relative stiffness of the infill to the column. After calculating λh , the ratio of effective width to the diagonal length of infill, (w_{eff}/d), can be read from the experimental curves provided by Stafford Smith and w_{eff} is determined [16].

2- Durrani, A.J., Y. Luo, and D.P. Abrams[18]

$$W_{\text{eff}} = \gamma \times \sqrt{L^2 + H^2} \sin 2\theta \quad (4.5)$$

$$\gamma = 0.32 \sqrt{\sin 2\theta} \left[\frac{H^4 E_w t_w}{m E_c I_c H_{\text{in}}} \right]^{-0.1} \quad (4.6)$$

$$m = \left[1 + \frac{6E_b I_b H}{\pi E_c I_c L} \right] \quad (4.7)$$

in which H and L are the storey height and the bay length of the frame, respectively, $\theta = \arctan(H/L)$ is the inclination of the diagonal to the horizontal, H_{in} is the net height of the infill panel, E_w is the elastic modulus of the infill wall, t_w is the thickness of the wall panel, E_c and E_b are the elastic

moduli of the frame column and beam material, respectively, and I_c and I_b are the second moments of area of the column and beam of the frame, respectively. W_{eff} is the effective width of the diagonal strut [18].

3- FEMA-356, Prestandard and commentary for the seismic rehabilitation of buildings [20]

In FEMA-356 it is mentioned that the elastic in-plane stiffness of a solid unreinforced masonry infill panel prior to cracking shall be represented with an equivalent diagonal compression strut of width, a , given by Equation (4.8). The equivalent strut shall have the same thickness and modulus of elasticity as the infill panel. It represents [20].

$$a = 0.175(\lambda_1 h_{col})^{-0.4} \times r_{inf} \quad (4.8)$$

where:

$$\lambda_1 = \sqrt[4]{\left(\frac{E_{me} \times t_{inf} \times \sin 2\theta}{4 E_{fe} I_{col} h_{inf}} \right)} \quad (4.9)$$

in which:

h_{col} = Column height between centerlines of beams, in.

h_{inf} = Height of infill panel, in.

E_{fe} = Expected modulus of elasticity of frame material, ksi

E_{me} = Expected modulus of elasticity of infill material, ksi

I_{col} = Second moment of area of column, in⁴.

L_{inf} = Length of infill panel, in.

r_{inf} = Diagonal length of infill panel, in.

t_{inf} = Thickness of infill panel and equivalent strut, in

θ = Angle whose tangent is the infill height-to-length aspect ratio, radians

λ_1 = Coefficient used to determine equivalent width of infill strut

Using these three different approaches, the effective width of struts have been determined. Accordingly, three separate models have been generated each based on one of the aforementioned approach.

The replacement of a complete wall panel with diagonal struts causes a reduction in the reactive mass in the model. This decrease in total mass of infills should be compensated with adding the mass difference to the model. To do so in a simple way, the mass of the struts are considered as zero and instead the total mass of infills at each floor is calculated and distributed uniformly over the floor slab.

Figures 36 and 37 illustrate the generated full-frame models of both blocks using the equivalent diagonal strut technique. Since the only difference between the three adopted techniques is the effective width values, they are all shown with one figure.

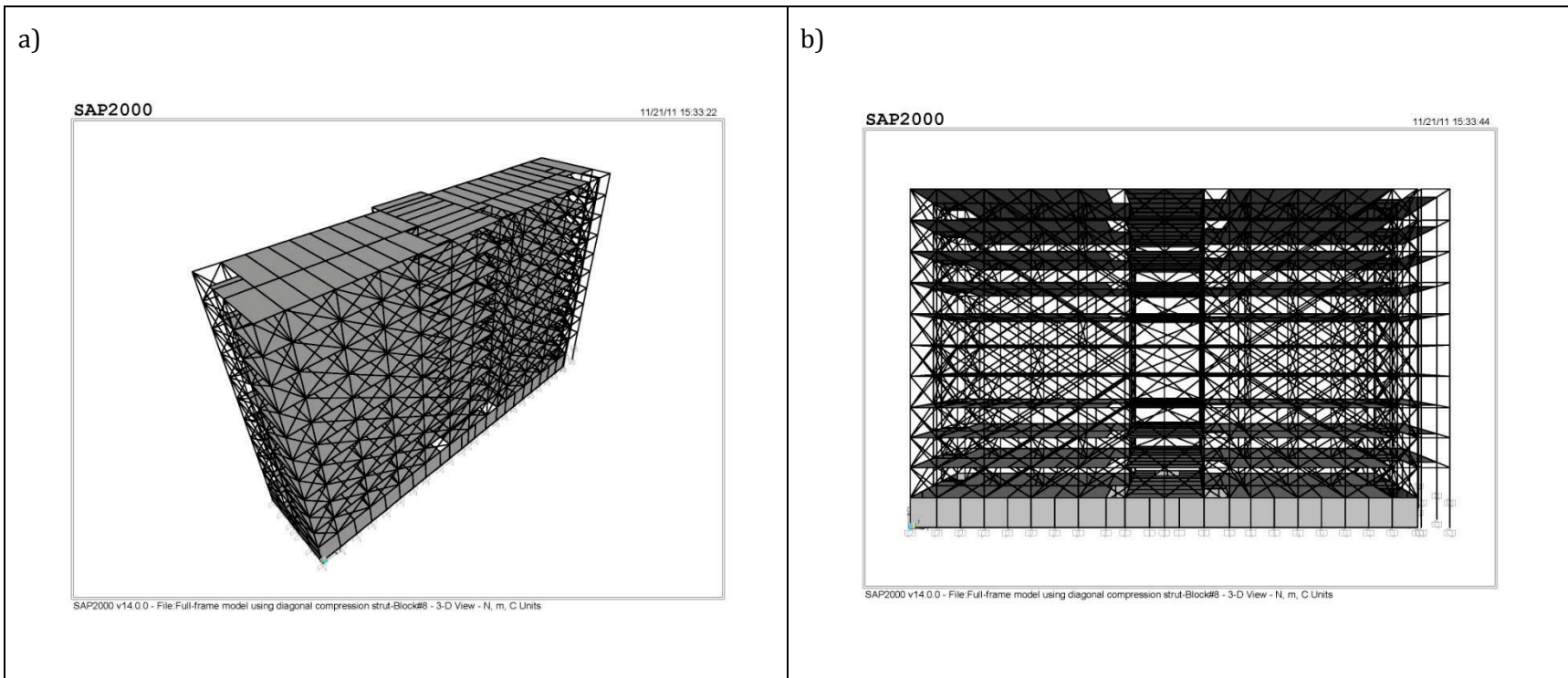


Figure 36- Full-frame model using diagonal compression struts - Block#8: a & b) 3D views;

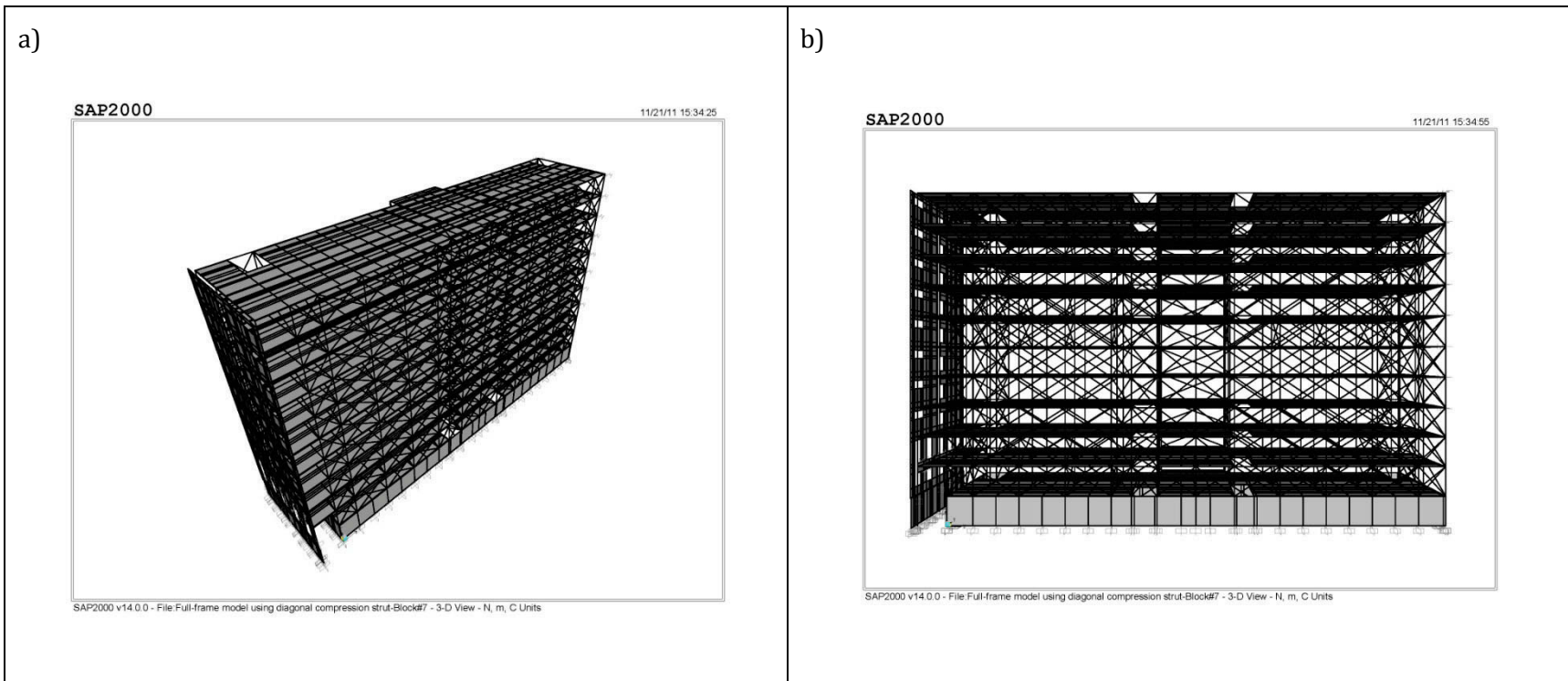


Figure 37- Full-frame model using diagonal compression struts - Block#7: a & b)3D views;

4.3 Calibration of numerical models using AVT results

Determining the real properties of masonry assemblies is a complicated task. It is due to the facts that: a masonry wall is a composite assembly of masonry units and mortar, by nature, the constitutive materials are not homogeneous, and in reality, the wall is not isotropic, i.e. it does not have identical properties in all directions. Hence, a common way to determine the mechanical properties of masonry walls is by experimental testing, which was not possible in our study. An alternative is using recommended properties available in the literature. Considering data from masonry standards [35, 37] and a masonry handbook [36], the smallest recommended compressive strength value (most conservative properties) was selected as the starting assumption in the models. Then, after completion of the initial frequency analysis, the results have been compared with those extracted from the AVT records and the material properties of masonry in the models were adjusted to match the first natural frequency of the continuum model of block#8 (the closest model to the AVT) in each horizontal direction and also to match the torsional frequency. In other words, the material properties resulting in the best match between the first three natural frequencies of continuum model of block#8 and AVT results have been selected. The revised masonry properties are then applied to all the FE models that included infill walls. Lastly, the calibrated (or adjusted) FE models are also subjected to frequency analysis and the results are compared to the AVT results. Finally, the model yielding results closest to the AVT results is retained for seismic analysis. The details will be discussed later in chapter 5.

It should be mentioned that the calibration described above was based on block#8 only due its simplicity compared to block#7. The same adjusted masonry properties, derived using block#8 results, have also been applied to block#7.

4.4 Time-history seismic analysis and development of Floor Response Spectra and Interstorey-Drift curves

In this step of the study, the calibrated models finally retained as described in section 4.3 are subjected to a series of horizontal base inputs including 12 synthetic ground accelerograms compatible with the NBC Uniform Hazard Spectra (UHS) for Montréal [38], corresponding to probabilities of exceedance of 2% in 50 years. These 12 synthetic time-histories have been adopted from the study done by Assi [39]. Note that this study used the seismicity specified in the 2005 edition of NBC, while the ground accelerations should be adjusted (actually lowered) according to NBC 2010. These synthetic records were generated using the stochastic approach presented by Atkinson and Beresnev [40]. A total number of 6 magnitude-distance (M-R) scenarios were used to cover the entire frequency range of interest. Due to the randomness of the generated records, two acceleration time-histories were used for each M-R scenario (Table 10). The scaling factor and PGA of each scaled record are listed in Table 11.

Table 10 - Characteristics of M-R scenarios considered for Montreal

Magnitude M	Epicentral distance (km)	Δt (s)	Length [s]	Return Period (years)	Records name	
					1 st record	2 nd record
6	30	0.01	8.89	2500	E60301	E60302
6	50	0.01	1241	2500	E60502	E60503
7	30	0.01	1704	2500	E70301	E70302
7	50	0.01	2055	2500	E70501	E70502
7	70	0.01	2408	2500	E70701	E70702
7	100	0.01	2308	2500	E701001	E701002

Table 11 – Scaling factor and PGA of scaled records

Records name	Scaling factor	PGA (g)
E60301	1.02	0.44
E60302	0.76	0.40
E60501	1.74	0.42
E60502	1.76	0.33
E70301	0.32	0.31
E70302	0.24	0.25
E70501	0.56	0.28
E70502	0.54	0.34
E70701	0.92	0.28
E70702	1.00	0.29
E701001	1.00	0.24
E701002	1.08	0.28

The records are scaled based on the UHS provided in NBC for Montreal considering the soil site condition of class C. To scale the records, firstly the Response Spectrum (RS) of each record is specified in terms of Pseudo Acceleration (PA) using the software SeismoSignal [41]. The RS of each record is then compared with the introduced UHS. Afterward, the RS is matched with UHS at three different periods using scaling factors. These periods represent the longest three modal periods of the buildings. Consequently, three scaling factors are computed for each record. Next, the entire RS is scaled by the factors. The scaled RS curves are drawn in the same graph as the UHS and the scaling factor resulting in the best match has been selected. Figures 38, 39, and 40 schematically show the procedure explained above for one record.

The scaled records are then applied as input to both principal horizontal directions (longitudinal and transverse directions of the structure) of each building independently as prescribed in the NBC 2005 (section 4.1.8.8) [4]. The linear time-history seismic analysis has been carried out using SAP2000 [34]. Then selecting two floors in each block (top floor #7 and middle floor #

3), Floor Response Spectra (FRS) and Interstorey-Drift curves were developed for each record. To produce the FRS, the response of each floor due to the particular record was extracted and presumed as the ground excitation for the NSCs mounted on that floor. The results will be comprehensively discussed in chapter 5.

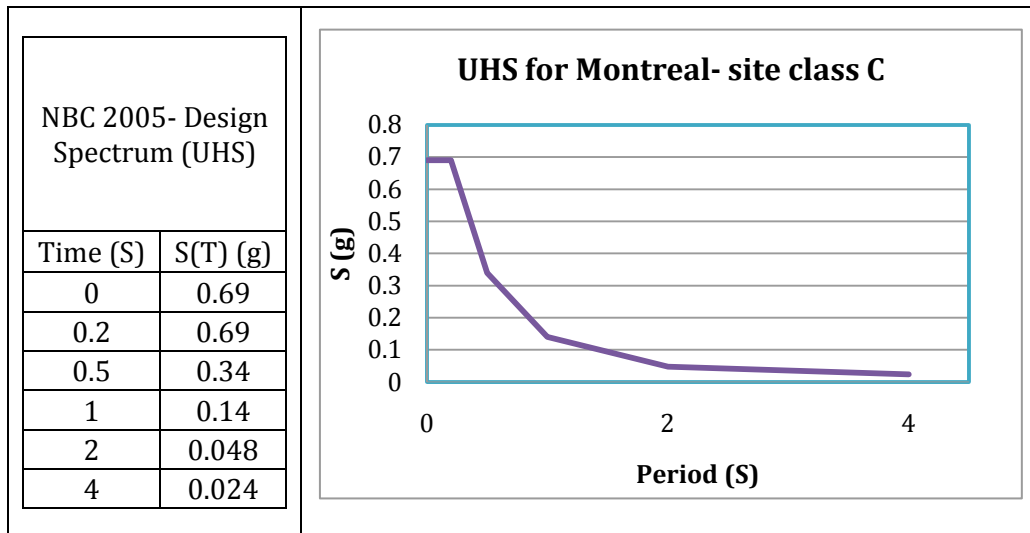


Figure 38- NBC 2005 UHS for Montreal

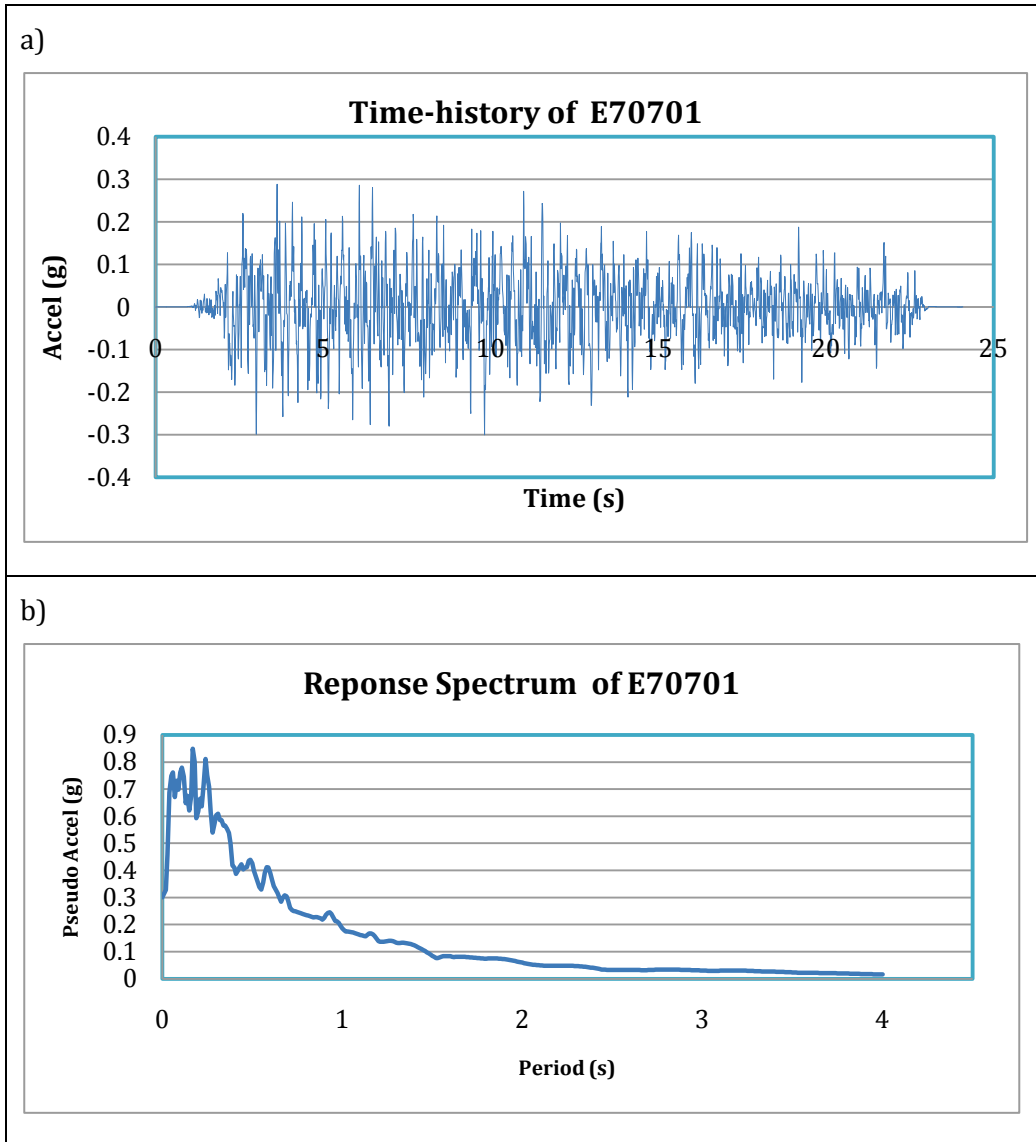


Figure 39- Example of ground motion record (E70701): a) Time-history, b) Response spectrum

Table 12 - Scale factor calculation based on first three modes-E70701

Fundamental periods of block#8, full-frame model using panel element		NBCC- S(T)	E70701	Scale Factor
Mode#1	0.60	0.30	0.39	0.769
Mode#2	0.41	0.44	0.42	1.047
Mode#3	0.35	0.52	0.57	0.915

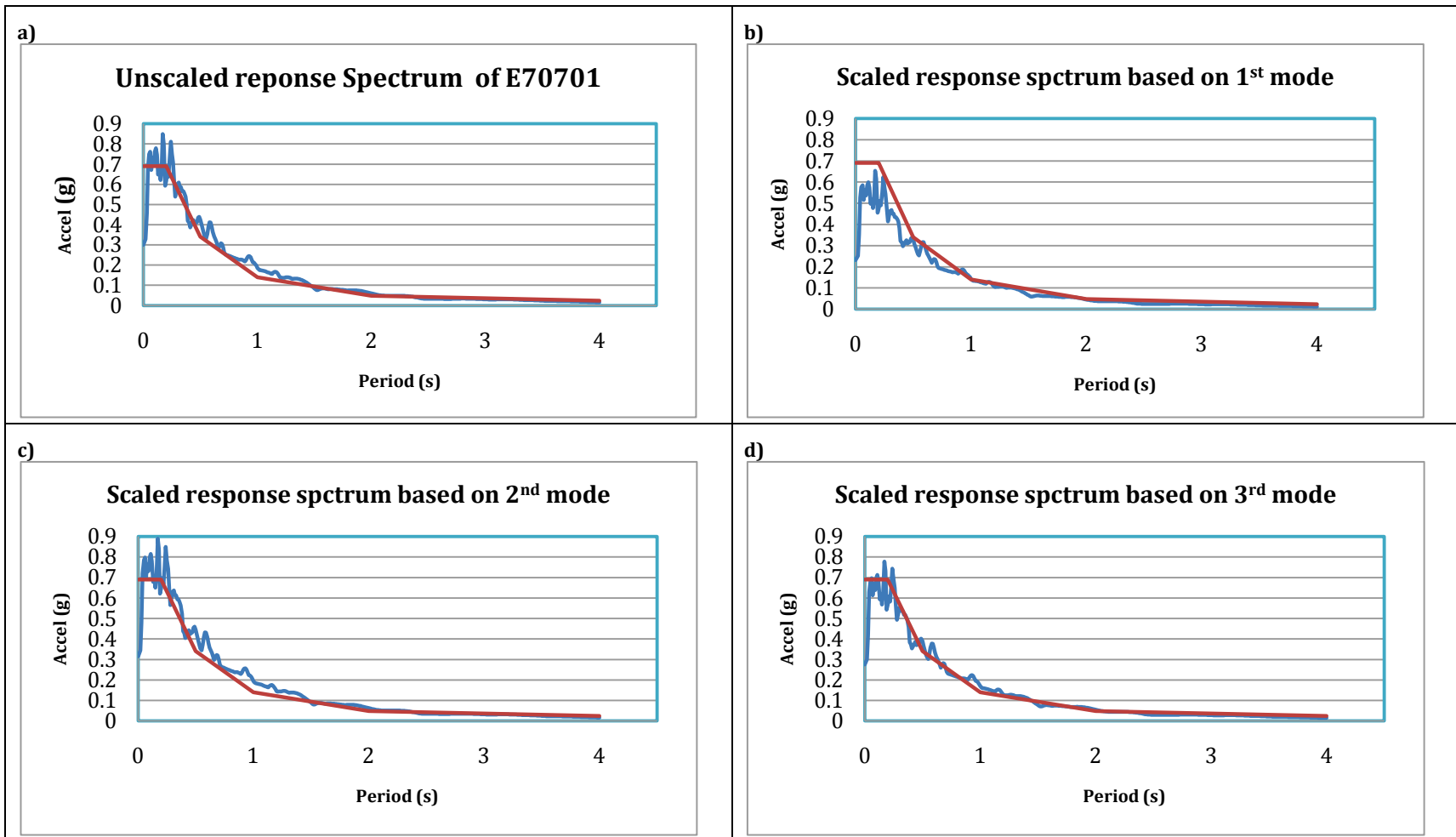


Figure 40- Comparison between response spectrum of E70701 and UHS: a)Unscaled RS; b)Scaled RS based on 1st mode; c) Scaled RS based on 2nd mode; d) Scaled RS based on 3rd mode (best match)

5 Results and discussion

So far in the thesis, the different aspects and assumptions of the numerical study have been presented in details. Now, the numerical results obtained for frequency analysis and seismic analysis will be presented and discussed in detail. It should be noted that this section presents the results derived after the calibration and verification of the FE models.

In the following discussions, the transverse direction is the direction along the smaller plan dimension of the buildings (weak direction) and the longitudinal means the direction along the larger one (strong direction).

5.1 Bare-frame model results

The periods and frequencies corresponding to the first fundamental modes of the bare-frame models of blocks #8 and #7 are listed in Tables 13 and 14, respectively. For block#7, two different models are presented: the first one is the model in which the block#7 is separated from block#9 and the connections are not defined, and the second model includes the connections. This is done to compare the effect of the seismic shear wall and the effect of connections on the dynamic properties of the building.

Table 13 - Bare-frame model results - Block#8

Block # 8		
Models	Bare-frame model (excluding masonry infill walls)	
Mode shape	Period (s)	Frequency (Hz)
1 st transverse mode	1.76	0.57
1 st longitudinal mode	1.56	0.64
1 st torsional mode	1.53	0.65
2 nd transverse mode	0.63	1.58
2 nd longitudinal mode	0.58	1.73
2 nd torsional mode	0.56	1.80

Table 14 - Bare-frame model results - Block#7

Block # 7				
Models	Bare-frame model (excluding masonry infill)			
	Not-connected to block#9		Connected to block#9	
Mode shape	Period (s)	Frequency (Hz)	Period (s)	Frequency (Hz)
1 st transverse mode	1.71	0.59	0.64	1.56
1 st longitudinal mode	1.57	0.64	0.31	3.19
1 st torsional mode	0.62	1.61	0.17	5.79
2 nd transverse mode	0.62	1.61	0.24	4.16
2 nd longitudinal mode	0.58	1.72	0.26	3.84

Considering the result presented in Tables 13 and 14, the following observations are made:

- 1- The difference between the natural frequencies (and periods) of block#8 and block#7-not connected to block#9- is not considerable except for the torsional mode where the added shear wall (Table 15) contributes very significantly to stiffen the building. Since the shear wall is attached to the end of block#7, it is far away from the CR and therefore, it is highly effective in resisting the torsional moments.

However, because the shear wall is oriented along the short direction of the building, it affects the longitudinal mode only slightly as expected. For the same reason (transverse orientation of shear wall), its effect should be observed mostly in the fundamental transverse mode but this behaviour cannot be seen in the results. It can be explained by the fact that in the model of block#7 excluding the connections to building #9, one end of the building is restrained by the shear wall while the other end is free to move. This makes the building torsionally irregular and the fundamental mode of block#7 is a combined translational-torsional mode, instead of a main translation, and the displacement is concentrated at the free end (Figure 41-b). Thus, the first mode of block#7 (not-connected model) cannot be compared directly with the nearly transverse mode of block#8.

Table 15 - Comparison between calculated natural frequencies of Block 8 and Block 7

Models	Bare-frame model (excluding masonry infill)		
	Block#8	Block#7(Not-connected to block#9)	Difference relative to block#7 (%)
Mode shape	Frequency (Hz)	Frequency (Hz)	
1 st transverse mode	0.57	0.59	-----
1 st longitudinal mode	0.64	0.64	0.09%
1 st torsional mode	0.65	1.61	59.30%
2 nd transverse mode	1.58	1.61	-----
2 nd longitudinal mode	1.73	1.72	0.5%

2- By comparing the two models of Block#7(Not-connected and connected models to Block#9), it can be inferred that the stiffening effect of connecting blocks #7 and #9 is noticeably more important than the effect of adding the shear wall only, and this trend can be observed in all the calculated modes of vibration listed in table 16.

Table 16 - Comparison between calculated natural frequencies of two models of block#7

Models	Block#7 - Bare-frame model (excluding masonry infill)		
	Not-connected to block#9	Connected to block#9	Difference relative to the Not-connected model (%)
Mode shape	Frequency (Hz)	Frequency (Hz)	
1 st translational mode	0.59	1.56	166%
1 st longitudinal mode	0.64	3.19	400%
1 st torsional mode	1.61	5.79	261%
2 nd transverse mode	1.61	4.16	158%
2 nd longitudinal mode	1.72	3.84	122%

- 3 In the model of Block #7 including connections, the first mode is also translational-torsional as there is torsional irregularity caused by the difference between the added stiffness contributed by the seismic shear wall to Block #7 and by connecting it to Block #9: the connected end to Block #9 is much stiffer than the shear wall end. Therefore, in contrary to the Not-connected model, in the fundamental mode of this model the displacement is mainly concentrated at the connected end to the shear wall (Figure 41-c).

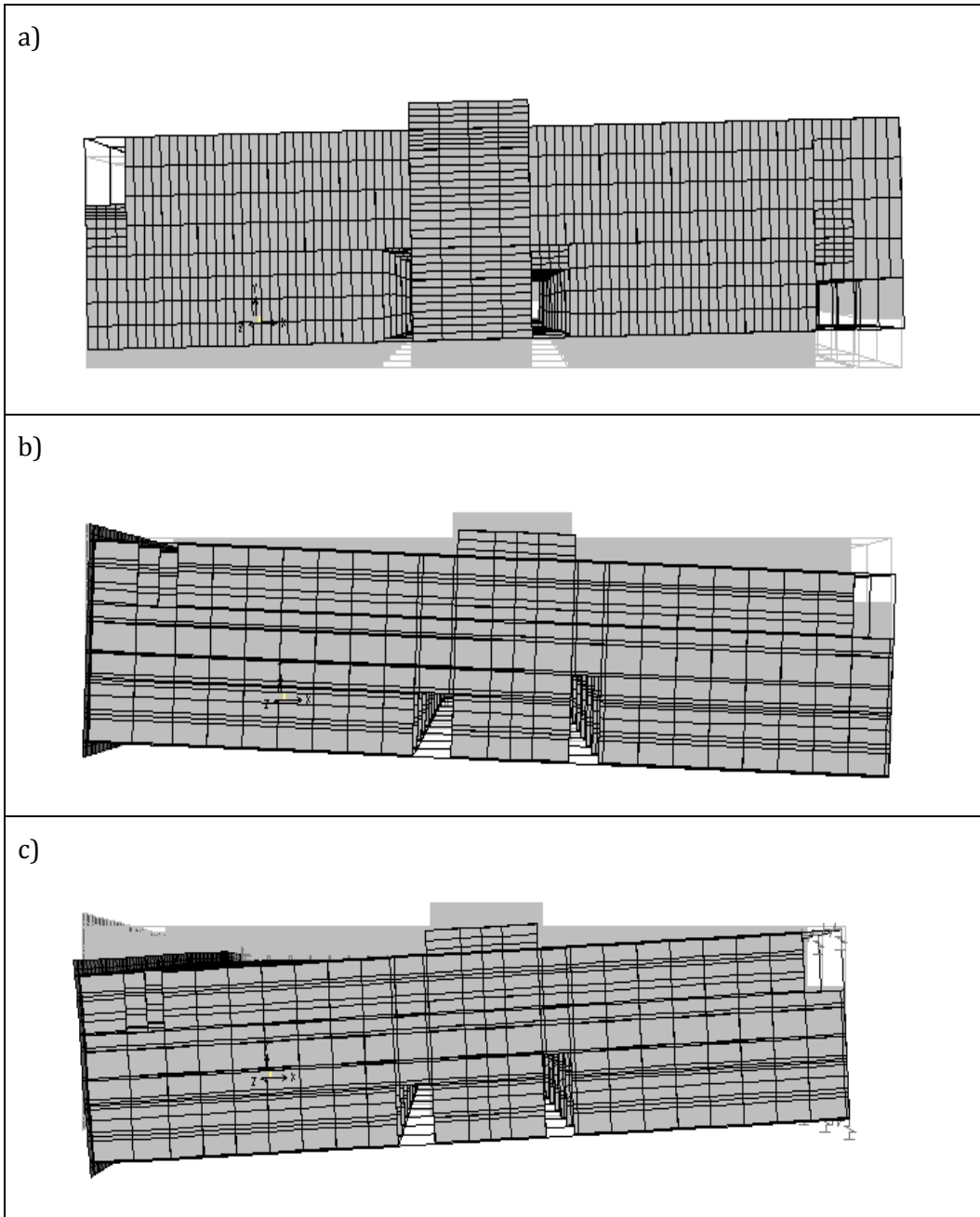


Figure 41- First mode of vibration of bare-frame models: a)Block#8; b)Block#7- Not connected model to block#9; c)Block#7- Connected model to block#9

5.2 Full-frame model results

In this section, the natural frequency results of all calibrated models of both blocks including the bare-frame model, continuum model, and diagonal compression strut model, which in turn comprises three different sub-models, are presented and compared with the AVT results in Tables 17-28. The bare-frame results are also included in this section since they are needed to discuss the calibration procedure and selection of the numerical model yielding results closest to AVT. The difference between the modal frequencies of each calibrated model and AVT result are calculated relative to the AVT frequencies and presented in percentage. In Tables 22 and 28 the difference is calculated relative to bare-frame models. The discussion of the results will follow the tables.

5.2.1 Results of Block#8

Table 17 - Comparison of bare-frame model and AVT results- Block#8

Block#8 - Bare-frame model												
Mode shape	1 st transverse mode		1 st longitudinal mode		1 st torsional mode		2 nd transverse mode		2 nd longitudinal mode		2 nd torsional mode	
	Period (s)	Frequency (Hz)	Period (s)	Frequency (Hz)	Period (s)	Frequency (Hz)	Period (s)	Frequency (Hz)	Period (s)	Frequency (Hz)	Period (s)	Frequency (Hz)
Bare-frame model	1.76	0.57	1.56	0.64	1.53	0.65	0.63	1.58	0.58	1.73	0.56	1.80
ARTEMIS-EFDD-Aug 2010	0.53	1.90	0.38	2.67	0.40	2.48	0.19	5.39	0.14	7.40	0.13	7.82
Difference	-----	70%	-----	76%	-----	74%	-----	71%	-----	77%	-----	77%

Table 18 - Comparison of full-frame model (continuum model) and AVT results- Block#8

Block#8 - Full frame model - Panel element (continuum model)												
Mode shape	1 st transverse mode		1 st longitudinal mode		1 st torsional mode		2 nd transverse mode		2 nd longitudinal mode		2 nd torsional mode	
Models	Period (s)	Frequency (Hz)	Period (s)	Frequency (Hz)	Period (s)	Frequency (Hz)	Period (s)	Frequency (Hz)	Period (s)	Frequency (Hz)	Period (s)	Frequency (Hz)
Continuum model	0.60	1.66	0.35	2.88	0.41	2.43	0.18	5.44	-----	-----	-----	-----
ARTEMIS-EFDD-Aug 2010	0.53	1.90	0.38	2.67	0.40	2.48	0.19	5.39	0.14	7.40	0.13	7.82
Difference	-----	12%	-----	8%	-----	2%	-----	1%	-----	-----	-----	-----

Table 19 - Comparison of full-frame model (Stafford Smith model for diagonal compression strut) and AVT results- Block#8

Block#8 - Full frame model - Diagonal compression strut (Stafford Smith model)												
Mode shape	1 st transverse mode		1 st longitudinal mode		1 st torsional mode		2 nd transverse mode		2 nd longitudinal mode		2 nd torsional mode	
Models	Period (s)	Frequency (Hz)	Period (s)	Frequency (Hz)	Period (s)	Frequency (Hz)	Period (s)	Frequency (Hz)	Period (s)	Frequency (Hz)	Period (s)	Frequency (Hz)
Stafford Smith	0.91	1.10	0.60	1.68	0.69	1.45	0.31	3.26	0.21	4.69	0.24	4.18
ARTEMIS-EFDD-Aug 2010	0.53	1.90	0.38	2.67	0.40	2.48	0.19	5.39	0.14	7.40	0.13	7.82
Difference	-----	42%	-----	37%	-----	41%	-----	40%	-----	37%	-----	47%

Table 20 - Comparison of full-frame model (Durrani & Luo model model for diagonal compression strut) and AVT results- Block#8

Block#8 - Full frame model - Diagonal compression strut (Durrani & Luo model)												
Mode shape	1 st transverse mode		1 st longitudinal mode		1 st torsional mode		2 nd transverse mode		2 nd longitudinal mode		2 nd torsional mode	
	Period (s)	Frequency (Hz)	Period (s)	Frequency (Hz)	Period (s)	Frequency (Hz)	Period (s)	Frequency (Hz)	Period (s)	Frequency (Hz)	Period (s)	Frequency (Hz)
Durrani AJ, Luo YH	0.90	1.11	0.60	1.66	0.69	1.45	0.30	3.36	0.21	4.79	0.23	4.29
ARTEMIS-EFDD-Aug 2010	0.53	1.90	0.38	2.67	0.40	2.48	0.19	5.39	0.14	7.40	0.13	7.82
Difference	-----	41%	-----	38%	-----	41%	-----	38%	-----	35%	-----	45%

Table 21 - Comparison of full-frame model (FEMA-356 model for diagonal compression strut) and AVT results- Block#8

Block#8 - Full frame model - Diagonal compression strut (FEMA-356 model)												
Mode shape	1 st transverse mode		1 st longitudinal mode		1 st torsional mode		2 nd transverse mode		2 nd longitudinal mode		2 nd torsional mode	
	Period (s)	Frequency (Hz)	Period (s)	Frequency (Hz)	Period (s)	Frequency (Hz)	Period (s)	Frequency (Hz)	Period (s)	Frequency (Hz)	Period (s)	Frequency (Hz)
FEMA-356 model	1.04	0.97	0.76	1.32	0.83	1.21	0.35	2.86	0.26	3.80	0.28	3.53
ARTEMIS-EFDD-Aug 2010	0.53	1.90	0.38	2.67	0.40	2.48	0.19	5.39	0.14	7.40	0.13	7.82
Difference	-----	49%	-----	50%	-----	51%	-----	47%	-----	49%	-----	55%

Table 22 - Comparison of the full-frame models with the bare-frame model

Block#8												
Mode shape	1 st transverse mode		1 st longitudinal mode		1 st torsional mode		2 nd transverse mode		2 nd longitudinal mode		2 nd torsional mode	
Models	Period (s)	Frequency (Hz)	Period (s)	Frequency (Hz)	Period (s)	Frequency (Hz)	Period (s)	Frequency (Hz)	Period (s)	Frequency (Hz)	Period (s)	Frequency (Hz)
Bare-frame model	1.76	0.57	1.56	0.64	1.53	0.65	0.63	1.58	0.58	1.73	0.56	1.80
Continuum model	0.60	1.66	0.35	2.88	0.41	2.43	0.18	5.44	-----	-----	-----	-----
Difference	193%	66%	-----	78%	-----	73%	-----	71%	-----	-----	-----	-----
Bare-frame model	1.76	0.57	1.56	0.64	1.53	0.65	0.63	1.58	0.58	1.73	0.56	1.80
Stafford Smith	0.91	1.10	0.60	1.68	0.69	1.45	0.31	3.26	0.21	4.69	0.24	4.18
Difference	-----	48%	-----	62%	-----	55%	-----	52%	-----	63%	-----	57%
Bare-frame model	1.76	0.57	1.56	0.64	1.53	0.65	0.63	1.58	0.58	1.73	0.56	1.80
Durrani AJ, Luo YH	0.90	1.11	0.60	1.66	0.69	1.45	0.30	3.36	0.21	4.79	0.23	4.29
Difference	-----	49%	-----	61%	-----	55%	-----	53%	-----	64%	-----	58%
Bare-frame model	1.76	0.57	1.56	0.64	1.53	0.65	0.63	1.58	0.58	1.73	0.56	1.80
FEMA-356	1.04	0.97	0.76	1.32	0.83	1.21	0.35	2.86	0.26	3.80	0.28	3.53
Difference	-----	41%	-----	52%	-----	46%	-----	45%	-----	54%	-----	49%

5.2.2 Results of Block #7

Table 23 - Comparison of bare-frame model and AVT results- Block#7

Block#7 - Bare-frame model						
Mode shape	1 st transverse mode		1 st longitudinal mode		1 st torsional mode	
Models	Period(s)	Frequency(Hz)	Period(s)	Frequency(Hz)	Period(s)	Frequency(Hz)
Bare-frame model	0.64	1.56	0.31	3.19	0.17	5.79
ARTEMIS-EFDD-Sep 2010	0.54	1.86	0.487	2.053	0.327	3.06
Difference	-----	16%	-----	-55%	-----	89%
ARTEMIS-EFDD-July 2011	0.53	1.83	0.5	2.00	0.35	2.88
Difference	-----	15%	-----	60%	-----	101%

Table 24 - Comparison of full-frame model (continuum model) and AVT results- Block#7

Block#7 - Full frame model - Panel element (continuum model)						
Mode shape	1 st transverse mode		1 st longitudinal mode		1 st torsional mode	
	Period(s)	Frequency(Hz)	Period(s)	Frequency(Hz)	Period(s)	Frequency(Hz)
Models						
Continuum model	0.47	2.1	0.25	4.00	0.18	5.63
ARTEMIS-EFDD-Sep 2010	0.54	1.86	0.49	2.05	0.33	3.06
Difference	-----	15%	-----	95%	-----	84%
ARTEMIS-EFDD-July 2011	0.55	1.83	0.5	2.00	0.35	2.89
Difference	-----	17%	-----	100%	-----	95%

Table 25 - Comparison of full-frame model (Stafford Smith model for diagonal compression strut) and AVT results- Block#7

Block#7 - Full frame model - Diagonal compression strut (Stafford Smith model)						
Mode shape	1 st transverse mode		1 st longitudinal mode		1 st torsional mode	
	Period(s)	Frequency(Hz)	Period(s)	Frequency(Hz)	Period(s)	Frequency(Hz)
Models						
Stafford Smith	0.58	1.72	0.31	3.21	0.19	5.32
ARTEMIS-EFDD-Sep 2010	0.54	1.86	0.49	2.05	0.33	3.06
Difference	-----	8%	-----	56%	-----	74%
ARTEMIS-EFDD-July 2011	0.55	1.83	0.5	2.00	0.35	2.89
Difference	-----	6%	-----	60%	-----	85%

Table 26 - Comparison of full-frame model (Durrani & Luo model model for diagonal compression strut) and AVT results- Block#7

Block#7 - Full frame model - Diagonal compression strut (Durrani & Luo model)						
Mode shape	1 st transverse mode		1 st longitudinal mode		1 st torsional mode	
	Period(s)	Frequency(Hz)	Period(s)	Frequency(Hz)	Period(s)	Frequency(Hz)
Models						
Durrani AJ, Luo YH	0.58	1.74	0.30	3.35	0.18	5.48
ARTEMIS-EFDD-Sep 2010	0.54	1.86	0.49	2.05	0.33	3.06
Difference	-----	7%	-----	63%	-----	79%
ARTEMIS-EFDD-July 2011	0.55	1.83	0.5	2.00	0.35	2.89
Difference	-----	5%	-----	68%	-----	90%

Table 27 - Comparison of full-frame model (FEMA-356 model for diagonal compression strut) and AVT results- Block#7

Block#7 - Full frame model - Diagonal compression strut (FEMA-356 model)						
Mode shape	1 st transverse mode		1 st longitudinal mode		1 st torsional mode	
	Period(s)	Frequency(Hz)	Period(s)	Frequency(Hz)	Period(s)	Frequency(Hz)
Models						
FEMA-356	0.61	1.64	0.31	3.23	0.18	5.43
ARTEMIS-EFDD-Sep 2010	0.54	1.86	0.49	2.05	0.33	3.06
Difference	-----	12%	-----	57%	-----	78%
ARTEMIS-EFDD-July 2011	0.55	1.83	0.5	2.00	0.35	2.89
Difference	-----	10%	-----	61%	-----	88%

Table 28 - Comparison of the full-frame models with the bare-frame model

Block#7						
Mode shape	1 st transverse mode		1 st longitudinal mode		1 st torsional mode	
Models	Period(s)	Frequency(Hz)	Period(s)	Frequency(Hz)	Period(s)	Frequency(Hz)
Bare-frame model	0.64	1.56	0.31	3.19	0.17	5.79
Continuum model	0.47	2.14	0.25	4.00	0.18	5.63
Difference	-----	27%	-----	20%	-----	3%
Bare-frame model	0.64	1.56	0.31	3.19	0.17	5.79
Stafford Smith	0.58	1.72	0.31	3.21	0.19	5.32
Difference	-----	9%	-----	1%	-----	9%
Bare-frame model	0.64	1.56	0.31	3.19	0.17	5.79
Durrani AJ, Luo YH	0.58	1.74	0.30	3.35	0.18	5.48
Difference	-----	10%	-----	5%	-----	6%
Bare-frame model	0.64	1.56	0.31	3.19	0.17	5.79
FEMA-356	0.61	1.64	0.31	3.22	0.18	5.43
Difference	-----	5%	-----	1%	-----	7%

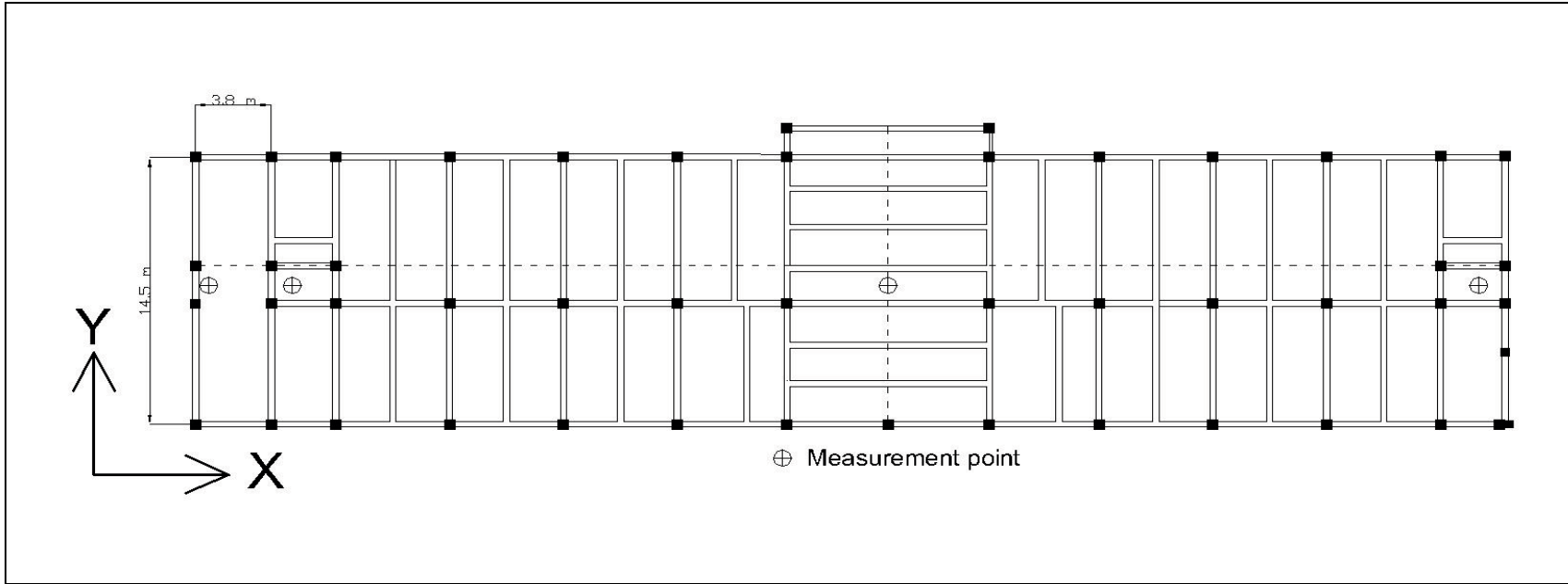


Figure 42- Layout of AVT measurement points distribution in second test series in block#7 and dimensions of balcony

5.3 FE Model Calibration with AVT results

As previously mentioned, the model calibration was based on block#8 due to its simplicity compared to block#7. To calibrate the material properties initially defined for masonry infills, the continuum model was finally selected among all different types of full-frame models to compare with AVT results. This choice was made because the continuum model (with infill panels) yielded the closest natural frequency results to the AVT extracted results (less than 12% difference-Table 18). The only parameter modified in the calibration process was the compressive strength of clay masonry, which was initially taken as the smallest value recommended in Table 9. Therefore, higher values of compressive strength needed to be considered based on Table 9. These different values have been inputted to the model to find the most suitable assumption resulting in the closest frequencies to the ones extracted from AVT. Then, the initial properties have been replaced by the calibrated properties (Table 29) in all the models. After the calibration, the continuum model remains again the closest to the AVT results, while still yielding smaller frequencies than AVT. Considering block#8, the maximum difference between the frequencies of this model and AVT extracted frequencies is 12 % which is deemed acceptable (Table 18).

Table 29 - Calibrated properties of terra cotta infill wall

<i>Terra cotta infill wall</i>	
Compressive strength (f_m')	22.96E+03 kN/m ²
mass per unit volume	2.0E+00 tons/m ³
weight per unit volume	1.96E+01 kN/m ³
modulus of elasticity	1.61E+07 kN/m ²
shear modulus (modulus of rigidity)	6.43E+06 kN/m ²
Poisson's ratio	0.25
Equivalent thickness	40 mm

5.3.1 Discussion of block#8 results

- As presented in Table 17, adding the *terra cotta* infill walls to the bare-frame model of block#8 changes the dynamic properties of the building significantly. The presence of infill walls results in considerable increase in natural frequencies of the building: [70%-77%] increase comparing the bare-frame model with AVT results (difference is calculated relative to the AVT results), and [41%-78%] increase comparing the bare-frame model with each full-frame model separately (difference is calculated relative to natural frequencies of each full-frame model). This increase in natural frequencies is due to the increased lateral stiffness of the building contributed by the masonry infill walls. The infill walls are approximately evenly distributed in both horizontal directions of Block 8 and as a result they increase the different natural frequencies by almost the same amount in each full-frame model.
- Considering the different full-frame models and the AVT frequencies (Tables 18-21), the continuum model shows the closest frequencies to the AVT results: the range is [1%-12%], which is deemed acceptable. Therefore, it can be concluded that in this particular case-study the best technique among the adopted methods for modeling the infill walls is the continuum model (panel element model). The other methods underestimate the stiffening effect of the infills by 40%, on average, in all modes of vibration examined (Tables 19-21).

5.3.2 Discussion of block#7 results

- The first AVT of block#7 has been conducted in September 2010. After calibrating the models of this block and comparing them with the AVT results, it was observed that the results were inconsistent. It means that the natural frequency extracted from AVT for the first mode (transverse mode) is higher than the first frequency of all full-frame models while for the second and third mode, AVT frequencies are less than the full-frame models. In other words, we cannot see a constant relative behaviour between the results of AVT and full-frame models (Tables 24-27). The first assumption for this discrepancy was that the modeling of the shear wall connection to the building in FE models was inappropriate. Therefore, various connection models for connecting the shear wall to the building have been tested as described previously. However, the different connecting systems yielded very similar results. The second assumption was in the in-plane modelling of the balcony slabs that link the shear wall to the former facade of the building. However, the balcony slab was located at the end of block#7 to which the shear wall is connected. It was previously exposed to the outside but after RDP, its occupancy has been changed to the office areas. The typical structural system of the balconies is composed of the continuous concrete slab (14.5 m × 3.8 m) supported by 4 columns and peripheral beams (Figure 42). Therefore, it was postulated that the balcony might not be strong enough to transfer the effect of the shear wall to the rest of the building, suggesting that the added shear wall is not contributing completely with the existing part, at least at very low ambient vibration levels. To investigate this possibility, a second series of AVT was carried out in July 2011. In this test, the number of measurement points at each floor was increased to 4 (Figure 42), with an with one sensor positioned right

before the balcony (i.e. inside the block when not retrofitted) and one at the end of the balcony slab, right behind the shear wall. This test was mainly done to check whether any particular in-plane racking flexibility could be attributed to the balcony slab. However, the second series of AVT results were the same as the first series. After these experimental and numerical simulations, it can only be concluded that the AVT results cannot fully capture the effect of the shear wall. A tentative explanation is related to the nature of the links between the seismic shear wall and the balcony slabs: the structural anchor bars may require a significant wall displacement to play their role, which is not observed under ambient vibrations. In other words, the AVT results suggest that under the very low-amplitude vibrations recorded during the tests (measured velocities in the range of [0mm/s-0.04 mm/s]) the shear wall is not involved in the structural response of the building and, therefore, its effect cannot be seen in AVT models. As a result, we conclude that the AVT results of block#7 cannot be used for masonry property calibration and further comparisons. This is another reason why block#8 was selected for calibration.

- Comparison between the full-frame and bare-frame models of block#7 (Table 28) shows [1%-27%] increase caused in modal frequencies after adding the infill walls. However, this increase is not as much as the increase observed in block#8, [41%-78%]. The main reason is that when disregarding the infill walls, block#7 is a lot stiffer than block#8 because of the presence of the concrete shear wall and the connection with block#9. As a result, the infill walls cannot affect the dynamic properties of block#7 as much as block#8. However, their effect is still considerable particularly when considering the continuum model, [3%-27%] (Table 28).

5.4 Effect of seismic retrofit and masonry infill walls on the performance of NSCs

To evaluate the effect of seismic retrofitting and the presence of *terra cotta* infill walls on the performance of NSCs, the continuum models and the bare-frame models of both blocks are subjected to a series of 12 generated accelerograms. Selecting two floors in each block (top floor #7 and middle floor # 3), Floor Response Spectra (FRS) and Interstorey-Drift curves were developed for each record in both orthogonal horizontal directions separately. It should be noted that the FRS curves presented are the average results over all the 12 input records. Regarding the Interstorey-drift curves, the results of one record is presented as an example and the maximum values of Interstorey-drift at both floors for all records are tabulated in Tables 30 and 31 expressed in percentage of story height.

5.4.1 Results and discussion for Block#8

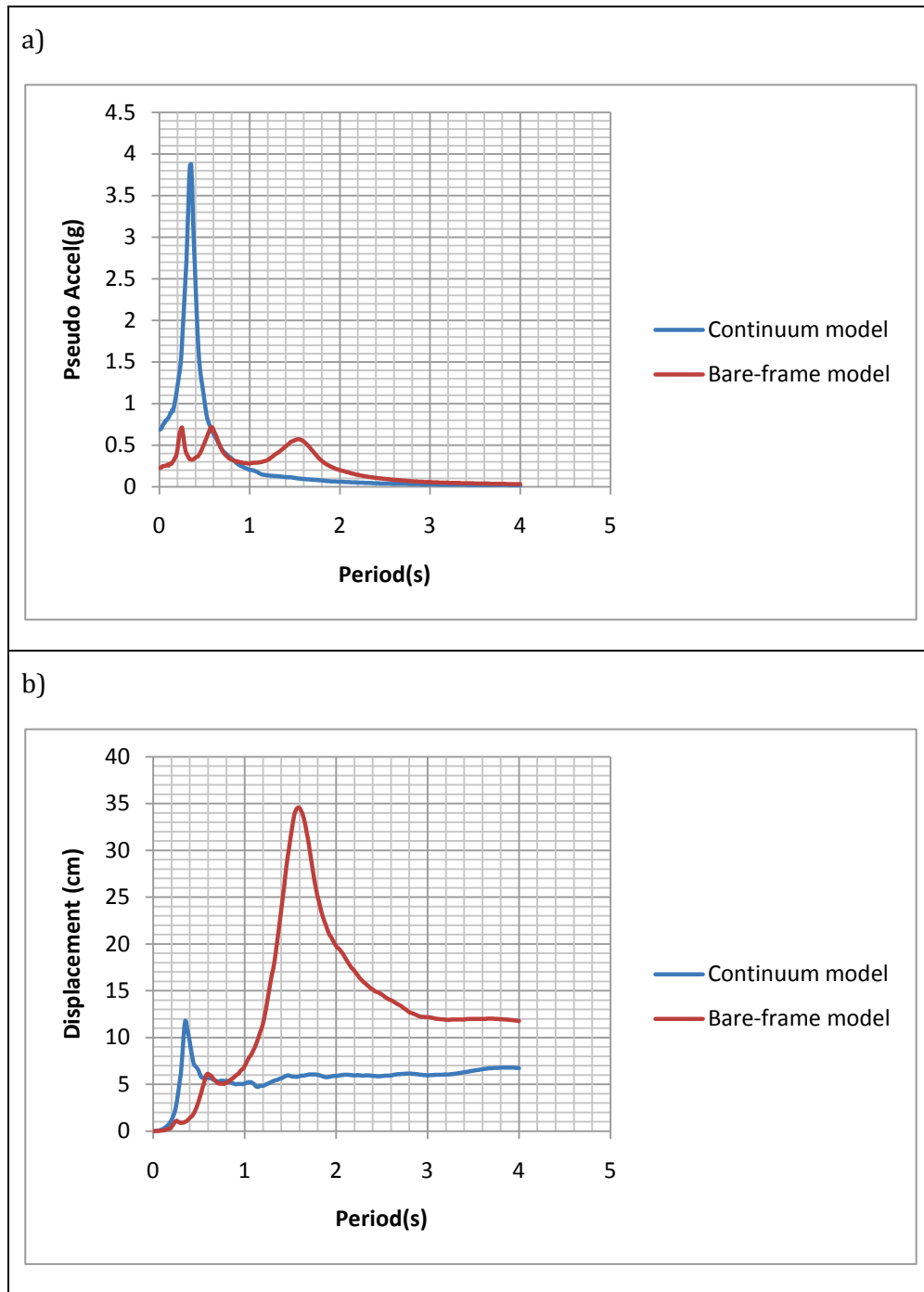


Figure 43 - Averaged FRS of block#8-7th floor-X-direction: a) Pseudo acceleration;
b) Displacement

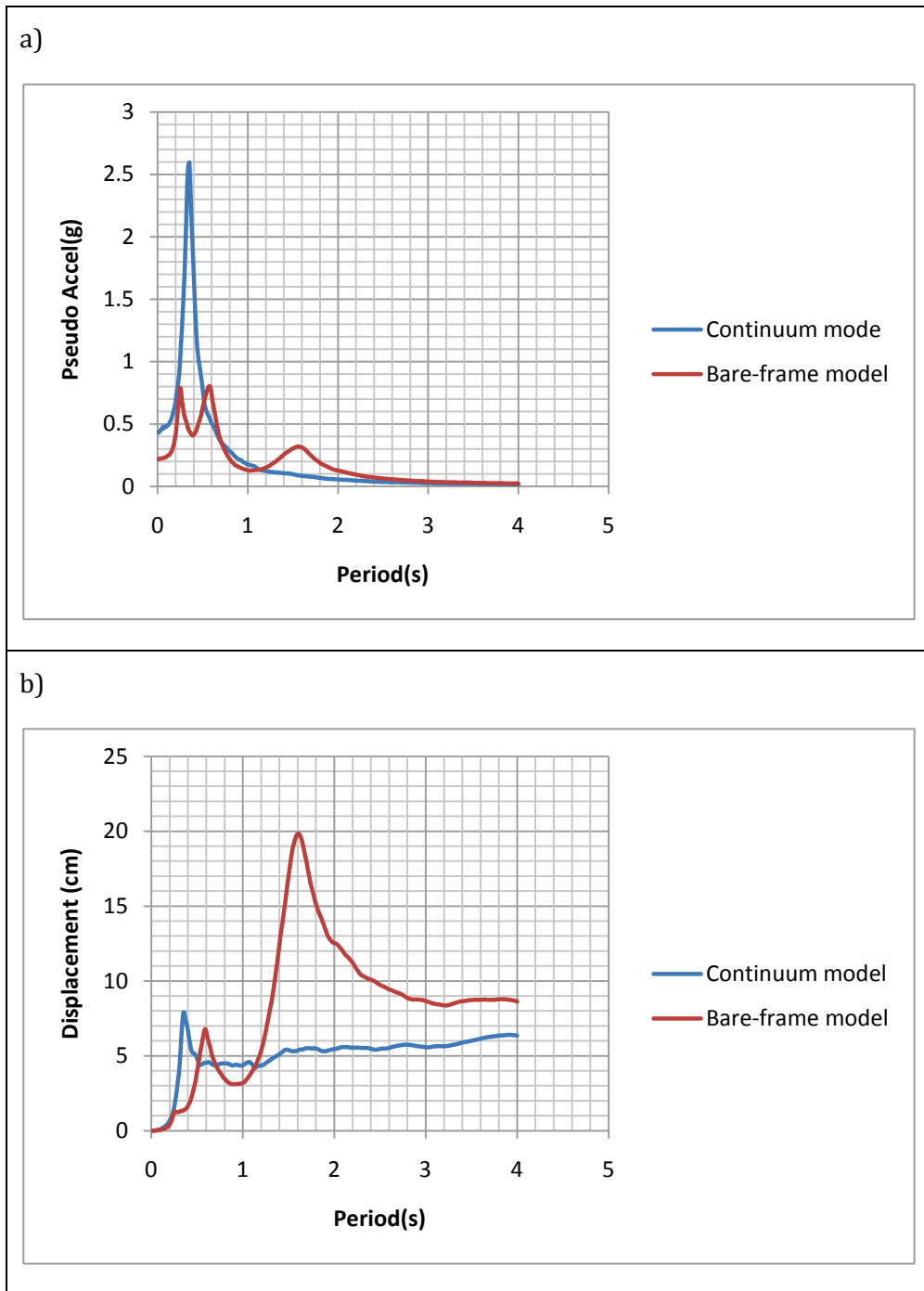


Figure 44 - Averaged FRS of block#8-3rd floor-X-direction: a) Pseudo acceleration;
b) Displacement

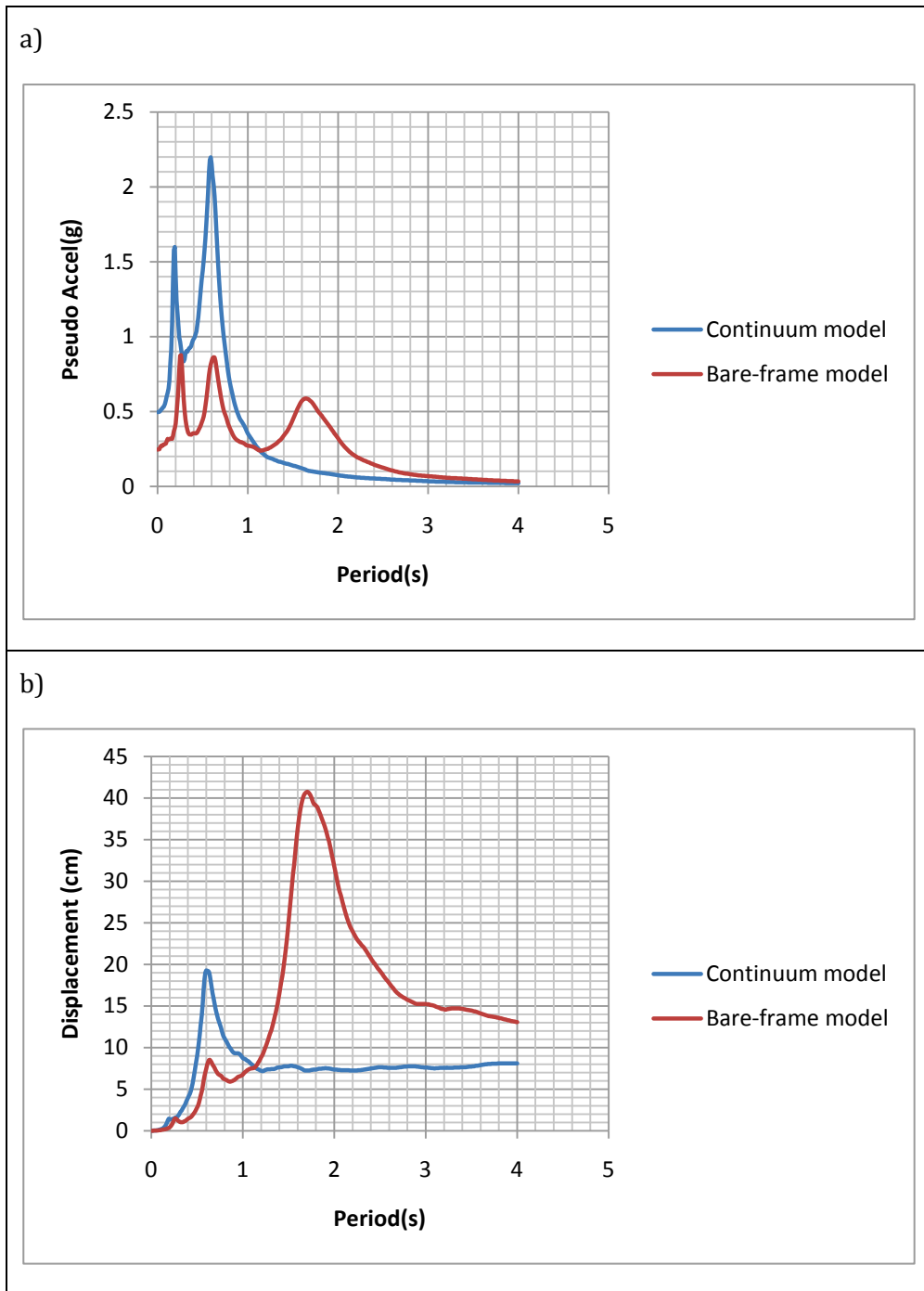
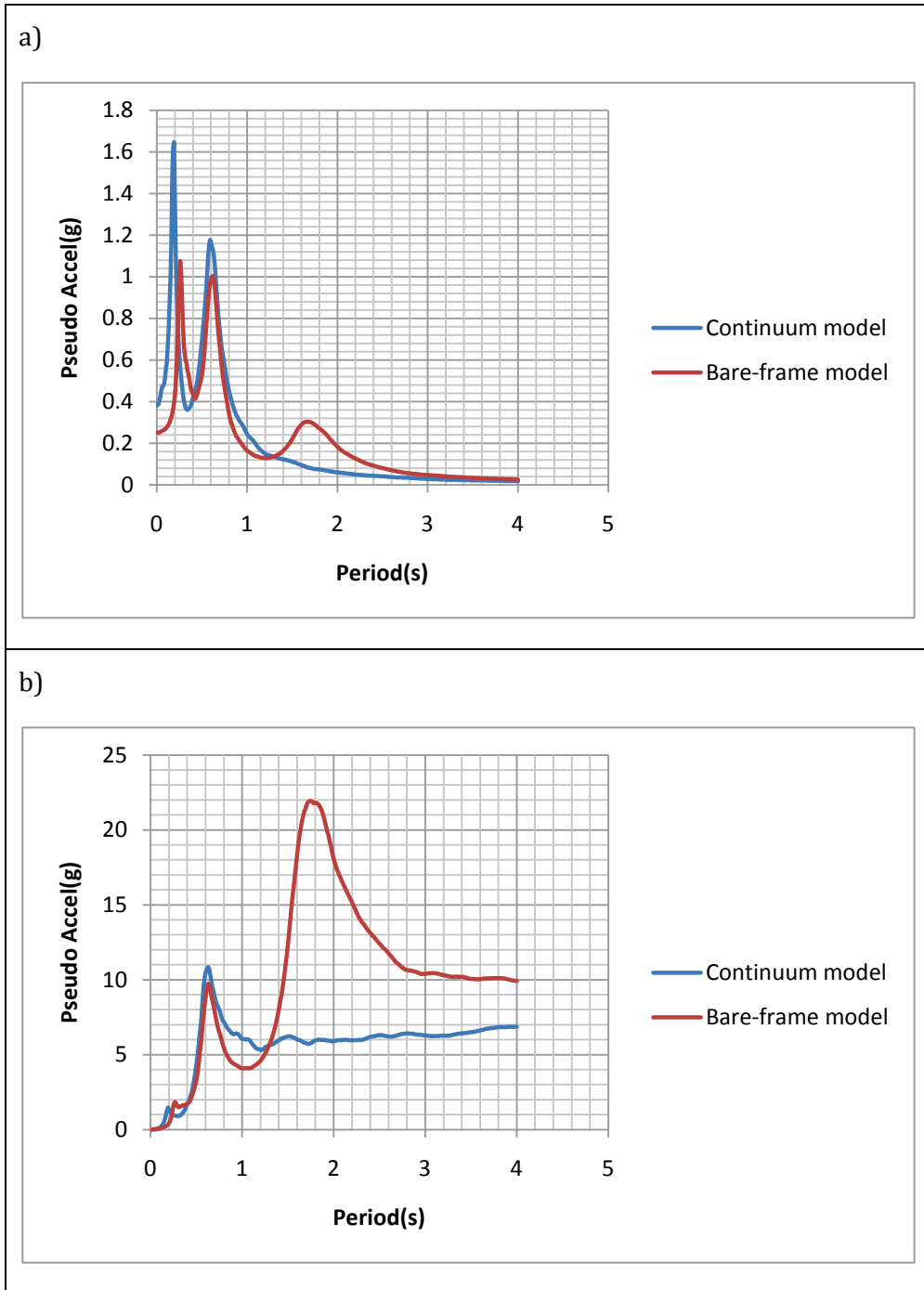


Figure 45 -Averaged FRS of block#8-7th floor-Y-direction: a) Pseudo acceleration;
b) Displacement



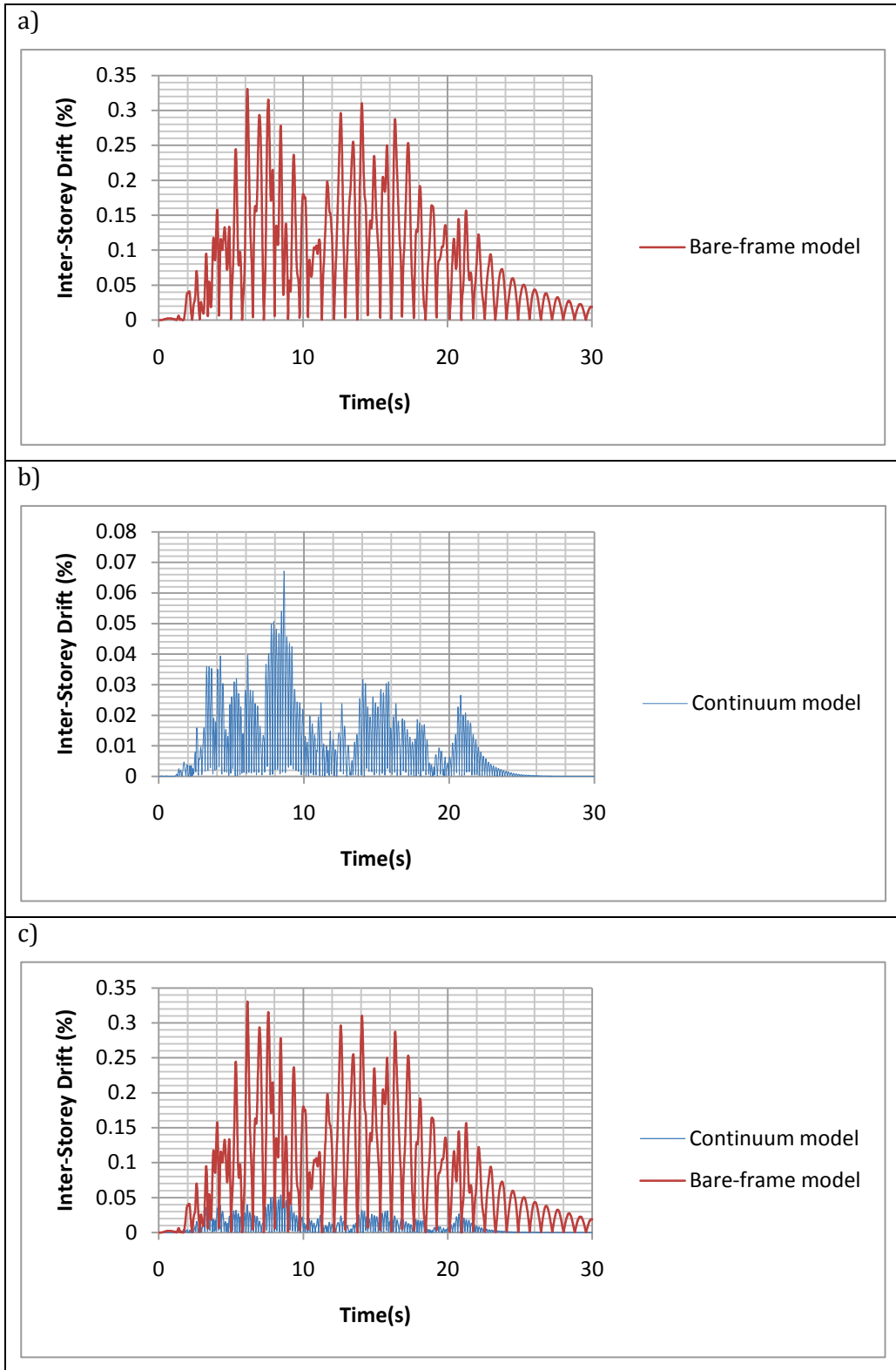


Figure 47 - Inter-storey drift curve - Block#8 - 3rd floor - X direction - E701001 record:
a) Bare-frame model; b) Continuum model; d) both models

Table 30 - Maximum Inter-storey drift - Block#8

Block#8 - Maximum Inter-storey drift (% of story height)								
MODEL	7 th floor- X direction		3 rd floor- X direction		7 th floor- Y direction		3 rd floor- Y direction	
	Bare-frame model	Continuum model	Bare-frame model	Continuum model	Bare-frame model	Continuum model	Bare-frame model	Continuum model
Records	(%)	(%)	(%)	(%)	(%)	(%)	(%)	(%)
E60301	0.30%	0.02%	0.22%	0.06%	0.50%	0.09%	0.24%	0.13%
E60302	0.25%	0.02%	0.17%	0.06%	0.40%	0.07%	0.22%	0.09%
E60501	0.34%	0.03%	0.27%	0.08%	0.36%	0.08%	0.30%	0.11%
E60502	0.29%	0.02%	0.29%	0.06%	0.34%	0.08%	0.28%	0.11%
E70301	0.22%	0.01%	0.23%	0.04%	0.32%	0.08%	0.26%	0.11%
E70302	0.29%	0.02%	0.21%	0.07%	0.37%	0.12%	0.25%	0.17%
E70501	0.28%	0.02%	0.24%	0.05%	0.39%	0.10%	0.28%	0.04%
E70502	0.20%	0.02%	0.26%	0.05%	0.35%	0.08%	0.31%	0.10%
E70701	0.25%	0.02%	0.27%	0.06%	0.36%	0.10%	0.36%	0.14%
E70702	0.30%	0.02%	0.39%	0.06%	0.45%	0.44%	0.46%	0.13%
E701001	0.28%	0.02%	0.33%	0.07%	0.43%	0.07%	0.47%	0.20%
E701002	0.38%	0.02%	0.27%	0.05%	2.84%	0.15%	0.46%	0.21%
Average	0.28%	0.02%	0.26%	0.06%	0.59%	0.12%	0.33%	0.120%

Table 31 - Modal periods and frequencies of bare-frame and continuum

Block # 8					
Bare-frame model	Mode Shapes	First mode		Second mode	
		Period	Frequency	Period	Frequency
	X direction	1.57	0.64	0.58	1.73
	Y direction	1.76	0.57	0.66	1.51
	Torsion	1.53	0.65	0.56	1.80
Continuum model	X direction	0.35	2.88	-----	-----
	Y direction	0.60	1.66	0.18	5.44
	Torsion	0.41	2.43	-----	-----

Figures 43 and 46 clearly show that the presence of masonry infill walls, resulting in a significant increase in the calculated fundamental frequencies of the building, causes the NSCs mounted on floors to experience larger accelerations, which may become critical for acceleration sensitive NSCs. However, for those NSCs which are sensitive to the inter-storey drift, the presence of masonry infill walls contributes to reduce the demand in drift, as seen in Figure 47 and Table 28.

Looking at the FRS in terms of Pseudo acceleration and displacement curves, a number of peaks are observed in each direction (X and Y). These peaks can be directly related to the natural frequencies of each model corresponding to each direction (Table 31). It is expected that the response of the main building (primary structure) at each floor shows the peaks at natural frequencies due to resonance. Then, the acceleration response of all floors is considered as the base acceleration for NSCs (Subsystem) to develop the FRS. As the floor response has higher energy content at natural frequencies of the primary structure, it is expected that the response of NSCs to this excitation (FRS) has also the peaks at the same frequencies.

Comparing the FRS provided for the 7th and 3rd floor shows that coming down along the height of the building, the effect of infill walls becomes smaller. This

is expected as the building is getting stiffer at lower floors which decrease the relative impact of infill walls. This can be seen clearly in Figure 46-a.

5.4.2 Results and discussion for Block#7

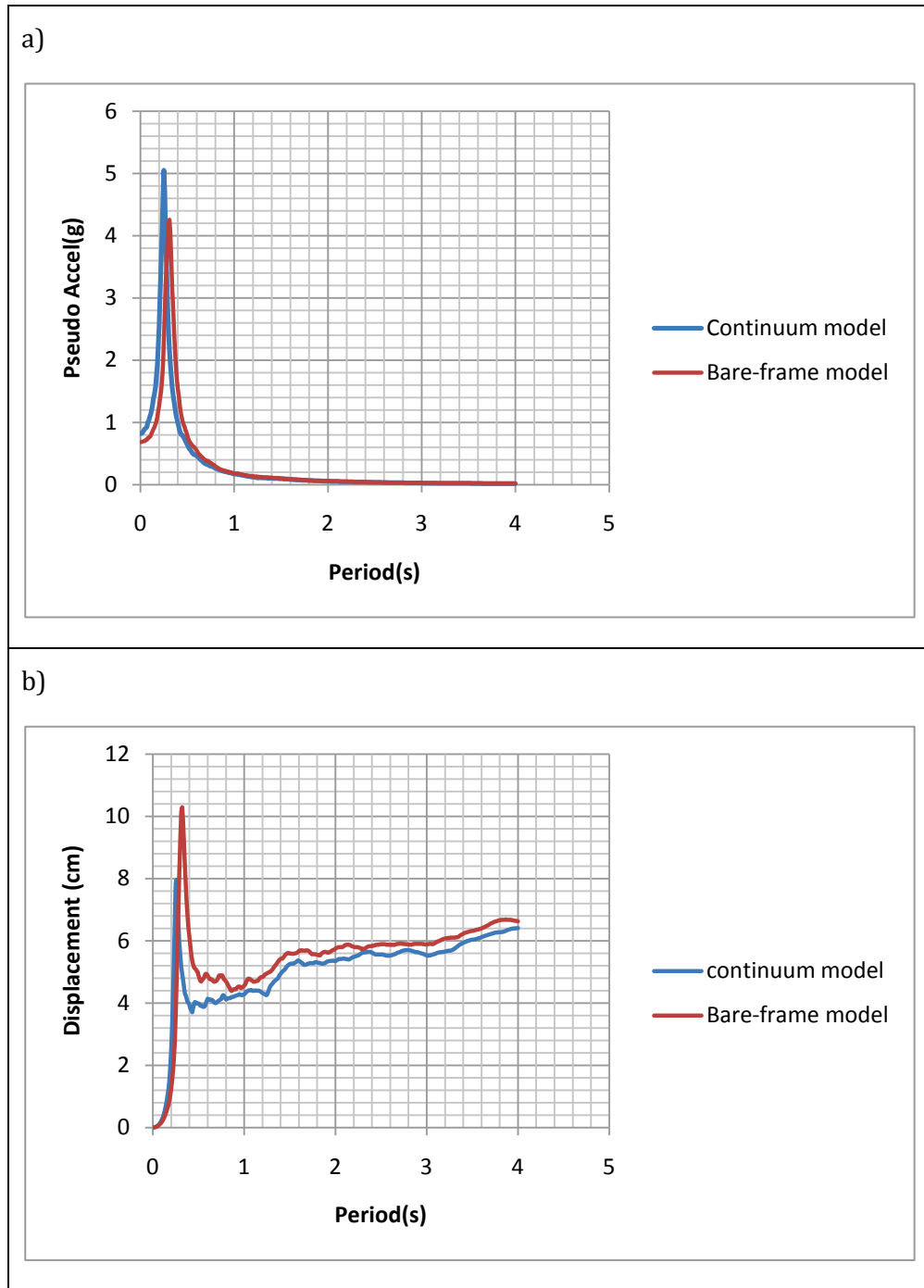


Figure 48 - Averaged FRS of block#7-7th floor-X-direction: a) Pseudo acceleration;
b) Displacement

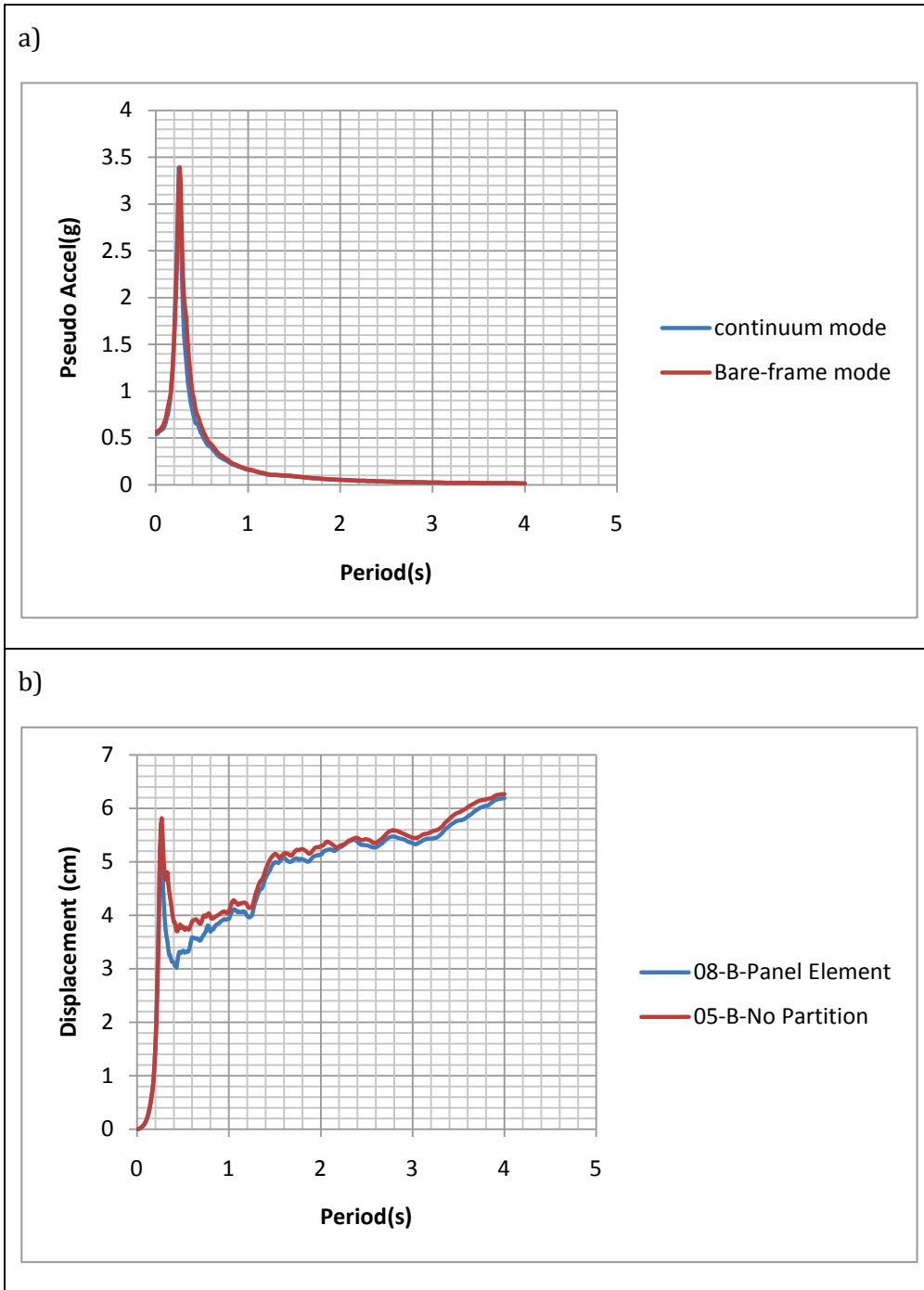


Figure 49 - Averaged FRS of block#7-3rd floor-X-direction: a) Pseudo acceleration;
b) Displacement

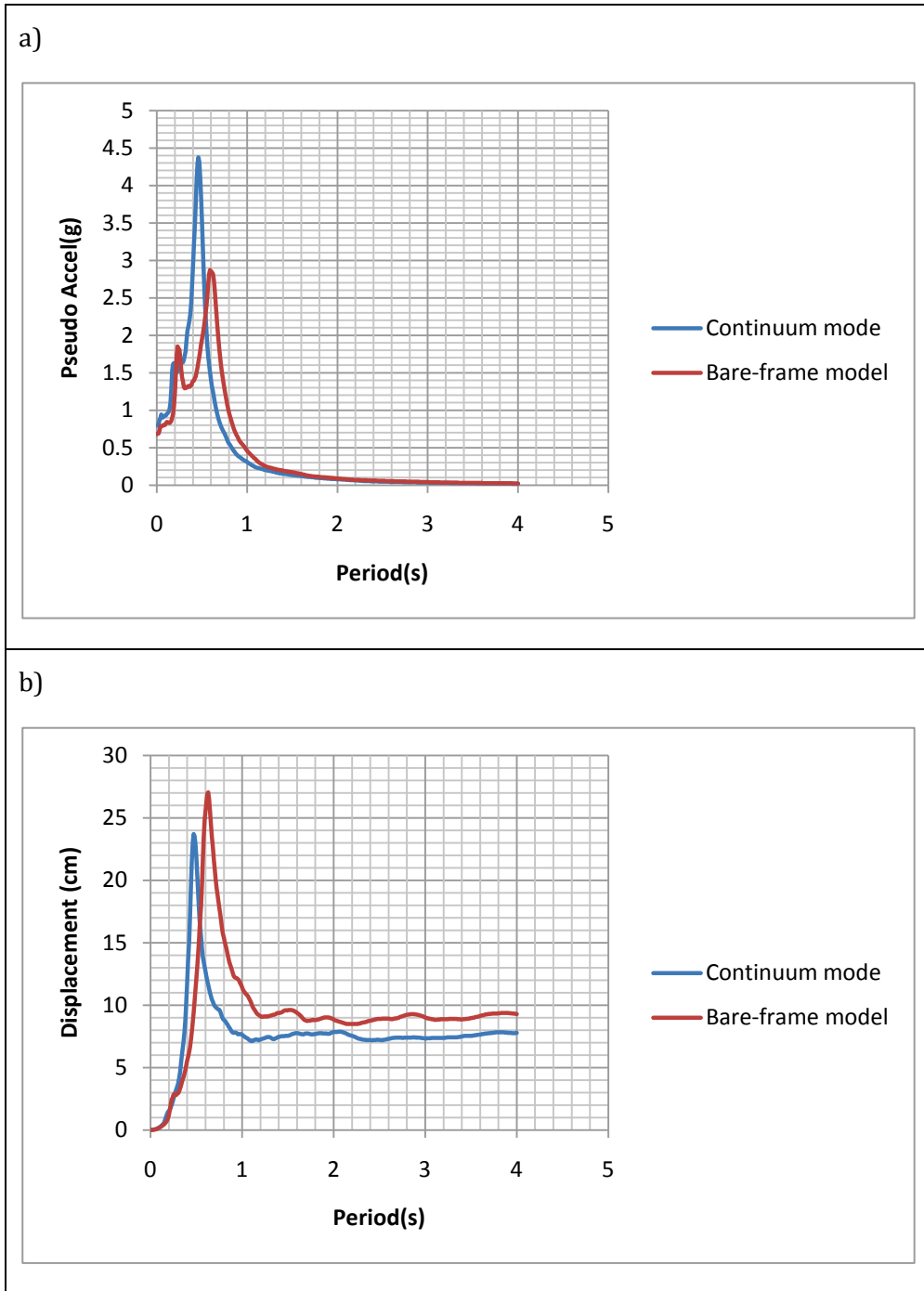


Figure 50 - Averaged FRS of block#7-7th floor-Y-direction: a) Pseudo acceleration;
 b) Displacement

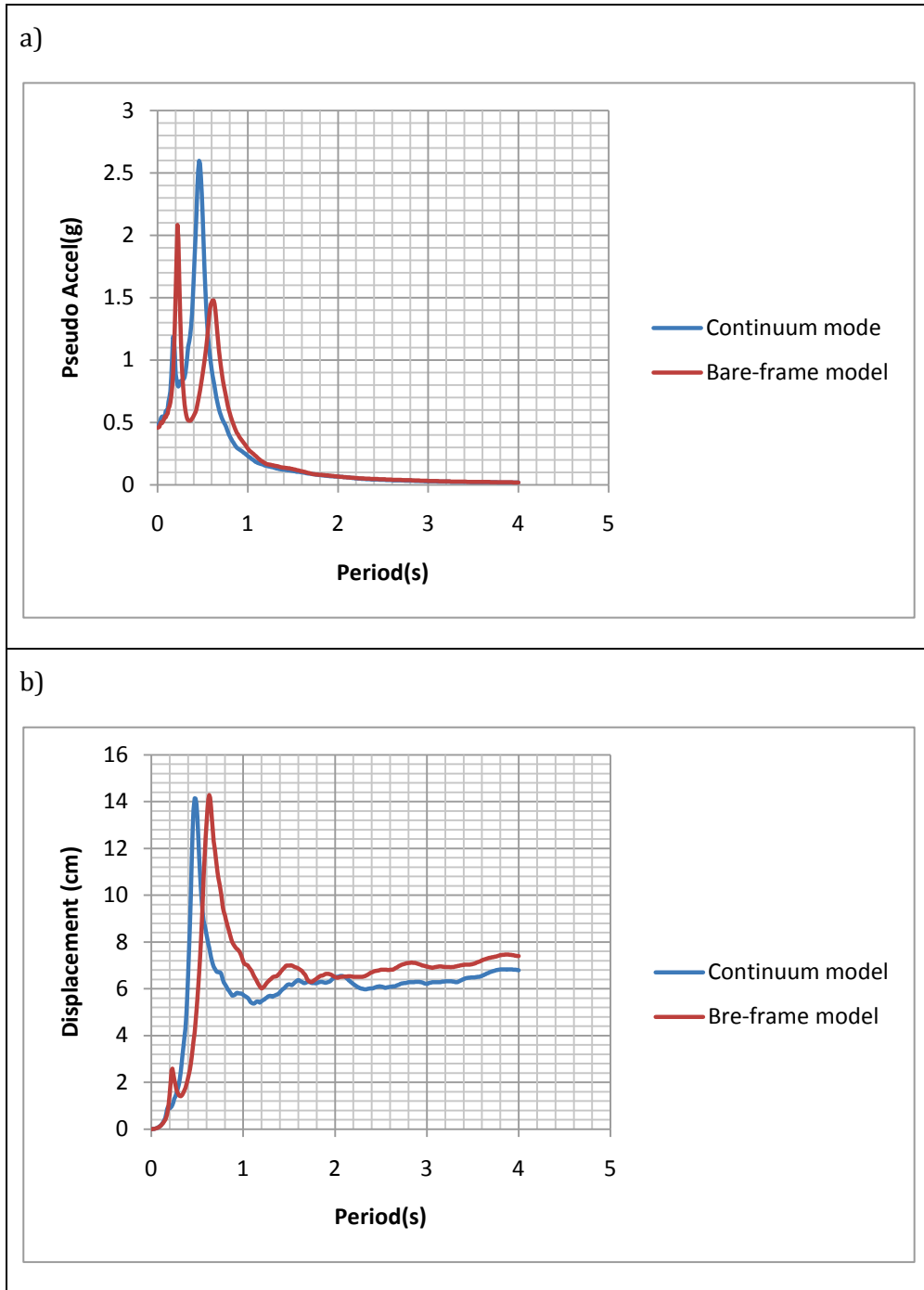


Figure 51 - Averaged FRS of block#7-7th floor-Y-direction: a) Pseudo acceleration;
 b) Displacement

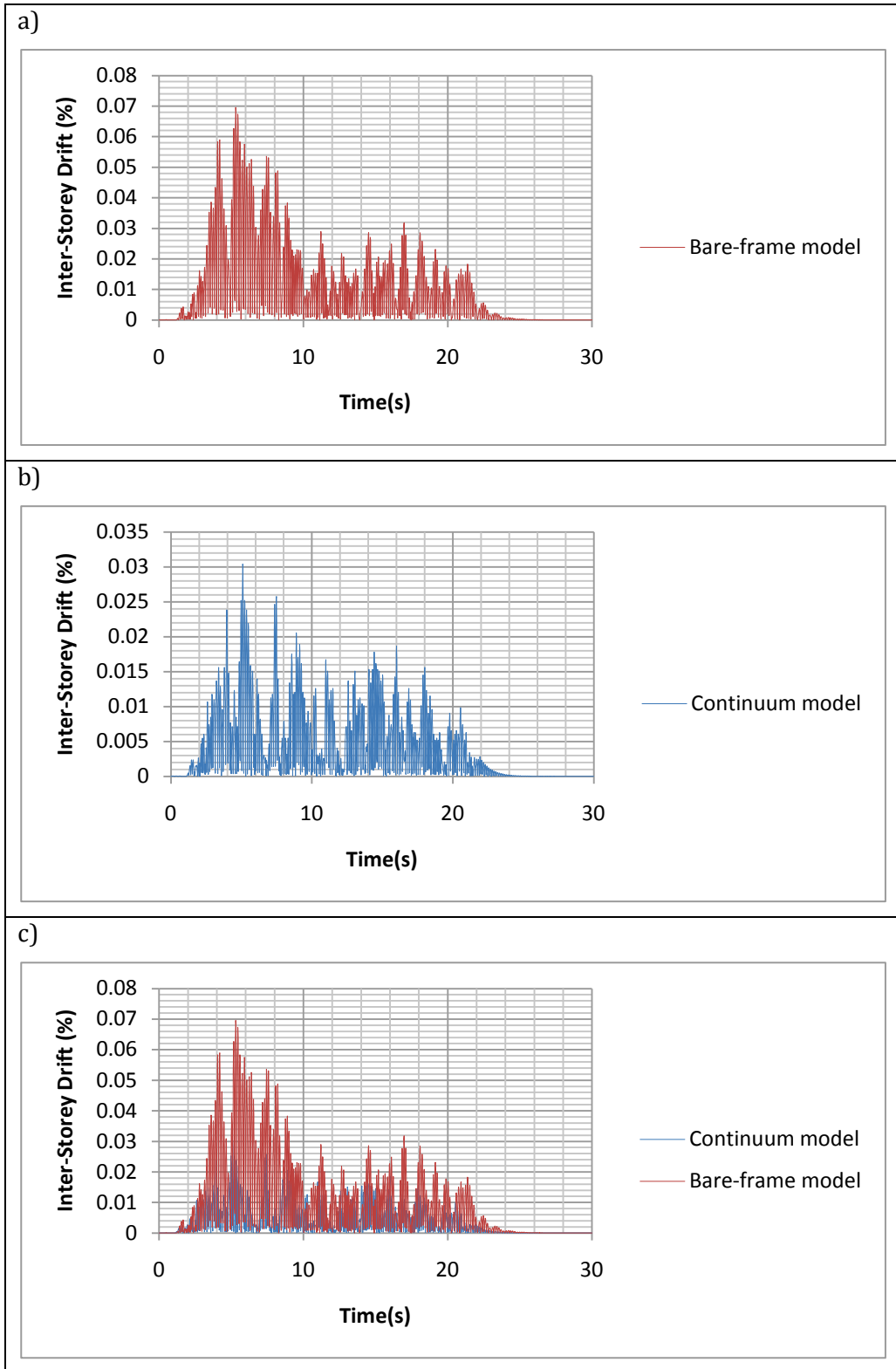


Figure 52 - Inter-storey drift curve - Block#8 - 3rd floor - X direction - E701001 record:

a) Bare-frame model; b) Continuum model; d) both model

Table 32 - Maximum Inter-storey drift - Block#7

Block # 7 - Maximum Inter-storey drift (%)								
MODEL	7 th floor- X direction		3 rd floor- X direction		7 th floor- Y direction		3 rd floor- Y direction	
	Bare-frame model	Continuum model	Bare-frame model	Continuum model	Bare-frame model	Continuum model	Bare-frame model	Continuum model
Records	(%)	(%)	(%)	(%)	(%)	(%)	(%)	(%)
E60301	0.15%	0.01%	0.08%	0.04%	0.16%	0.07%	0.20%	0.10%
E60302	0.15%	0.01%	0.09%	0.04%	0.12%	0.08%	0.14%	0.11%
E60501	0.13%	0.01%	0.08%	0.03%	0.14%	0.07%	0.16%	0.10%
E60502	0.14%	0.01%	0.06%	0.04%	0.10%	0.07%	0.13%	0.10%
E70301	0.13%	0.01%	0.06%	0.04%	0.12%	0.10%	0.14%	0.14%
E70302	0.12%	0.01%	0.09%	0.04%	0.19%	0.08%	0.22%	0.12%
E70501	0.15%	0.01%	0.06%	0.04%	0.13%	0.06%	0.16%	0.08%
E70502	0.12%	0.01%	0.06%	0.03%	0.13%	0.07%	0.15%	0.10%
E70701	0.13%	0.01%	0.07%	0.03%	0.17%	0.07%	0.20%	0.10%
E70702	0.16%	0.01%	0.06%	0.04%	0.16%	0.07%	0.20%	0.10%
E701001	0.14%	0.01%	0.07%	0.03%	0.12%	0.09%	0.13%	0.13%
E701002	0.13%	0.01%	0.06%	0.03%	0.23%	0.08%	0.29%	0.11%
Average	0.14%	0.01%	0.07%	0.04%	0.15%	0.08%	0.18%	0.11%

Table 33 – Natural periods and frequencies of bare-frame and continuum models

Block 7					
Bare-frame model	Mode Shapes	First mode		Second mode	
		Period	Frequency	Period	Frequency
	X direction	0.31	3.19	0.26	3.84
	Y direction	0.61	1.63	0.23	4.36
	Torsion	-----	-----	-----	-----
Continuum model	X direction	0.25	4.00	-----	-----
	Y direction	0.47	2.14	-----	-----
	Torsion	0.18	5.63	-----	-----

In general, similar conclusions made for block#8 can be made for block#7. It includes the increase in acceleration and decrease in inter-storey drift caused by the presence of masonry infill walls. However, in block#7 the difference between bare-frame and continuum models is less than for block#8 that is essentially an isolated building while block #7 as retrofitted benefits from the presence of the added shear wall and the connection to block#9.

In block #7, the peaks observed in FRS and the displacement curves in each direction can be again related to the resonant frequencies of the main building. These periods and frequencies are summarized below in Table 33.

6 Conclusions and Future Work

The main objective of this thesis was to examine the effects of seismic retrofitting and presence of *terra cotta* infill walls on the dynamic characteristics of the buildings. The other goal was to evaluate the impact of the aforementioned parameters on the performance of non-structural components of the buildings during a design earthquake. To address these objectives, experimental and numerical studies have been conducted on two separate buildings (Blocks #7 and #8) of Sainte-Justine Hospital in Montreal.

The results of ambient vibration tests and finite element models showed that considering masonry infill walls in modeling significantly influences the dynamic properties of the structures. The presence of infill walls is expected to cause an increase in natural frequencies (or decrease in natural periods) of the buildings. In this particular case study, adding the masonry infill walls to the models decreased the fundamental period of blocks #8 and #7 by nearly 200% and 40%, respectively. Therefore, disregarding this effect in seismic design as commonly done by engineers will result in underestimated earthquake load (i.e. selecting a lower acceleration on Design Spectrum).

The results of frequency analysis on four types of full-frame models (i.e. the continuum model and three different compression strut models) were compared with ambient vibration results and it was concluded that the continuum model gives the closest results to the tests; this means that the panel elements can simulate the linear effect of the infill walls on the dynamic response of the buildings better than the strut models. Although this is confirmed in the linear range of response, we have no experimental evidence to calibrate the finite element models at larger deformations. We believe that the linear range of response is appropriate in this application because of the post-critical nature of the structures.

To address the influence of infill walls and seismic retrofitting on the performance of non-structural components, the floor response spectra and inter-storey drift curves were developed for two floors of each block (floor levels 3 and 7) considering a series of 12 earthquake records compatible with the NBC 2005 uniform hazard spectrum for Montreal. The numerical simulation results showed that the presence of partitions (global lateral stiffening) can lead to two main effects: 1- Acceleration-sensitive components attached to upper floors are subjected to the higher acceleration when the building is stiffer and 2- Displacement-sensitive components are experiencing lower drifts, which is beneficial to their seismic performance.

The effect of seismic retrofitting on the dynamic behaviour of block#7 was studied by comparing the finite element models of this block with block#8, which was not-retrofitted seismically. The comparison showed that seismic rehabilitation had a pronounced effect on the torsional behaviour of the block#7. The results showed that connecting block#7 to the adjacent block#9 had more global stiffening effect (reduction of fundamental periods) than adding the concrete shear wall alone.

For block#7, it was observed that AVT results cannot fully capture the stiffening effect of the shear wall. A possible explanation may be related the nature of the links used to connect the seismic shear wall to the building. It should be noted that the ambient vibrations measured have very low amplitude and maybe insufficient to engage the shear wall into a fully coupled response as would be expected in strong shaking. To fully account for this effect in analysis would require non-linear modeling which is outside the scope of this study but could be explored in a more comprehensive future study.

Appendix A:

Acceleration floor response spectra

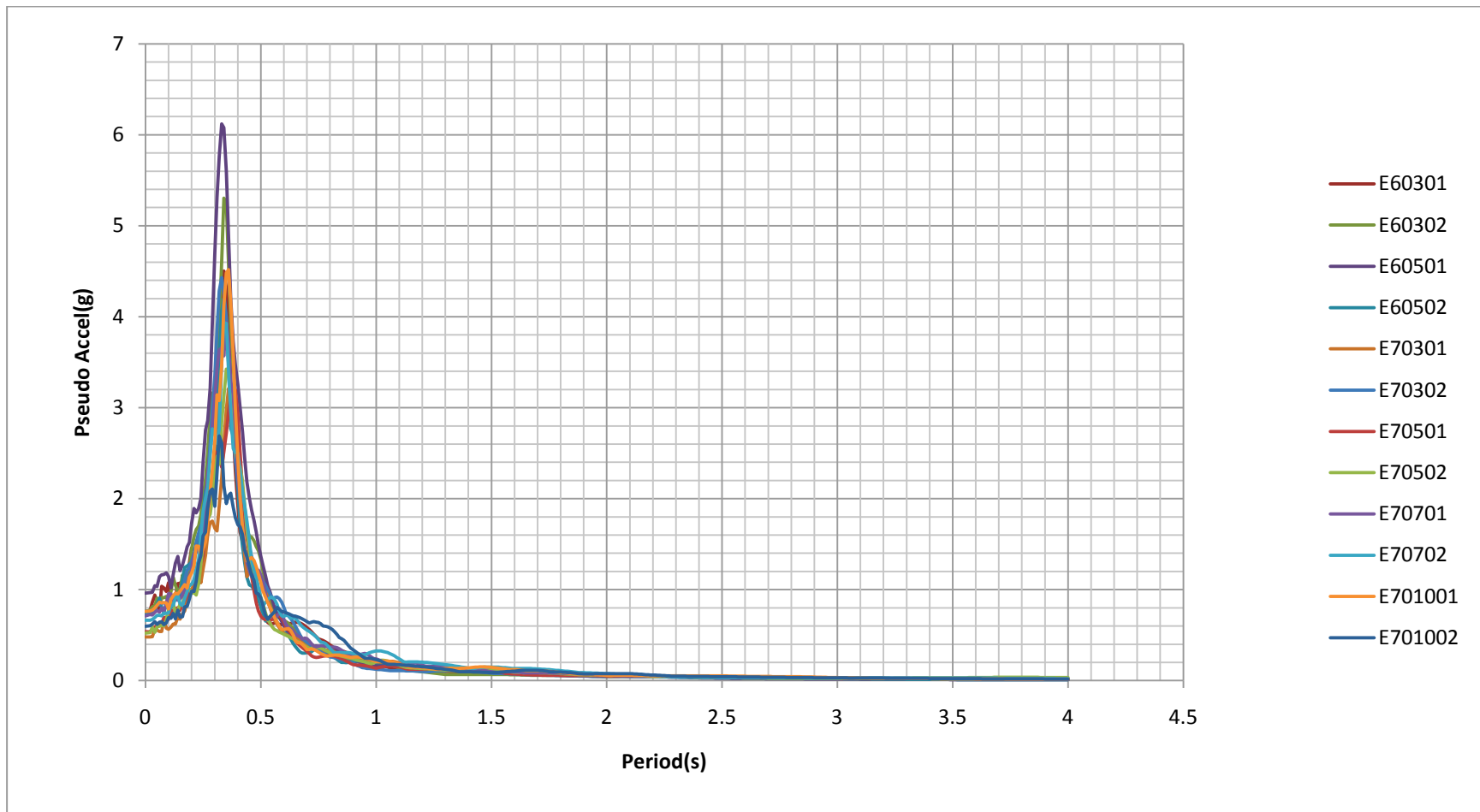


Figure 53 - Floor Response acceleration, Block#8, Continuum model, 7th floor, X-direction

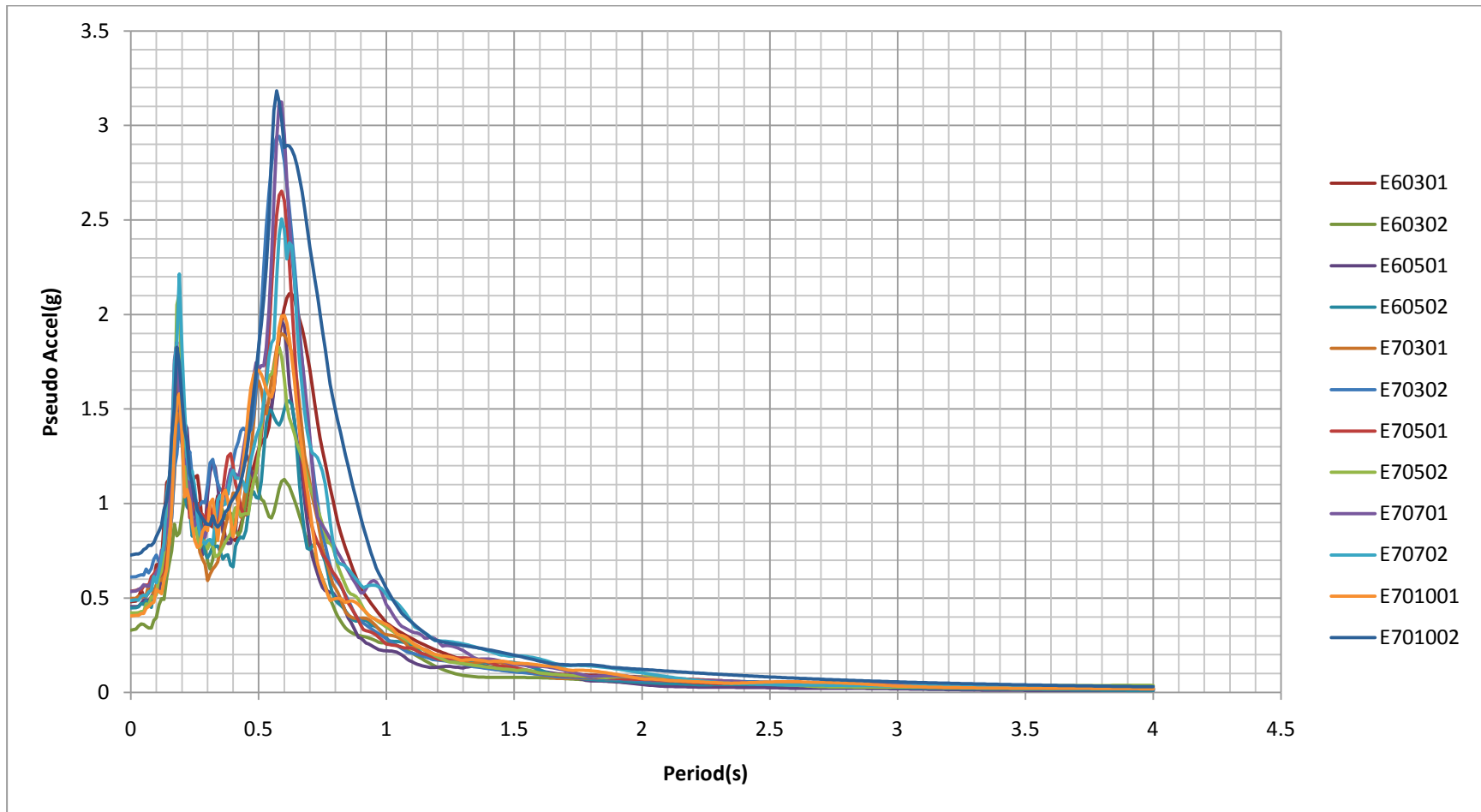


Figure 54 - Floor Response acceleration, Block#8, Continuum model, 7th floor, Y-direction

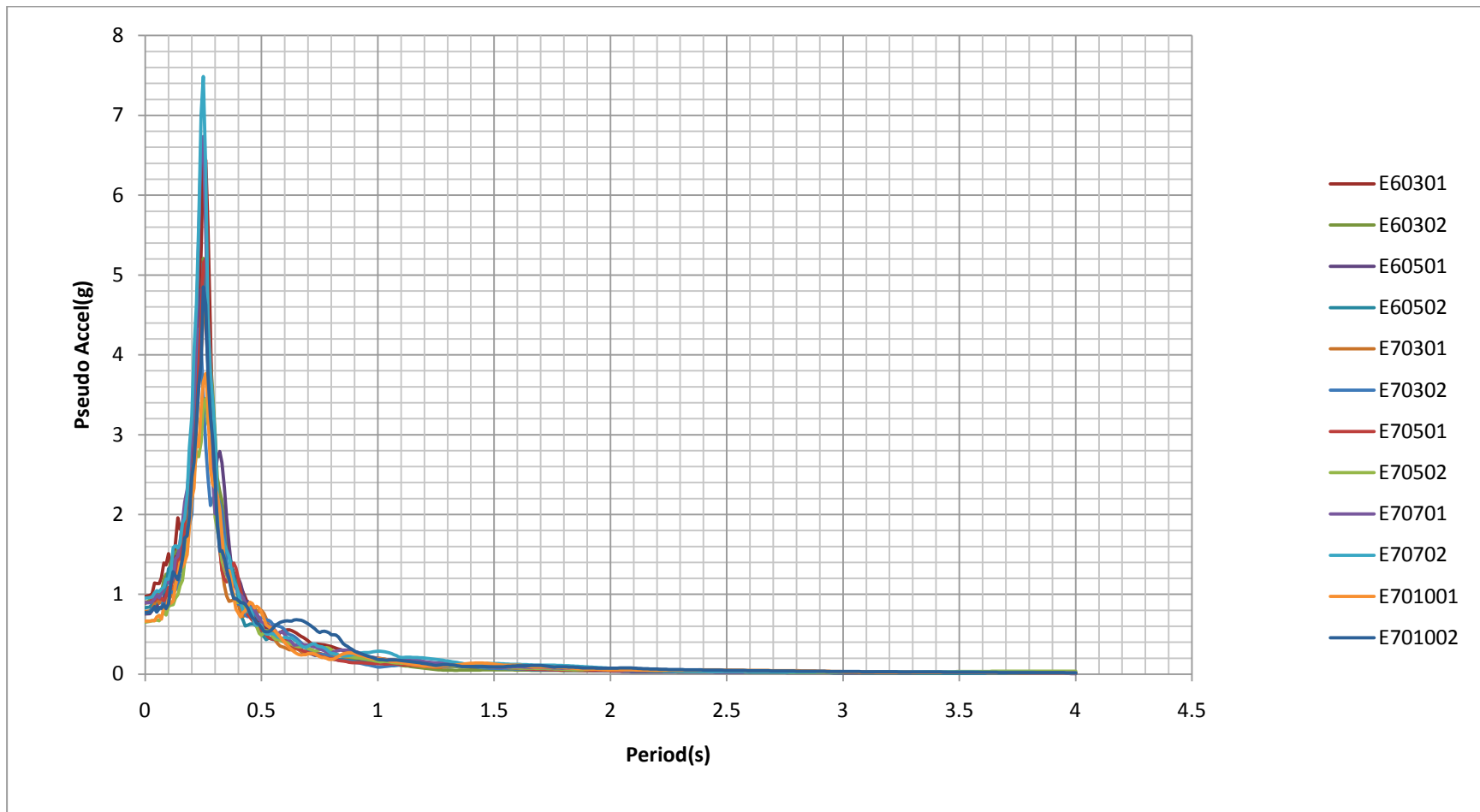


Figure 55 - Floor Response acceleration, Block#7, Continuum model, 7th floor, X-direction

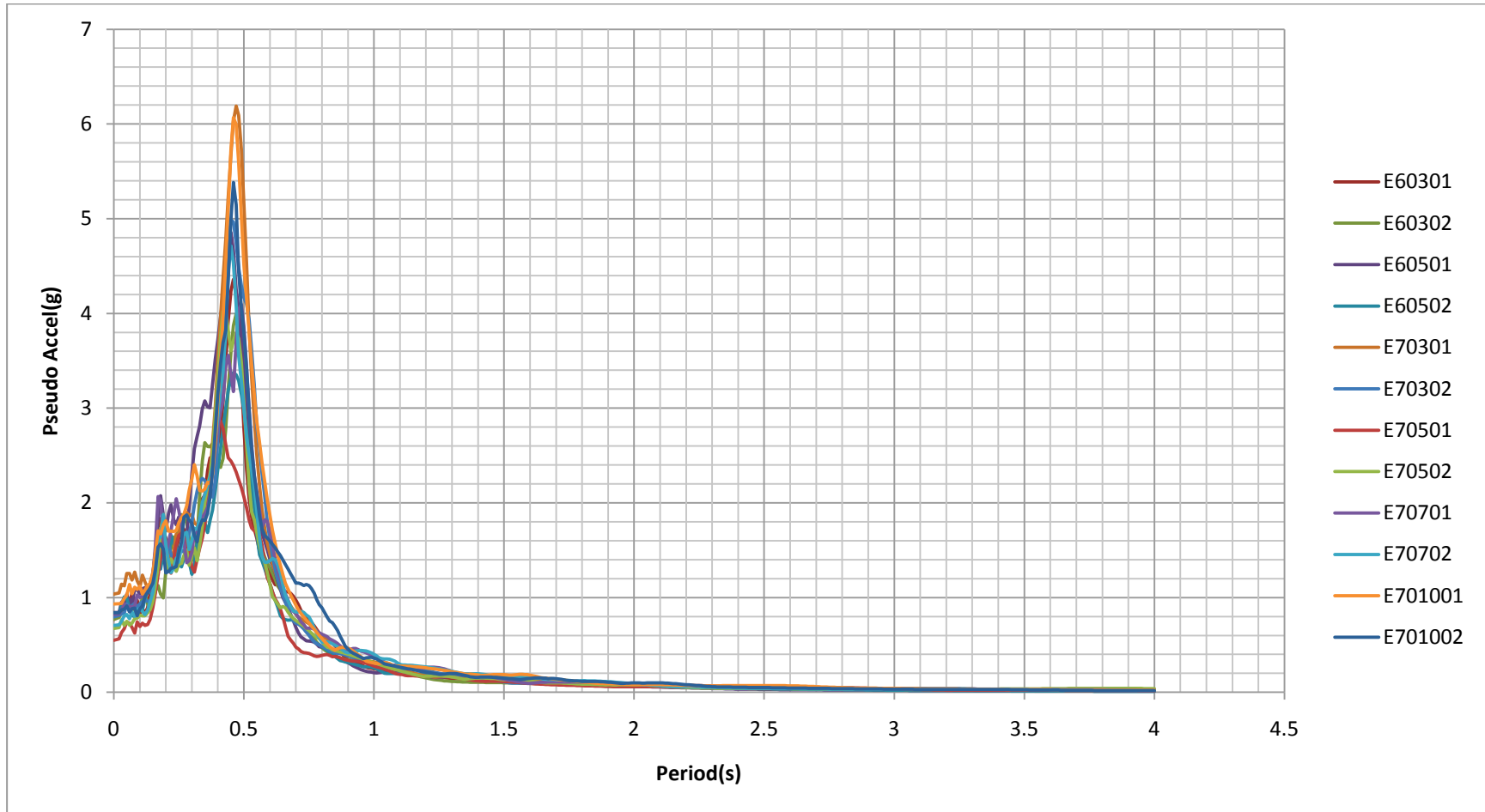


Figure 56 - Floor Response acceleration, Block#7, Continuum model, 7th floor, Y-direction

References

1. ASSOCIATION-CSA, C.S., *Seismic risk reduction of operational and functional components (OFCs) of buildings, CAN/CSA-S832-06*, 2006.
2. Chartrand, V., *Seismic Retrofitting of the Ste-Justine Hospital in Montreal*, in *Civil Engineering 2009* Massachusetts Institute of Technology.
3. Hospital, S.J. *Ste-Justine Hospital website*. 2011; Available from: <http://www.chu-sainte-justine.org/Home/default.aspx>.
4. National Research Council Canada, I.f.R.i.C., *National Building Code of Canada (NBCC)*, 2005.
5. Villaverde, R., *Fundamental concepts of earthquake engineering*, 2009: CRC Press.
6. Canada, P.W.a.G.S. *National Resource Canada*. 2011; Available from: <http://earthquakescanada.nrcan.gc.ca/index-eng.php>.
7. Gilles, D., *In situ dynamic characteristics of reinforced concrete shear wall buildings*, in *Department of Civil Engineering and Applied Mechanics 2011*, McGill University: Montreal, QC.
8. Bendat, J.S. and A.G. Piersol, *Random data: analysis and measurement procedures 2000*: John Wiley & Sons, Inc.
9. Solution, S.V., *ARTEMIS Extractor, Software for Operational Modal Analysis*, 2010.
10. Memari, A., Aghakouchak, AA., Ghafory Ashtiany, M., Tiv, M., *Full-scale dynamic testing of a steel frame building during construction*. *Engineering Structures*, 1999. 21(12): p. 1115-1127.
11. Su, R.C., AM. Sheikh, MN. Lam, NTK., *Influence of nonstructural components on lateral stiffness of tall buildings*. *The Structural Design of Tall and Special Buildings*, 2005. 14(2): p. 143-164.

12. Chang, C., T. Chang, and Q. Zhang, *Ambient vibration of long-span cable-stayed bridge*. Journal of Bridge Engineering, 2001. 6: p. 46.
13. Farrar, C. and G. James III, *System identification from ambient vibration measurements on a bridge*. Journal of Sound and Vibration, 1997. 205(1): p. 1-18.
14. Polyakov, S.V., *On the Interaction between Masonry Filler Walls and Enclosing Frame when Loaded in the Plane of the Wall*. Earthquake Engineering, 1960: p. 36-42.
15. Holmes, M., *Steel frames with brickwork and concrete infilling*. Proceedings of the Institution of Civil Engineers, 1961. 19: p. 473 – 478.
16. Stafford Smith, B., *Methods for predicting the lateral stiffness and strength of multi-storey infilled frames*. Building Science, 1967. 2(3): p. 247-257.
17. Shing, P.B. and A.B. Mehrabi, *Behaviour and analysis of masonry-infilled frames*. Progress in Structural Engineering and Materials, 2002. 4(3): p. 320-331.
18. Durrani, A.J., Y. Luo, and D.P. Abrams, *Seismic retrofit of flat-slab buildings with masonry infills*. Technical Report, 1994: p. 1-8.
19. Luo, Y., *Evaluation, Modeling, and Retrofit of Flat-Slab Buildings subjected to Seismic Loading*, 1995, Rice University.
20. FEMA and ASCE, *FEMA-356, Prestandard and commentary for the seismic rehabilitation of buildings*, 2000.
21. Mainstone, R.J. and B.R. Station, *On Stiffnesses and Strengths of Infilled Frames* 1974: Building Research Station.
22. Hendry, A.W., *Structural brickwork* 1981: Halsted Press.

23. Eldakhakhni, W.W., *Non-linear finite element modeling of concrete masonry-infilled steel frames*2000: Drexel University.
24. El-Dakhakhni, W.W., *Experimental and analytical seismic evaluation of concrete masonry-infilled steel frames retrofitted using GFRP laminates*, 2002, Drexel University.
25. El-Dakhakhni, W.W., M. Elgaaly, and A.A. Hamid, *Three-strut model for concrete masonry-infilled steel frames*. JOURNAL OF STRUCTURAL ENGINEERING, 2003. 129(2): p. 177-185.
26. Mohyeddin-Kermani, A., H.M. Goldsworthy, and E. Gad, *A Review of the Seismic Behaviour of RC Frames with Masonry Infill*, 2008.
27. KORKMAZ, K.A., F. Demir, and M. Sivri, *Earthquake assessment of R/C structures with masonry infill walls*. International Journal of Science & Technology, 2007. 2(2): p. 155-164.
28. S.P.A., M., *Manuale tromino ENG TR-ENGY PLUS October 2008*, M. S.P.A., Editor 2008.
29. Oppenheim, A.V., R.W. Schaffer, and J.R. Buck, *Discrete-time signal processing*. Vol. 1999. 1989: Prentice hall Englewood Cliffs, NJ:.
30. Norton, M.P. and D.G. Karczub, *Fundamentals of noise and vibration analysis for engineers*2003: Cambridge Univ Pr.
31. Chopra, A.K. and F. Naeim, *Dynamics of Structures—Theory and Applications to Earthquake Engineering*. Earthquake Spectra. Vol. 23. 2007. 491.
32. Brincker, R., L. Zhang, and P. Andersen, *Modal identification of output-only systems using frequency domain decomposition*. Smart Materials and Structures, 2001. 10: p. 441.
33. Schott, J.R., *Matrix analysis for statistics*. 2nd ed2005: Wiley-Interscience.

34. Computers and Structures, I.C., *SAP 2000-advanced 14.0.0*, 2009.
35. Committee, M.S.J., *Specification For Masonry Structures (ACI 530.1/ASCE 6-92/TMS 602-902)*. American Concrete Institute International, 2005.
36. Amrhein, J.E., *Reinforced masonry engineering handbook: clay and concrete masonry*1998: CRC Press.
37. Committee, M.S.J., *Building code requirements for masonry structures (ACI 530-05/ASCE 5-05/TMS 402-05); Specification for masonry structures (ACI 530.1-05/ASCE 6-05/TMS 602-05); Commentary on building code requirements for masonry structures (ACI 530-05/ASCE 5-05/TMS 402-05); Commentary on specification for masonry structures (ACI 530.1-05/ASCE 6-05/TMS 602-05)*2005: Masonry Society.
38. Halchuk, S. and J. Adams, *Fourth Generation Seismic Hazard Maps for Canada*, 2001. p. 0638.
39. Assi, R., *Seismic analysis of telecommunication towers mounted on building rooftops*, in *Department of Civil Engineering and Applied Mechanics*2006, McGill University: Montreal.
40. Atkinson, G.M. and I.A. Beresnev, *Compatible ground-motion time histories for new national seismic hazard maps*. Canadian Journal of Civil Engineering, 1998. 25(2): p. 305-318.
41. Antoniou, S. and R. Pinho, *SeismoSignal*, in *Version 3.2*. 02008.42.
42. National Information Service for Earthquake Engineering, University of California, Berkeley. 1997; Available from: http://nisee.berkeley.edu/bertero/html/nonstructural_components.html
43. Petley,Dave,2009; Availablefrom: <http://www.landslideblog.org/2009/03/beichuan-photos-of-aftermath-of-natural.html>